LASER CLEANING OF PRECIOUS METALS

Thesis submitted in accordance with the requirements of the University of Liverpool for the degree of Doctor in Philosophy

by Margarida Calejo Pires

December 2007

Declaration

I hereby declare that all of the work contained within this dissertation has not been submitted for any other qualification.

Signed:

(Margarida Calejo Pires)

Date: 31st Dec. 2007

TABLE OF CONTENTS

List of Figures

List of symbols and units

Quantity		Symbol	Units
Ablation rate		A_{bl}	
Absorption coefficient (optical)		α	m^{-1}
Absorption length (optical) Penetration depth		L_α	m
Absorbance, Absorptivity		**A**	
Adiabatic Coefficient		γ	
Angle (optical)		θ	o
Area		**A***	m^2
Beam Spot or Section Diameter		d_σ	m
Density		ρ	Kg m^{-3}
Distance (any direction), thickness		ℓ	m
Elasticity or Young Modulus		**Y**	Pa
Electric charge		**q**	C
Electric potential		**U**	V m^{-1}
Electrical permittivity of air		ε_a	F m^{-1}
Energy		**E**	J
Enthalpy		**H**	J
Fluence		**F**	J m^{-2}
Force		**f**	N
Heat Capacity	specific	C_m	J kg^{-1} K^{-1}
	volumetric	$C_v=\rho\, C_m$	$J{\cdot}m^{-3}{\cdot}K^{-1}$
Heat		**H**	J
Heat Flux		**Q**	W m^{-3}
Intensity, Irradiance, Power density		**I**	W m^{-2}
Length, distance (any direction)		ℓ	m
Liquid surface tension		γ_l	N m^{-1}
Mass		**m**	Kg
Momentum	Material object	**p**	Kg m s^{-1}
	photon		J s m^{-1}
Overlap (pulse scan)		OL	
Penetration depth (optical) / Absorption length (optical)		L_α	m
Photon oscillation frequency		υ	Hz
Poisson ratio		ϑ	
Power		**P**	W
Pressure		p_r	Pa
Pulse duration or length		τ_p	s
Pulse Repetition Rate		f_p	Hz
Reflectance, Reflectivity		**R**	
Reflection coefficient		$r_\perp$, $r_\parallel$	
Refractive index	substrate	$n_u - ik_u$,	
	contamination	$n_c - ik_c$	
Strain		ε	
Stress (compressive or tensile)		σ	Pa

Temperature		T	K
Temperature variation		ΔT	K
Thermal conductivity		K	$W\ m^{-1}\ K^{-1}$
Thermal diffusion length, Thermal penetration depth (1D),		δ	m
Thermal diffusivity Thermal diffusion coefficient		κ	$m^2\ s^{-1}$
Thermal expansion coefficient	linear	β	K^{-1}
	volumetric	3β	K^{-1}
Thickness		ℓ	m
Time duration		Δt	s
Time – pulse duration		τ_p	s
Time - variable		t	s
Transmission coefficients		$t_\perp, t_\parallel$	
Transmittance, Transmissivity		T	
Variable, angle		θ	o
Variable, space orthogonal to surface		z	m
Variable, number		n	
Variable, space parallel to surface		(x, y)	m
Variable, time		t	s
Velocity, speed	general	v	$m\ s^{-1}$
	light	c	
	sound	v_s	
Volume		V	m^3
Wavelength		λ	m
Young or Elasticity Modulus		Y	Pa

Subscripts	
Phase: solid, liquid, vapour	*s, l, v*
Energy: incident, absorbed, reflected, transmitted	*i, a, r, t*
Object layers	*c, u*

Constants			
Planck constant		h	$6.626\ E^{-34}\ J\ s$
Velocity of light in air		c_0	$3\ E^8\ m\ s^{-1}$
Velocity of sound (depends on T)	air	v_s	$3.44\ E^2\ ms^{-1}$
	water		$1.5\ E^3\ ms^{-1}$
	steel		$5.1\ E^3\ ms^{-1}$

Acknowledgements

My very first words of gratefulness and deep recognition are due to my supervisor Prof. Ken Watkins that along these years, always guided and supported my work and my difficulties with his kind scientific and human hosting.

Also my gratefulness to those that conducted my research activity and skills development until this point: Prof. Carvalho Rodrigues, Dr. Ribau Teixeira and Prof. Bill Steen.

My recognition and thanks are also due to those that created the necessary conditions to carry this research work, Dr. C. Freitas, Dr. R. Salimbeni, Prof. Olinda Conde, Dr. Martin Sharp, Prof. J. Rebordao and the British Royal Mint.

My thanks also to all the colleagues that helped me with the use of sophisticated analysis equipment and with the interpretation of he results, without whom this work would not be possible, Teresa Ferraz, Teresa Santos, Luis Geraldes, Luis Coutinho, Mª José Oliveira.

My thanks are due also to those contributing enlightening discussions of my ideas, opening new windows and establishing bridges in my route in research; thank you Carmel Curran, thank you Salvatore Siano, thank you Walter Perrie, thank you Gerard Sliwinsky, thank you Jens Hildegarden, thank you Alexandre Cabral, thank you Geoff Dearden.

To all the other persons that helped me in a way or other to accomplish this work, namely Prof. C. Pond, Jennie Kay, Andrea Jones, Andrea Dearden, Ana Espergueira and Aldora Amaral

And to all my family and my friends and very very deeply to my "kids", thank you for believing in me.

Abstract

Laser cleaning, a process of selective interaction of laser radiation with materials based on differentiated optical properties of contamination and underlying substrate, was foreseen by Arthur Schallow one of the laser inventors. Since then, numerous applications have been developed along with a large research effort in understanding the associated mechanisms.

However laser cleaning of precious metal surfaces has proven to be a delicate intervention due to the need of preserving the surface gloss characteristic of these metals, associated with a relatively low melting point and a usually thin corrosion or contamination layer.

Laser cleaning of precious metal – Gold and Silver, contaminated with continuous films of ambient corrosion – silver sulphide, industrial contamination – lubricant oil, and human intervention – overpainted gold, was studied in experimental conditions, in order to overcome previously reported difficulties, mainly the dulling of the precious metal surface and study the laser surface interaction processes and cleaning mechanisms.

A large range of laser sources was experimented for cleaning the contaminated surfaces with wavelength of 10.6 μm- CO_2 laser, 1.06 μm- Nd:YAG laser and respective harmonics in visible and ultraviolet range and 248 nm- KrF excimer laser. Diverse pulse duration ranges were also used such as microsecond pulses of CO_2 and Short Free Running Nd:YAG laser, hundreds of nanoseconds from Long Q-Switched lasers and few nanosecond pulses of electro-optical Q-Switched Nd:YAG lasers and Excimer lasers and finally femtosecond pulse duration from a fibre laser.

Laser cleaning condition was assessed using Optical and Electron Microscopy equipped with X-ray Energy Dispersive Spectroscopy, Colorimetry and, sporadically, Fourier Transform Infrared Spectroscopy and Optical Interference Profilometry.

For each set of material surface and contamination, it was found a range of operating conditions for laser cleaning resulting in a damage free

surface. The successful conditions were found for "non-thermal wavelengths" and pulse durations, meaning UV laser wavelengths or femtosecond pulse durations.

A specific Laser Cleaning mechanism was proposed concerning each laser cleaned surface, regarding the experimental applied parameters, and the assessment analysis results.

INTRODUCTION

"I did a lot of stuff to show that lasers were really not death rays. That's one reason I invented the laser eraser..."

Nobel Laureate Arthur Schawlow

Beauty and rarity of gold, silver and alloys lead that the ancients considered them to be of noble birth compared to other metals; for this reason, and also due to precious metals scarceness they were used mainly for the activities considered at that time the more noble, namely religion, war and authority.

But precious metals associated with authority were used not only in ornaments of rulers and very influent persons but also for money, which coinage has been always, in organised societies, a sign of power and domination.

Nowadays, the use of precious metals, mainly silver and gold has spread into many other fields such as optical devices and circuits, electronics and medicine.

Silver is the whitest and brightest of all metals, meaning that it is the metal with a more flat and higher value reflectivity spectrum in the optical region of electromagnetic radiation; thereof it is used for coatings on reflective optical components. But silver presents also the highest electrical and thermal conductivity of all pure metals and, for this reason it is also used in electrical equipment and electronic component contacts. Beyond these industrial applications silver is also an anti-bacterial agent and so it is also used in medicine for medical devices and implants.

Gold is a bright yellow metal, very resistant to corrosion, oxidation and sulfidation. Because it remains tarnish free for long, gold is much used in jewellery and religious decorations. Due to its chemical stability, gold alloys are often used in orthodontic appliances, for dental restoration and fillings. Gold is also used in electronic devices employing low voltage and current, where surface tarnish films need to be avoided.

Indeed precious metals include other rare transition metals, named the platinum group (or shortly platinum) located in period 5 and 6 of group VIII B of the periodic table; these are ruthenium, rhodium, palladium, osmium, iridium and platinum. However, due to their scarceness and latter use in Europe, in the XIII century, their application in jewellery,

coinage, medicine and electronics industry is found, but much rarer and therefore the present work does not include them.

Although recognised as "Noble" since the beginning of ancient civilizations, indicating the resistance that these metals have to corrosion and to combine with other elements, the fact is that gold and silver are also subject to degradation arising from use, weathering and vandalism, for which further conservation and restoration are required.

The use of lasers in conservation and restoration of precious artefacts was introduced in Venice, in 1972, when John Asmus [1, 2] in collaboration with Laboratorio San Gregorio, developed and implemented a methodology to perform holographic records of precious artworks, severely eroded by local weathering and pollution.

Based on his accomplishments in Venice, technical research and development at the University of San Diego, USA, and further sabbatical work for three years at Laser Department of Maxwell Laboratories, Asmus definitely triggered the use of lasers to clean and restore precious artworks.

In spite of John Asmus pioneer work and dissemination effort, laser cleaning had a limited acceptance by the scientific and conservation community and at a first stage during the 1970's and 80's, this laser processing of materials was mainly applied to remove particles from substrates or black crust from stones and almost always confined to experimental studies and laboratorial work.

Laser cleaning to remove micron and sub-micron particles from silicon wafers and stencil mask substrates for the semi-conductors industry has been studied and developed at the end of the 80's by two different groups at IBM, Germany [3], with UV pulsed lasers and the University of Iowa [4], USA, with IR TEA CO_2 laser pulses and latter on by a team in Singapore and Osaka, using both UV and IR pulsed lasers [5-6].

Laser cleaning applied to the removal of continuous layers from metallic substrates was initially applied in an industrial environment, to the removal of paint layers [7], to the removal of rust, oil and grease [8], but

also to remove corrosion layers in artworks [9, 10, 11] and in the electronics industry [12-16].

Laser cleaning applied to silver and alloys was reported by C. Degrigny and V. Zafiropulos (2001), J. Lee and Y. Koh (2001) and latter by M. Sokhan and D. McPhail (2003), all of them studied the cleaning of contaminated or tarnished silver threads used in ancient textile embroideries.

Degrigny, Zafiropulos *et al* [17], in the sequence of previous work by Degrigny and others at Arc' Antique, France, made an experimental study on the effect of laser wavelength and ambient gas in the cleaning of tarnished silver surfaces. Test samples, including silvered brass, silver alloy artefacts and silver thread-textile composites, where irradiated with a Q-Switched Nd:YAG laser and then analysed by scanning electron microscopy (SEM) and X-ray photon spectroscopy (XPS).

Except for slightly tarnished pure silver on brass, where the cleaning tests were considered acceptable, the cleaning process was considered incomplete or else caused adverse features on the silver alloy surfaces. Modifications of the surface colour and shine, such as surface whitening, yellowing and dulling, occurred at energy density values above 0.08 J cm^{-2} for the 3rd harmonic wavelength (355 nm) of the Nd:YAG laser.

Moreover, the cleaning process didn't show clear improvements in experiments of laser cleaning of tarnished silver in inert atmosphere, except for the decrease of silver surface yellowing. Silver yellowing was detected when irradiating silver surfaces at high fluencies and was caused by the formation of silver oxide (Ag_2O).

J Lee, J. Yu and Y. Koh [18] studied also the influence of the incident Nd:YAG laser radiation for the cleaning of silver ribbons wrapping silk fibres. Concerning the used wavelengths (1064, 532, 266 nm), at approximately the same energy density (2.6 J cm^{-2}), it was observed by optical microscopy, that IR and visible wavelengths caused melting and colour changes on the silver surface and thermal damage of the silk.

However the UV laser radiation revealed a bright silver surface without damaging the silk.

The laser cleaning threshold for the referred wavelengths was also determined by those authors, based on optical microscopy examination, being 0.06 J cm^{-2} at 266 nm, 0.2 J cm^{-2} at 532 nm, and 0.6 J cm^{-2} at the fundamental wavelength.

M. Sokhan, F. Hartog and D. McPhail [19] , using also a Q-switched Nd:YAG, emitting in the fundamental (1064 nm) and 2nd harmonic wavelength (532 nm) have analysed the effects of cleaning by laser soiled silver threads, assessing the results by surface analysis techniques such as focused ion beam (FIB) and secondary ion mass spectroscopy (SIMS).

Varying the laser fluence from 0.2 to 2 J cm^{-2} they found the same features that Degrigny, Zafiropulos *et al* [17] and Lee *et al* [18] namely the colour change of the irradiated surface. Based on the results of the referred surface analysis techniques, M. Sokhan *et al* concluded that different chemical reactions took place during laser surface irradiation and attributed the surface colour changes to surface chemistry alterations, like oxidation and sulphidation; these chemical alterations were also dependent on the cleaning environment.

More recently, Siatou, Charalambous, Argyropoulos and Pouli (2006) presented an experimental study on laser cleaning of artificially corroded metals, including silver samples.

In this study, A. Siatou *et al* [20], irradiated the surface of silver alloy coupons with Nd:YAG laser at infrared (1064 nm) and ultraviolet (355 nm) wavelength as well as with KrF excimer lasers, with nanosecond pulses. Once again they refer surface melting for surface irradiation with the IR wavelength at very low fluence (0.1 J cm^{-2}), surface whitening with the 355 nm laser pulses, but they found a good surface quality after cleaning with excimer laser pulses at 248 nm and with 10 ns pulse duration.

Laser cleaning of gold is much more difficult to find in the published literature, possibly due to the fact that its use is rarer than that of silver and also because gold does not corrode in most common environments. As a matter of fact, corrosion appearing in gold objects is found to be due to the presence of other metals e. g. alloyed [21] or layered [22] with gold.

Laser cleaning of industrial contamination from gold contacts was referred by Ohba, Kuzukzwa and Sakairi (1998). In this paper, Ohba *et al* [23] present an experimental study concerning laser cleaning of signal control relays having gold-silver alloy contacts. The relay contact, contaminated with organic material such as machine oil were irradiated with a scanned CO_2 laser beam at 16 J cm^{-2}, that caused the burn off or dissociation of the organic film covering the precious metal contact. The aim of this paper is mostly the study of the causes affecting contact resistance, and so no much more information is given concerning the laser cleaning process.

The present research work had as departure point a literature review on laser cleaning and associated mechanisms, supported by the vast bibliographic collection existing at the Laser Group, The University of Liverpool.

Analysing the published literature, at the beginning and along the duration of this work, it become evident that a systematic research on the experimental cleaning of precious metal surfaces was lacking. Moreover, no indication was found in the reviewed literature on laser cleaning of precious metals, about the possible mechanisms of laser cleaning involved. More than that, new laser sources with new temporal pulse regimes become available, presenting new challenges to the study of the cleaning process by laser and associated physical mechanisms.

After the reception of the first set of silver coins and blanks provided by the Royal Mint, an experimental approach was taken, using several lasers to clean different sets of surfaces and contaminations.

Cleaning of silver and gold was experimented with wavelengths from the mid infrared, using CO_2 laser at 10.6 μm, to the ultraviolet of KrF excimer

laser at 248 nm, including the three first harmonics of Nd:YAG laser at 1064 nm, 532 nm and 355 nm.

Pulse length temporal regime applied to laser cleaning in this research work varied from a few microseconds- pulsed CO_2 and short free running Nd:YAG, through the nanosecond regime- excimer, long Q-switch and standard Q-switch Nd:YAG lasers to pico or femtosecond pulses emitted by fibre lasers.

Single pulse, multiple pulse, scanning beam with partial overlap, dry and wet cleaning were used varying the irradiation within a large range of fluencies, in order to identify and optimise the operation parameters adequate to clean precious metals with laser.

Several surface analysis techniques were systematically used, including optical and electron microscopy for surface observation, energy dispersive X-ray spectroscopy for elemental analysis and colorimetry for surface appearance control. Sporadically, when necessary, Fourier transform infrared spectroscopy, X-ray diffraction and optical interference profilometry was also used.

Considering contaminated precious metals also a large range of samples were experimented for laser cleaning with a more or less degree of success. Silver coins and blanks were supplied by the Royal Mint, with small localized depositions, or lines and traces of oil on the surface, or sulphatation covering the whole surface. Gold and silver plates, bought from commercial jewellery stores, were deliberately contaminated by tarnishing or overpainting.

From this diverse experimental work three successful case studies were enhanced and are presented next, on the basis of their representativeness of real situations of silver tarnishing of valuable artefacts, silver objects contaminated in industrial environment by machine oil and paint layers on gold surfaces simulating renovative interventions found in religious decorations:

Case 1. Laser cleaning of tarnished silver; successful cleaning with low fluence and low repetition rate UV nanosecond pulses.

Shining silver surfaces are aimed in jewellery and houseware, religious artefacts and icons. However these surfaces tend to corrode or tarnish in regular environment, due to the presence of airborne hydrogen sulphide and carbonyl sulphide, reducing brightness, purity and conductivity of the exposed surfaces.

Cleaning tarnished silver is usually achieved by mechanical or chemical methods or both simultaneously, leading in any case to an uncontrolled loose of surface material.

The goal of cleaning by laser of tarnished silver consisted mainly in removing the contaminated layer without noticeable alteration of the surface appearance, such as colour or brightness. This was succeed with low fluence and low repetition rate UV nanosecond pulses

Case 2. Laser cleaning of oiled silver blanks; successful cleaning with moderate fluence and low repetition rate UV pulses.

The industrial environment where the production of silver or silver alloy objects takes place, such as medical and electronic devices or coins, is prone to the contamination of the silver objects with machine oil lubricants. This organic film contamination not only alters the colour of the silver surface but mostly alter the properties of silver that indicate its use, like the high electrical conductivity and anti-bacteriological effect.

Cleaning the contaminated surface without modification of surface flatness, needed for a reflective optical surface or to minimize the impedance between electrical contacts was a challenge, mainly due to the fact that the thin organic film formed by the oily contamination was mostly transparent for visible and near visible radiation. Successful cleaning was achieved with moderate fluence and low repetition rate UV pulses.

Case 3. Laser cleaning of over-painted gold; successful cleaning with low energy near infrared femtosecond laser pulses.

Gold cannot be oxidized by oxygen, for ambient pressure and temperature range, even in much polluted environments.

Gold and gilded decorations are largely used in churches and religious ornaments. However during XIX century, several restoring campaigns overpainted the golden surfaces with a white layer, with the goal of covering damaged areas or just for a question of fashion.

Gold was cleaned by laser with low energy near infrared femtosecond laser pulses.

For each one of these practical situations where laser cleaning was studied and successful, that is, for each pair surface – contamination, a different laser cleaning mechanism is proposed and discussed, regarding the experimental applied parameters, and the assessment analysis of the cleaned surface.

Therefore, a systematic experimental study on laser cleaning of precious metals – silver and gold, was realized, in a diversified range of available wavelengths and temporal pulse duration including femtosecond pulsed lasers.

From this experimental study, three successful cases of laser cleaning of precious metals are here enhanced and described with more detail, being considered representative of also three different problems occurring in everyday life and each one associated to a different mechanism of laser cleaning.

PART I LASER CLEANING – MECHANISMS

"Through adjustments in the laser's color, pulse length and energy ... it often is possible to emphasize only one of (laser cleaning) interactions. Thus in a sense the laser may be "tuned" to produce a specific result" [1]

1. INTRODUCTION

Although invented almost half a century ago, developments concerning new laser media, new cavity and amplifier configurations and pulse shaping devices together with technological evolution of laser systems allowing better emission control and reliability, result in continuous innovation in scientific and industrial applications for matter manipulation and materials processing.

Laser cleaning, one of the laser applications that has seen considerable development in last decades, involves a large range of physical, chemical and quantum-mechanical phenomena that can occur in parallel or sequentially, resulting in many different laser cleaning mechanisms that are still the object of discussion and research.

Since Asmus' work, specific models for specific laser cleaning phenomena and mechanisms have been developed and published in the scientific literature.

In what follows a general overview of the published literature concerning the several basic phenomena and mechanisms associated with laser cleaning is presented, as well as the models that support the understanding of the phenomena involved.

2. PHENOMENA OF LASER - MATERIALS INTERACTION

When a laser beam, described as a coherent electro magnetic wave or a photon flux propagating in a confined region of space, hits or passes through a passive material, the material causes modifications in the laser beam, involving usually changes in the energy content, propagation direction, polarization and propagation speed. In addition, the energy of the beam causes modifications in the material, involving usually the

transformation of incident electromagnetic energy into kinetic excitation of free electrons, in metallic materials, or vibrational excitation of bonding electrons, in non-metals. These forms of electronic excitation are then randomised by collision processes and transformed in several other forms of energy, namely thermal energy.

The transformations of radiating energy (described either as electromagnetic or photonic energy) into other forms of energy are here designated as "Primary Phenomena" of laser interaction with materials. These primary phenomena include photo-thermal, photo-mechanical, photo-chemical, and photo-electrical energy transformations. The phenomena in which radiating energy does not change to other forms of energy, but just modifies its properties are also here considered and designated by optical phenomena.

The primary energy transformations, in turn, can induce other energy changes in the material media, such as thermo-chemical or thermo-mechanical. These physical phenomena, here designated by "Secondary Phenomena" are generally the ones responsible for laser cleaning, in some situations acting alone (only one of these phenomena in presence) but mostly often in conjunction or in cascade association.

In other situations however, the transformation of radiant energy in local electronic and lattice excitation is so fast that the radiation pulse ends before local thermal equilibrium is reached. This is the case of very short pulse laser interactions, in which material removal might occur by non-thermal phenomena.

2.1 Primary Phenomena

In what follows and whenever possible, this text will be kept in the domain of linear optical phenomena, those in which the relative change of optical radiation intensity interacting with the material is not dependent on the radiation intensity [23]. Being in this domain of linearity, the interaction of a more complex electromagnetic wave or light beam

with a material can be analysed as the superposition of waves or beams with specific and simpler characteristics.

Moreover, the optical, thermal and mechanical properties of the materials will be considered constant, for a given physical state of the irradiated material. In reality, the properties of materials change with temperature and pressure, physical entities that are obviously and desirably altered in the course of laser materials processing. However, the assumption of the constancy of the physical properties of the materials does not change the nature of the physical phenomena in presence and allows for a simpler analysis. In turn, the consideration of temperature and pressure dependent physical properties leads to much more complex mathematical relations that are beyond the scope of this work.

The term intensity, I, or more commonly used irradiance of an electromagnetic field is used meaning power density, that is, the average power carried by the incoming radiation crossing or incident on the unit area, A^*; it will denote also the equivalent concept of the average energy flux [23], E, per unit time, t, and unit area, A^*:

$$I = \frac{E}{A^* \Delta t} = \frac{P}{A^*} = \frac{n_{ph} h\upsilon}{A^* \Delta t} \qquad \text{(Eq. 1)}$$

this is, in an electromagnetic description, the radiant power density (P/A^*), or in a photonic description, the photon flux density (n_{ph} is the number of photons and $h\nu$ the energy of a single photon).

The physical quantity, E/A^* is generally named energy density or fluence. Considering the intensity of a laser beam, A^* is the area of or the beam cross section and Δt the irradiation time or pulse temporal length τ_p, if a single pulse is considered.

2.1.1 Optical Phenomena

When an electromagnetic wave or photon flux, such as a monochromatic light beam, is incident on an interface between two media, it will split at the surface, into a reflected beam, propagating in same media that the

incident one and a refracted beam interacting and transmitted to the second media. Reflected and transmitted beams will propagate further in directions that are distinct from each other, and also generally distinct from the propagation direction of the incident wave.

Snell's law [25] experimentally deduced, determines the relation between the propagation directions of the incident, reflected and refracted waves:

$$n_i \sin \Theta_i = n_i \sin \Theta_r = n_t \sin \Theta_t, \qquad \text{(Eq. 2)}$$

where n_i and n_t are the refractive index of the incidence and transmitting media, and Θ_i, Θ_r and Θ_t are the angles between the normal to the discontinuity surface at the incidence point and the propagation directions of the incident, reflected and transmitted waves.

The amplitude and phase of the reflected and transmitted waves at the interface between the two media, in the very usual situation of plane electromagnetic waves propagating in non magnetic isotropic media, can be related with the amplitude and phase of the incident wave using the Fresnel coefficients [25] for the perpendicular and parallel polarization components of the electromagnetic field.

$$r_\perp = \frac{n_i \cos\theta_i - n_t \cos\theta_t}{n_i \cos\theta_i + n_t \cos\theta_t} \qquad r_{//} = +\frac{n_t \cos\theta_i - n_i \cos\theta_t}{n_i \cos\theta_t + n_t \cos\theta_i} \qquad \text{(Eq. 3 a)}$$

$$t_\perp = +\frac{2n_i \cos\theta_i}{n_i \cos\theta_i + n_t \cos\theta_t} \qquad t_{//} = +\frac{2n_i \cos\theta_i}{n_i \cos\theta_t + n_t \cos\theta_i} \qquad \text{(Eq. 3 b)}$$

However, these coefficients are not very useful when studying materials processing by radiating energy, mostly because the instantaneous values of amplitude and phase of electromagnetic waves are changing in a very short temporal range and also because it is more convenient to consider the optical phenomena occurring in material objects with finite thickness, and not just at discontinuity interfaces between two media.

More useful parameters to describe the average energy content of the reflected or refracted wave, in relation with the average energy content of the incident wave, are the reflectance (R), transmittance (T) and absorbance (A), parameters that describe the macro optical properties of

each material, and are dependent on the incidence angle and wavelength.

These optical parameters are defined as ratios between the power carried by the electromagnetic wave, being the power density or irradiance the time average of the Poynting vector, over one complete period of the wave. Therefore, the optical parameters can be defined by the expressions [25]:

$$R = \frac{P_r}{P_i} \qquad T = \frac{P_t}{P_i} \qquad A = \frac{P_a}{P_i} \qquad \text{(Eq. 4)}$$

where P_i, P_r, P_t and P_a are the radiant power respectively incident on, reflected by, transmitted through or absorbed into the material object (Fig. 1).

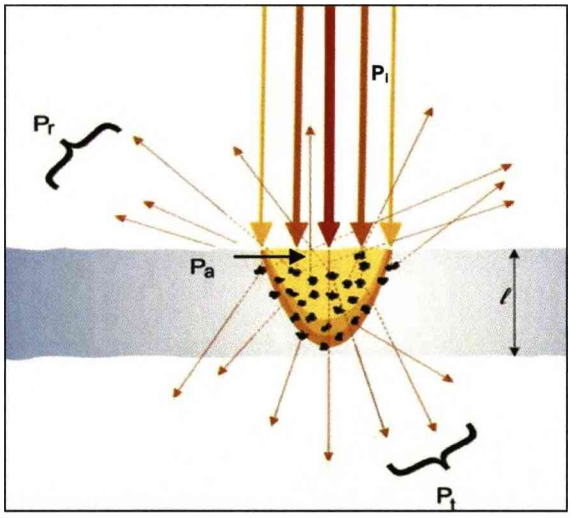

Fig. 1. Optical phenomena in material objects with finite thickness (ℓ)

- reflection, transmission and absorption

Moreover, in agreement with energy conservation:

$$P_r + P_t + P_a = P_i \Rightarrow R + T + A = 1 \qquad \text{(Eq. 5)}$$

Although reflection is a surface phenomenon, very much dependent on surface conditions, absorption and transmission take place along the thickness of the material object. In order to describe their evolution, along the propagation path (ℓ), an absorption (more exactly attenuation) coefficient α, is defined as [23]:

$$\alpha = -\frac{1}{I}\frac{dI}{d\ell} \quad \Leftrightarrow \quad I(\ell) = I_i \cdot e^{-\alpha\ell} \quad \Leftrightarrow \quad T = e^{-\alpha\ell} \qquad \text{(Eq. 6)}$$

the above equivalences being valid in media that are linear and homogeneous and for which the attenuation by scattering is insignificant. The second relation is the Beer-Lambert's law, and the third is Bouger law.

Related with energy absorption and with the absorption coefficient, another useful parameter can be defined, the optical penetration depth or optical absorption length $L_\alpha = 1/\alpha$, meaning the length over which the incident optical energy is attenuated by the factor $1/e$.

The absorption coefficient, α, is dependent on the incident radiation wavelength, λ, as well as on the optical properties of the absorbing material, according the relation [23]:

$$\alpha = \frac{4\pi\ k}{\lambda} \qquad \text{(Eq. 7)}$$

where k is the imaginary term of the complex refractive index of the material.

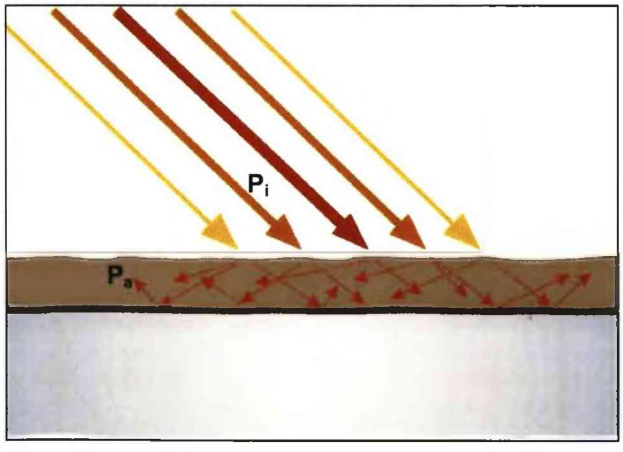

Fig. 2. Optical phenomena-multiple diffuse reflections in the contamination layer

Although not very common in laser cleaning, it might happen that the refractive index of the contamination layer is much higher than the refractive index of the adjacent material. In this case, the partial reflection of the incident laser power (P_i) occurring at the contamination-

substrate boundary is not negligible and multiple internal reflections in the contamination layer are possible, increasing the optical path (ℓ) inside the material (Figure 2), increasing the absorbed laser power (P_a) and decreasing the transmission to the substrate [26].

The importance of these optical parameters in laser cleaning is that they can provide useful information about laser wavelength and power levels that would be more efficient in removing a contamination from a material surface. The penetration depth can be an especially meaningful parameter in laser cleaning, because it allows the modulation of the laser energy as a surface or volume heat source where the laser energy is absorbed.

Pasquet *et al* [27-28] have shown the importance of the optical properties of the contamination for the quality of the laser cleaning process.

Using ferrous materials having different type of corrosion with differentiated absorbance properties in respect to the different laser wavelengths used, it was observed that when the corrosion absorbance to the incident wavelength was high – for example, a Fe_3O_4 corrosion layer on iron irradiated with a Nd:YAG laser at 1064 nm, the corrosion layer melted but was not removed from the substrate; when the corrosion absorbance to the incident wavelength was low – for example, a Cr_2O_3 corrosion layer on steel, irradiated with the same wavelength, the removal of the oxide layer was total in the irradiated area.

Pasquet *et al* [29] have also shown that the alteration of the optical properties of corrosion layers, due to electrochemical confinement, could lead to clear improvements in laser cleaning of corroded ferrous metals.

Autric et Oltra [30], considering the experimental results and microscope observations, proposed two different physical processes for laser cleaning of oxidized metals; for transparent oxide layers, a thermo-mechanical process consisting of thermal expansion and shear stress (buckling) is proposed, while for absorbing oxides the removal is due to selective ablation by vaporization.

2.1.2 Photo-Thermal Phenomena

Part of the laser energy flux, incident in a material object is transmitted across the object surface and is absorbed through the material. Two opposite situations can be given as example (Fig. 3): in opaque materials this energy is absorbed in a very thin layer at the surface, that is, the optical penetration depth (L_α) is much smaller than the object thickness. For transparent objects, having an absorption length that is much larger than the object thickness, most of the incident energy is transmitted through the thickness of the object and the energy absorbed across the material is insignificant.

However, absorbed at the surface or through the object, the electromagnetic energy results in an increase in the energy of the particles. This increase of energy is locally randomized through elastic collisions and in the case of non-radiative energy transitions, is transferred to phonons by inelastic collisions and thermal energy by the increase of lattice vibrational energy.

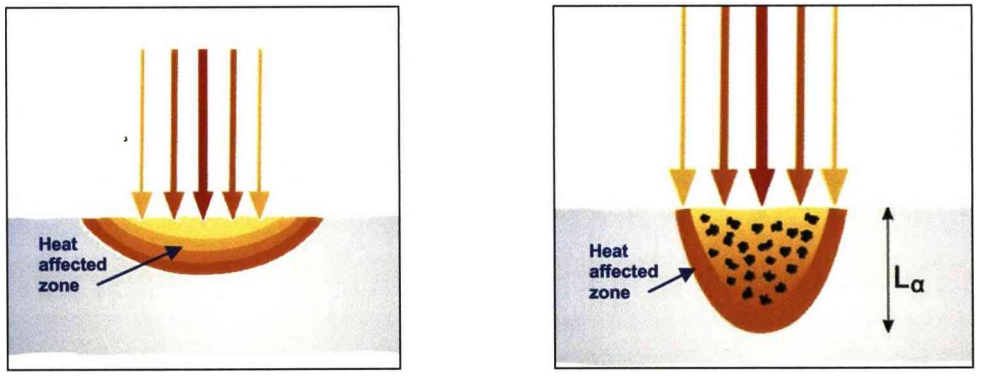

Fig. 3. Laser energy absorption:
surface absorption (left) and volume absorption (right)

The thermal energy or heat, originates a local increase of temperature (ΔT), and heat transfer to the surrounding material by conduction and to the removed material (contamination) by convection (Figure 4); the heat re-radiated by the object itself is not considered here because it is usually negligible in laser processing and cleaning

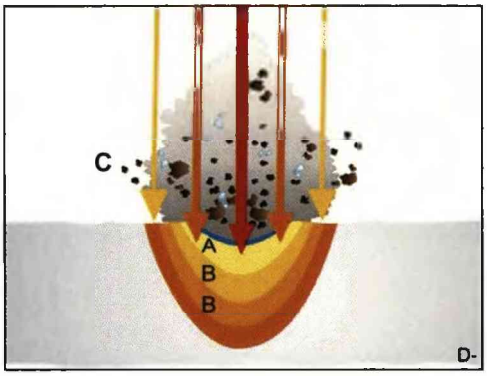

Fig. 4. Photo-thermal phenomena
A – Laser absorbing zone = volume heat source, $T_A = T_0 + \Delta T$
B – Heat conduction zone, $T_0 < T_B < T_A$
C – Heat convection zone, vapour, liquid droplets and particles
D – Non affected zone, $T = T_0$

The temperature changes at some point of the heated volume of the irradiated material depend on the thermal properties of the material, and for isotropic and homogeneous materials can be expressed in terms of the heat flux (Q), by the heat transfer equation [31]:

$$Q = \rho c_m \frac{\partial T}{\partial t} - K\nabla^2 T - \rho c_m v \nabla T, \qquad \text{(Eq. 8)}$$

where $K/\kappa = \rho c_m$.

In equation 8, the left side accounts for the heat source (Figure 4). The right side terms account respectively for the local temperature change, the heat lost by conduction, and the heat lost by a convection fluid moving out at speed v.

A. *Considerations regarding the heat source*

When the heat source is the laser energy absorbed by the object, the volumetric density of the absorbed laser power P_i; can replace the heat flux Q, in the heat transfer equation (equation 8) and so:

$$\frac{AP_i}{V} = \rho c_m \frac{\partial T}{\partial t} - K\nabla^2 T - \rho c_m v \nabla T \qquad \text{(Eq. 9 a)}$$

for superficial absorbing materials (opaque) or, for materials with significant optical penetration depth (semi transparent) with surface reflectance R and bulk attenuation coefficient α:

$$(1-R)\ \alpha\ I_i e^{-\alpha z} = \rho c_m \frac{\partial T}{\partial t} - K\nabla^2 T - \rho c_m v \nabla T \qquad \text{(Eq. 9 b)}$$

In these equations, K represents the thermal conductivity, κ the thermal diffusivity, c_m the specific heat, ρ the density of the material and V the volume of the laser affected zone.

Also in the above equation, it is assumed that the laser absorbed radiation is instantaneously transformed into heat, $H = A.E_i$, in spite of H being time dependent as well as E throughout the pulse temporal profile. However, local thermal equilibrium is achieved in a range of a few picoseconds, that is much shorter that the typical nanosecond pulse length used for laser cleaning (5-50 ns), and other thermal phenomena on the material (few microseconds). Therefore, this simplification is justified.

B. *Considerations regarding the substrate layers*

Although the optical and thermal parameters of each material generally modify with temperature increase, the alteration is abrupt in the case of physical change of state in the absorbing material that might be the contamination layer or the underlying substrate in the case of laser cleaning.

Moreover, in most laser cleaning processes, the convection heat is carried out by the removed material, in the vapour or solid state and seldom in the liquid state (Figure 3). So the heat transfer equation must be distinctly written for the liquid and the solid phases [32] of the absorbing layer(s):

$$Q_l = \rho_l c_{ml} \frac{\partial T}{\partial t} - K_l \nabla^2 T - \rho_v c_{mv} v_v \nabla T \qquad \text{(Eq. 10 a)}$$

and

$$Q_s = \rho_s c_{ms} \frac{\partial T}{\partial t} - K_s \nabla^2 T \qquad \text{(Eq. 10 b)}$$

where the subscripts were added to the parameter symbols, to refer to the solid state (*s*), the liquid (*l*) and the vapour (*v*) and the heat flux, *Q* is:

$$Q = \frac{AP_i}{V}$$ for superficial absorbers (Eq. 11 a)

or

$$Q = (1 - R)\ \alpha I_i e^{(-\alpha z)}$$ for volume absorbers (Eq. 11 b)

In this situation where several layers in different physical states (solid, liquid, vapour) are present, special attention is required concerning the definition and calculation of the heat source (Fig 5), affecting each layer possessing different optical and thermal parameters characteristic for each physical state (Eq. 12 a, b). Moreover, the instantaneous position and progressing speed of the vapour-liquid (v_l) and the liquid-solid interfaces (v_s) [32] must also be taken in consideration.

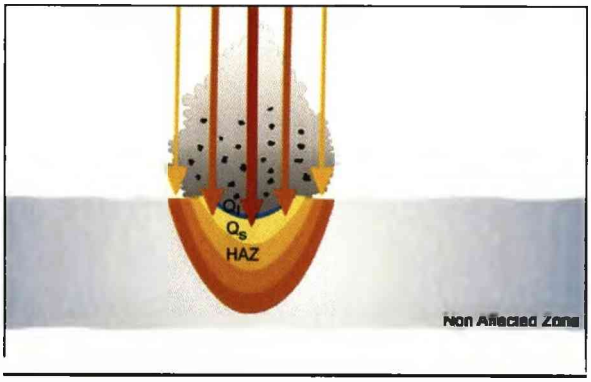

Fig. 5. Laser heat source in a multi-phase system
Q_l – heat source due to laser absorption in the liquid layer
Q_s –heat source due to laser transmitted to the solid layer

In the absence of a plasma cloud and with moderate vapour production rate, the heat source in the liquid phase, Q_l, is mainly due to the absorbed laser energy, through the liquid interface. However, the heat source in the solid phase, Q_s, is due to the thermal conduction from the liquid layer, added to the absorbed laser power at the liquid-solid interface, if the optical penetration depth in the liquid phase is larger than the liquid layer thickness:

$$Q_l = (1 - R_l)\ \alpha_l I_{il} e^{(-\alpha z)} = T_v (1 - R_l)\ \alpha_l I_i e^{(-\alpha z)}$$ (Eq. 12 a)

and, considering the solid material to be a superficial absorber

$$Q_s = \frac{T_v T_l A_s P_i}{V_s} \exp\left[-\left(\frac{z-\ell_l}{\sqrt{2\kappa t}}\right)\right] \qquad \text{(Eq. 12 b)}$$

where ℓ_l is the thickness of the liquid layer, and the subscripts *s, l, v,* are concerning the solid liquid and vapour phases.

C. Considerations regarding the heat losses

Considering again equation 8, there are explicit two processes of heat loss; the first one due to thermal conduction ($K\nabla^2 T$), and a second one due to the convection by the removed material ($\rho c_m v\nabla T$).

In the cases where one of these processes is clearly dominant and the other one might be neglected, equation 8 is simplified:

- for processes mainly thermal, without meaningful loss of material:

$$Q = \rho c_m \frac{\partial T}{\partial t} - K\nabla^2 T, \qquad \text{(Eq. 13 a)}$$

- and

$$Q = \rho c_m \frac{\partial T}{\partial t} - \rho c_m v\nabla T = \rho c_m \frac{\partial T}{\partial t} - \rho \frac{\Delta H}{\Delta t} \qquad \text{(Eq. 13 b)}$$

for processes for which thermal dissipation can be neglected and material removal is dominant, such as ablation, cold ablation or spallation, where ΔH is the enthalpy of the removal phenomena and Δt the time interval for laser irradiation.

D. Particular solutions of the heat transfer equation

The manipulation of the heat transfer equation in the general form requires the use of numerical methods, but several simplifying assumptions might be done. H. S. Carslaw and J. C. Jaeger [33] have

assumed a set of different object geometries, such as infinite and semi-infinite solid, plane plate, rod, parallelepiped, sphere and cone, in order to devise possible solutions for the referred equation. J. F: Ready [34] based on the work of Carslaw and Jaeger considered a laser beam as the heat source; again several simplifying assumptions were made concerning the energy distribution in the laser beam, uniform, gaussian, "top hat", and the relative dimensions of the beam transversal section and the considered object, such as point source or extended source. Later, Ready and W. W. Duley [35, 36] have applied the developed solutions to different aspects of laser materials processing.

A set of solutions of the above equation that can be found in several referred books, will be presented next, in very simplified situations but very useful in many practical laser applications including laser cleaning. Unless stated otherwise the following situation is considered- a uniform and constant intensity laser beam heating an homogeneous material, with no convection or radiation losses, nor phase changes in the material.

CW laser irradiation of opaque or surface absorbing materials

The temperature increase in the irradiated material is a function of the position of the considered point with respect to the absorbing surface and the irradiation time. During the irradiation time or pulse length, the temperature increase in the material is [37]:

$$\Delta T(z,t) = \frac{AI_i}{K}\left[\sqrt{4\kappa t}\cdot ierfc\left(\frac{z}{\sqrt{4\kappa t}}\right)\right] \qquad \text{(Eq. 14)}$$

and, at the absorbing surface [38]:

$$\Delta T(0,t) = \frac{AI_i}{K}\sqrt{4\kappa t/\pi} \qquad \text{(Eq. 14 a)}$$

where I_i, is the incident irradiance, F_i, the incident fluence and *ierfc* is the "integral of the complimentary error function".

CW laser irradiation of semi-transparent or volume absorbing materials

In the case of less absorbing or semi-transparent materials with very low thermal conduction, the laser energy is absorbed in an homogeneous volume, and for short irradiation times the temperature distribution follows the optical distribution, so [39]:

$$\Delta T(z,t) = \frac{1}{\rho c_m} \frac{(1-R)F_i}{L_\alpha} e^{-z/L_\alpha} \qquad \text{(Eq. 15)}$$

and, at the absorbing surface

$$\Delta T(0,t) = \frac{1}{\rho c_m} \frac{(1-R)F_i}{L_\alpha} \qquad \text{(Eq. 16)}$$

where R is the surface reflectance, F_i is the fluence incident at the surface and L_α is the optical penetration depth of laser radiation in the material; in this equation conduction losses were neglected and it was considered that the optical absorption length, L_α, is smaller than the contamination thickness.

CW laser irradiation of a two layers object

The practical situation in most cases of laser cleaning is that there is a more or less uniform contamination layer, covering the underlying material, each one with its own optical and thermal properties and parameters.

If the contamination layer has a high absorption coefficient α_c to the incident laser radiation wavelength, that is, if the laser energy is mainly absorbed at the contamination surface and also the optical penetration depth is smaller than the laser spot size in the contamination surface, a solution of the laser generated heat transfer equation for the contamination layer might be written [36]

$$T_c(z,t) = \frac{I_{ac}}{K_c}\sqrt{4\kappa_c t}\sum_{n=-\infty}^{\infty}\zeta^{|n|}\,ierfc\left[\frac{|z-2n\ell|}{\sqrt{4\kappa_c t}}\right] \qquad \text{(Eq. 17. a)}$$

and for the underlying substrate:

$$T_u(z-\ell,t) = 2\frac{I_{ac}}{K_u}\sqrt{\frac{4\kappa_u t}{\pi}}\zeta'\sum_{n=0}^{\infty}\pi^{1/2}\zeta^n\,ierfc\left[\frac{z-\ell}{\sqrt{4\kappa_u t}}+\frac{(2n+1)\ell}{\sqrt{4\kappa_u t}}\right] \qquad \text{(Eq. 17. b)}$$

where:

$$\zeta = \frac{K_c\sqrt{\kappa_u}-K_u\sqrt{\kappa_c}}{K_c\sqrt{\kappa_u}+K_u\sqrt{\kappa_c}} \text{ and } \zeta' = \frac{K_u\sqrt{\kappa_c}}{K_c\sqrt{\kappa_u}+K_u\sqrt{\kappa_c}}$$

with ℓ, the contamination thickness, *c* the subscript for contamination parameters and *u* the subscript for the parameters of the underneath substrate.

A perfect thermal contact between contamination layer and underneath material is assumed, so $T_c(\ell, t) = T_u(z-\ell, t)$, at contamination – substrate interface for any *t*.

Repeated pulse laser irradiation

In most cases, laser cleaning is performed with pulsed laser systems, at a variety of pulse length (τ_p) ranges and repetition rates [39, 40, 41, 42].

During a single laser pulse, the local temperature increase for opaque (a) and semi-transparent materials (b) is:

$$\Delta T(z,t) = \frac{I_a}{K}\left[\sqrt{4\kappa t}\cdot ierfc\left(\frac{z}{\sqrt{4\kappa t}}\right)\right],\ t<\tau_p \qquad \text{(Eq. 18. a)}$$

and

$$\Delta T(z,t) = \frac{1}{\rho c_m}\frac{(1-R)F_i}{L_\alpha}e^{-z/L_\alpha},\ t<\tau_p \qquad \text{(Eq. 18. b)}$$

and

$$\Delta T(z,t) = \frac{I_a}{K}\left[\sqrt{4\kappa t}\cdot ierfc\left(\frac{z}{\sqrt{4\kappa t}}\right) - \sqrt{4\kappa(t-\tau_p)}\ ierfc\left(\frac{z}{\sqrt{4\kappa(t-\tau_{p)}}}\right)\right],\ t>\tau_p$$

(Eq. 18. c)

For repetitively pulsed lasers incident upon semi-transparent materials with reduced thermal diffusion, the temperature increase is due to optical absorption as well as thermal conduction after each pulse [39]:

$$\Delta T(0,t) = \frac{1}{\rho c_m}\frac{(1-R)F_i}{L_\alpha}\left(1+\sqrt{\frac{\pi L_\alpha d_\sigma f_p}{4\kappa}}\right),\ \text{if } L_\alpha >> \delta \qquad \text{(Eq. 19)}$$

where L_α is the optical penetration depth, δ is the thermal penetration depth, d_σ is the beam spot diameter on the surface and f_p is the pulse repetition rate.

This and other solutions of the heat transfer equation allow the calculation, for example, of the actual temperature in some point of the material object at some moment in time, or the temporal evolution of the temperature of a point or a surface, or isothermal propagation in the laser irradiated material, or the maximum temperature achieved at the material surface after a laser pulse.

2.1.3 Photo-Mechanical Phenomena

Most of the phenomena designated by "photo-mechanical", in the reviewed literature, refer in fact to mechanical processes such as generation of pressure or stress, acoustic or shock waves, resulting from material thermal expansion and displacement due to local temperature increase after laser energy absorption. Therefore, these phenomena are not indeed primary photo-mechanical phenomena but photo-thermo-mechanical phenomena, and will be considered in the aim of secondary phenomena of laser materials interaction.

The "Photo-Acoustic" or "Opto-Acoustic" effect, discovered by A. G: Bell (1880), when referred to solid materials, is also a photo-thermal-acoustic

phenomenon, arising in consequence of the thermal expansion generated by the absorption of the electro magnetic energy flux in the material object.

However the laser photons incident on a material surface have specific quantum mechanical properties which can induce directly mechanical effects [31], independent of temperature increase, due to the photon momentum and pressure.

The basic equations for quantification of photonic pressure are:

- Energy of a photon (Plank's Law):

$$E_{ph} = h\upsilon \qquad \text{(Eq. 20)}$$

- Momentum of a photon, using Einstein equivalence:

$$p_{ph} = h\upsilon / c = h / \lambda \qquad \text{(Eq. 21)}$$

Therefore, the total photon pressure of a laser beam, $p_{r\ beam}$, on the surface [31] is:

$$p_{r\ beam} = \frac{P_{beam} / c}{\pi\ d_{\sigma}^{2} / 4} \qquad \text{(Eq. 22)}$$

where h is the Planck constant, $\nu = c/\lambda$, the photon oscillation frequency, c, the speed of light, P_{beam}, the incident laser beam power and d_{σ} the beam diameter on the surface, that is the diameter of the area directly irradiated by the incident laser beam.

Although the force exerted on the surface by the incoming photon beam is negligible when compared with the adhesion forces in a laser cleaning process, the existence of this force must be taken in consideration when analysing the dependence of the cleaning efficiency with the beam incidence angle.

2.1.4 Photo-Chemical Phenomena

Photo-chemical primary phenomena is due to the absorption of laser photons, resulting in excited states of present species, or bond breaking (dissociation) of molecules, with energies matching the bonding energies of the absorbing media.

Photo-chemical processing of materials by laser includes different aspects such as photodissociation, isotope separation, or laser induced or enhanced chemical reactions.

In laser cleaning, the photo-chemical phenomena mostly found are chemical dissociation, also called laser ablation, cold ablation or non-thermal ablation. These designations arose because the breaking of the chemical bonds causes strong expansion forces releasing the dissociation products, and the increase of thermal energy of the processed material is usually of minor importance.

The general laser induced photo-chemical dissociation can be described [43], in a simplified way, by:

$$AB + M + h\nu = A+B + M$$

or

$$AB + h\nu_1 = (AB)^* \qquad \text{and} \qquad h\nu_2 + (AB)^* = A + B$$

where *AB* is a molecule, *AB** the excited molecule, *M* the environmental media, and *A* and *B* the particles, atoms or ions resulting from the photo induced chemical reaction.

In principle, photo-chemical dissociation, also named photolysis, can occur whenever the energy of a single photon matches the bonding energy of the chemical components of the irradiated material, regardless the irradiance of the absorbed energy flux (multi photon processes not considered here). The intensity of the laser beam will determine the amount of material being processed.

However very often, complex molecules have several different bonds of different energies holding the molecular components of the contaminant

material together as well as to the original surface; but very often too, several of these bonds have dissociation energies with approximate values, so photo molecular dissociation can follow different "routes", even when using the same laser wavelength, originating different dissociation products.

The graphic below depicts the energy of 1 photon of each different laser source, comparing them with some values of covalent bonds.

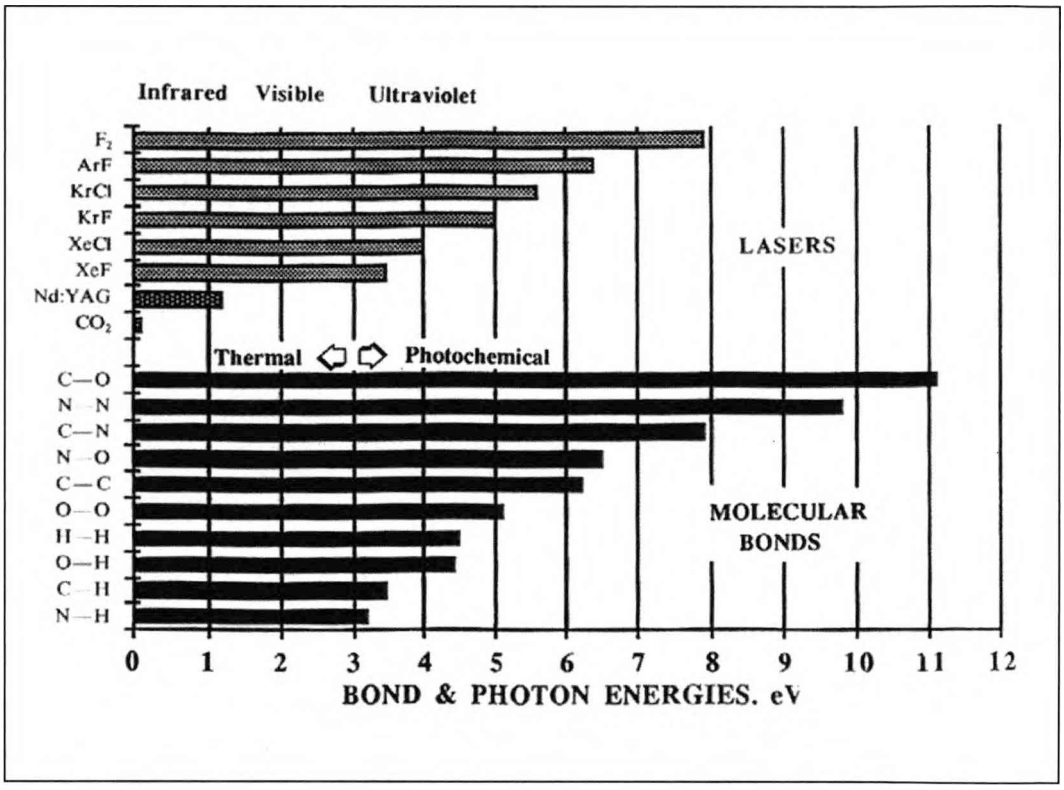

(from Gower, M C; "Excimer Lasers: Current and Future Applications in Industry and Medicine", in "*Laser Processing in Manufacturing*", p. 190)

To study the interaction phenomena and resultant chemical dissociation, Fotakis *et al* [44] used laser-induced fluorescence analysis of the laser irradiated area. They found that the spectrum of the emitting species was broadening towards the visible as long as the number of incident pulses was increasing, and this broadening was more pronounced for laser pulsed irradiation at 248 nm than at 193 nm.

These modifications on the registered spectra were considered indicative of the presence of new products resulting from enhanced reactivity and mobility of the species present in the irradiated material.

Although usually of minor importance, thermal effects usually accompany photo-chemical phenomena, because the quantum efficiency of photo-chemical phenomena is less than unity; the remainder energy may be conducted to the surrounding material and transformed into heat. The relative importance of the photo-thermal phenomena depends on the wavelength of the incident energy flux and increases with increasing irradiation time or pulse length.

2.1.5 Photo-Electrical

Generally speaking photoelectrical effects are those in which the electrical properties of the irradiated material are changed due to the light or laser irradiation.

The photoelectrical effect is mainly associated with the release of electrons, named photoelectrons, from a solid surface irradiated by laser. Yet, this effect is only observed with very short pulses (pico or femtosecond pulses) [43], and not very often used in laser cleaning.

However, the optical breakdown of the air or other dielectric media at ambient temperature, in the waist of a high power focused laser beam might also be considered a photoelectrical effect, and this optical breakdown or photo-ionization of the air is a physical phenomenon that has been used for laser cleaning [45].

The high intensity electric field of the laser pulse can cause photoionization of the air or other surrounding media, releasing free electrons and generating a localized plasma, via avalanche ionization or multi-photon absorption [23, 45]. The avalanche ionization and the multi-photon absorption can be expressed as a reaction respectively according to:

$(M + h\nu) + e^- \rightarrow M^* + e^- \rightarrow M^+ + 2e^-$ and $M + n\, h\nu \rightarrow M^+ + e^-$

where M is a neutral molecule, M^* the excited molecule and M^+ the ionized molecule of the media, $h\nu$ the laser photon energy and e^- a free electron.

Dense plasma still absorbs the laser pulse radiation, becoming increasingly hot and expanding very fast, leading to a blast wave with a shock front.

The propagation of the shock wavefront can be described by the Sedov Taylor equation:

$$r \approx \left(\frac{E_{pl}}{\rho_0} \right)^{1/(2+n)} t^{2/82+n)} \qquad \text{(Eq. 23)}$$

where r is the radius of the wavefront, E_{pl} the fraction of laser energy coupled into the plasma plume, ρ_0 the density of the gas media (usually air), t the time of propagation, and n a small integer dependent of the frontwave propagation regime.

Lee *et al.*[4] presented also an analysis and experimental measurements of the propagation of a shock wavefront assuming spherical expansion. Here, the shock wave is generated in a thin water layer in consequence of explosive vaporization after laser irradiation.

In general, the avalanche ionization, growing with the wavelength, is more efficient in the infrared, while the multiphoton absorption, requiring more energetic photons, is dominant in the visible and ultraviolet range.

2.2 Secondary Phenomena

Under this topic several phenomena taking place in laser cleaning processes can be mentioned, most of them driven by thermalization, that is, the temperature increase in the absorbing material, such as thermo-chemical and the most often mentioned the thermo-mechanical phenomena.

Once a material volume is irradiated by laser energy, its energy content will increase dependent on the laser intensity, the surface conditions and the optical properties of the material.

In photothermal phenomena, the absorbed laser radiation is transmitted to the lattice in the form of heat, increasing the temperature of the absorbing volume as well as that of the neighbouring material, mainly by conduction but also by convection and radiation.

The temperature increase of the heated material (which in laser cleaning might be the contaminant, substrate, assistance fluid, or other surrounding media) will result in thermodynamic effects, such as expansion of the material, phase change from solid to liquid or vapour and the formation of a more or less dense plasma.

In any case an expansion of the heated material will occur, resulting in strain and stress exerted in one or many of the materials and phases in contact. This stress can be transient and generates an elastic response of the material within a certain set of conditions, but can also generate shock or blast waves travelling in the solid material (substrate, contamination) or in the surrounding media, usually the air.

The temperature increase due to laser absorption can also lead to chemical decomposition, combustion or other transformations in the heated material, breaking and releasing molecules of the contaminant.

2.2.1 Transient Heating

In the thermoelastic regime, a short laser pulse incident on the absorptive surface, either the contamination surface or the substrate surface, results in the process of transient heating without phase change, thermoelastic expansion and subsequent contraction of a restricted volume. The expansion and contraction of the heated volume within the thermoelastic regime might be expressed as a surface displacement with associated acceleration, causing also displacement of surface adherent particles or films.

The constrained localized volume expansion and contraction causes also pressure on adjacent material creating a stresspulse that propagates on the object surface and into the substrate and contamination layer. The stress pulse is reflected back and forth at the free boundary.

Repetitive laser pulses with short duration (nano or picosecond) might generate thermoelastic stress waves with enough magnitude to lead to acoustic waves propagating into the material and surrounding media [40]. This effect is usually known as photo-acoustical or opto-acoustic effect.

A simplified 1D model, for an absorbing, free and solid surface irradiated by a uniform laser pulse, will take in account the local surface temperature increase, ΔT (equation 13 and 14), and normal expansion amplitude $\Delta\ell$, for absorbing surfaces (a) or semi-transparent substrates (b):

$$\Delta \mathrm{T}(0,t) = \frac{1}{\rho c_m} \frac{AF_i}{\sqrt{4kt}} \qquad \text{(Eq. 24 a)}$$

or

$$\Delta \mathrm{T}(0,t) = \frac{1}{\rho c_m} (1-R) F_i \frac{e^{\alpha \ell}}{\sqrt{4\kappa t}} \qquad \text{(Eq. 24 b)}$$

and:

$$\Delta \ell(t) = \beta \ \delta \ \Delta \mathrm{T}(0,t) \qquad \text{(Eq. 24 c)}$$

where β is the linear thermal expansion coefficient and δ the thermal diffusion length.

According to Tam *et al* [46], and Lu *et al* [47], this thermal expansion, although minimal, can induce strong acceleration on the particle or substrate surface during short laser pulse irradiation, resulting in the ejection of small particles (Figure 6).

The transient force per unit area applied to a particle or film layer adjacent on the substrate surface is [47]:

$$p_r(t) = \beta \ Y \ \Delta \mathrm{T}(0,t) \qquad \text{(Eq. 25)}$$

where Y is the Young modulus of the absorbing material (either particle or substrate).

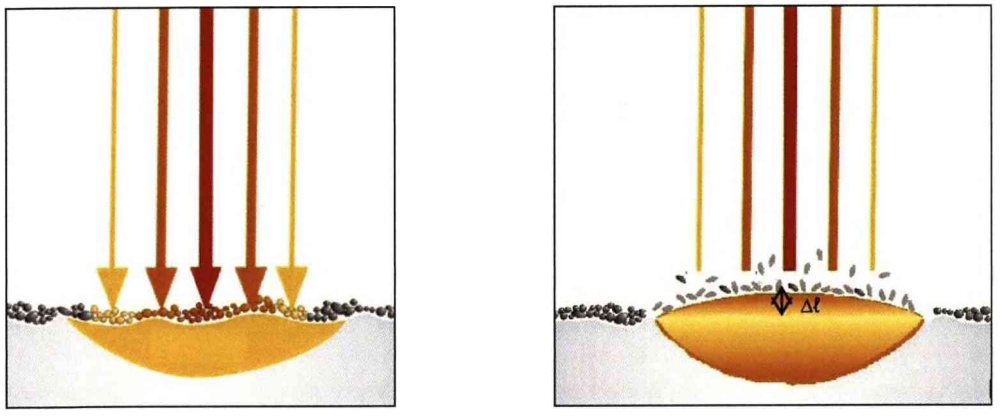

Fig. 6. Particle removal due to substrate expansion

The thermal expansion and subsequent contraction of the heated volume are in fact a straining of the heated material ε, causing compressive or tensile stress σ, in the restrained adjacent solid material (Figure 7).

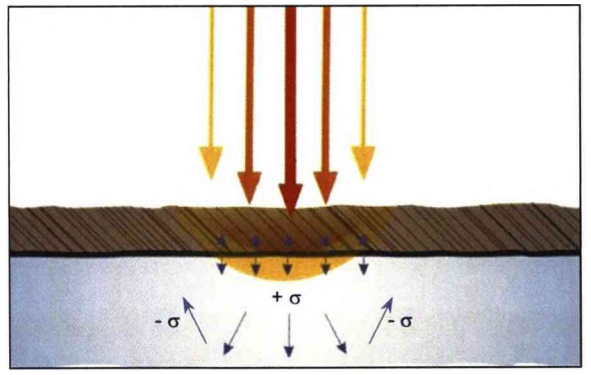

Fig. 7. Thermal stress propagation
after laser thermalization and expansion

If the material is isotropic and there are no other significant stresses to be considered, the thermo-elastic stress can be expressed according the following expression, simplified for one-dimensional expansion:

$$\sigma(t) = \frac{Y}{(1-2\vartheta)}\ \varepsilon\ (t) = \frac{Y}{(1-2\vartheta)}\ \beta\ \Delta T(t) \qquad \text{(Eq. 26)}$$

where Y is the elasticity or young modulus of the material, $\varepsilon = \Delta\ell/\ell$ the thermal expansion strain and ϑ the Poisson ratio.

The thermoelastic stress pulse or acoustic wave propagates with exponential attenuation according to:

$$\frac{\partial^2 \ell}{\partial t^2} = v^2 \frac{\partial^2 \ell}{\partial z^2} - \beta \frac{\partial T}{\partial z} \qquad \text{(Eq. 27)}$$

and at the material (contamination or underneath substrate) interface with the surrounding media, it is reflected with an acoustic reflection coefficient :

$$R_{ac} = \frac{\rho_2 v_2 - \rho_1 v_1}{\rho_2 v_2 + \rho_1 v_1} \qquad \text{(Eq. 28)}$$

where ρ is the material density, v is the speed of sound into the material and 1 and 2 are subscripts related with material where the back or forward pulse propagation takes place.

At a solid or liquid to air interface the acoustic reflection coefficient, $R_{ac} \approx -1$, because the acoustic air impedance is usually much lower than that of the contamination, substrate or liquid film. This fact implies that a compressive stress wave locally originated by thermal expansion will reflect at the air interface, becoming a tensile stress wave.

Kane, Arnold, Luk'Yanchuk, Pleasants *et al* [48, 49, 50, 51], have developed more complex models, taking in consideration phenomena such as true pulse shape and energy distribution on the substrate as well as particle deformation and dynamic effects to explain the removal of small particles from solid substrates by laser irradiation.

Hsu and Lin [52] have numerically simulated laser generated thermoelastic stress waves with commercially available FEM software. Using this model for the study and comparison of temperature distribution, surface displacement and acceleration, they concluded that the surface displacement acceleration increases with the increase of pulse energy and the decrease of the beam spot size.

Bloisi *et al* [53, 54] developed also a specific model for the expansion of a contaminated surface when the opposite object face was irradiated by a pulsed laser – "verso laser cleaning" - to determine the threshold conditions for effective cleaning and object thickness.

2.2.2 Thermal Phase Change

Longer laser pulses with higher energy content but lower peak power can cause on the absorbing surface, the contamination or the substrate surface, phase changes such as vaporization that can occur without plasma formation [38, 40] or in the presence of weakly absorbing plasma having low electronic density.

Evaporation pressure is applied for laser cleaning if associated with a meaningful vaporization of the irradiated surface, and in the absence of an optically thick plasma formation. In this mechanism, momentum transfer from the vapour to the solid surface would produce a recoil pressure, responsible for the removal of the contamination.

The propagation of the vapour front, that is, the interface between the expanding vapour and the ambient gas, will produce a recoil pressure on the absorbing surface that might lead to material removal.

The pressure p_s on the solid surface can be related with the laser incident energy I_i, via a coupling coefficient, χ_m, such as [55]:

$$p_s = \chi_m I_i \qquad \text{(Eq. 29)}$$

2.2.3 Thermo-Dynamic Effect

If a short laser pulse is focused on a solid target generating high intensity irradiation, physical state changes are observed associated with regular or explosive liquid or vapour material ejection, as well as vapour and plasma in fast expansion [40]. The evaporated material from the contamination, substrate or assistance fluid, and generated plasma

expansion cause intense impact pressure on the material surface originating shock or blast waves propagating in the surrounding media.

The initial impact pressure is built up by the volumetric gain of particles during the transition from the condensed to the vapour state and further by the volumetric expansion of the vapour and plasma due to absorption and thermalization of the incident laser radiation [56].

Due to the high values of laser irradiance incident upon the absorbing surface a fast vaporization occurs. Accompanying the high rate of vapour production at the target surface, vapour ionization takes place due to further absorption of laser radiation, generating an intense plasma plume, also absorbing the incident laser radiation and generating a shock wavefront expanding at supersonic speed [40].

Aden *et al* [56] measured experimentally the evolution of the blast wave and made simulation of this blast wave in order to make clear the role each physical phenomenon: the volumetric thermal expansion of the evaporating material and the detonation dynamics of the laser absorbing plasma. They concluded that, although both processes contribute and may occur simultaneously during the removal of material, the "piston" effect of fast evaporation dominates for lower power densities or reduced absorptivity and the "detonation" effect due to the energy absorption and fast expansion of the plasma, is predominant for high absorption and high incident power densities.

In the detonation effect, the shock wavefront, that is a pressure discontinuity between the hot and dense plasma and the non-affected surrounding fluid, expands and propagates away with supersonic speed.

Siano and Pini [57] assuming also the model of the detonation wave for very high laser intensities, referred the mathematical expressions describing the parameters of the shock wavefront propagation, such as front propagation radius (r_f) and speed (v_f), pressure (p_f), as well as the pressure (p_{surf}) and momentum (M) on the absorbing surface:

$$v_d = \left[2 \frac{\left(\gamma^2 - 1\right) I_d}{\rho_0} \right]^{1/3} \qquad \text{(Eq. 30)}$$

$$r_f = v_f . t \,,\; t_0 < t \leq \tau_d \qquad r_f = v_f \;\; f\left(\tau_d, t\right),\; t > \tau_d \qquad \text{(Eq. 31)}$$

$$p_f = \frac{\rho_0}{\gamma + 1} v_f^2 \qquad p_{surf} = \left(\frac{\gamma + 1}{2\gamma} \right)^{2\gamma/(\gamma-1)} p_f \qquad \text{(Eq. 32)}$$

$$M = \int_0^{\infty} p_{surf}(t)\, dt \qquad \text{(Eq. 33)}$$

where v_d is the speed of the detonation front, v_f the speed of the shock front, I_d the fraction of laser irradiance used in the detonation, γ the adiabatic coefficient and ρ_0 the density of the gas media in contact with the surface, t_0 the starting delay of the detonation, and τ_d the detonation time, such as $t_0 + \tau_d = \tau_{lp}$, the laser pulse length. The function $f(\tau_d, t)$ in the definition of the instantaneous propagation speed of the shock wavefront, posterior to the detonation depends on the propagation regime of the blast wave (planar, spherical, or other).

2.2.4 Thermo-Chemical Effect

In many situations of laser cleaning, the heat generated by absorption of laser radiation may activate chemical reactions on the irradiated material, or between the radiated material and the environmental media.

The thermo-chemical (pyrolytic) phenomena can be distinguished from the photo-chemical (photolytic) primary phenomena [43], because in the first case, mostly driven by IR laser wavelengths, the thermalization of the laser energy is faster than the chemical reaction, while in the latter case, mostly driven by UV radiation, the beginning of the chemical reaction takes place before thermalization, although temperature increase may go on during laser irradiation.

Some examples of thermo-chemical phenomena are the decomposition of calcite ($CaCO_3$) into calcium oxide (CaO), releasing carbon dioxide (CO_2):

$CaCO_3 \rightarrow CaO + CO_2$

or the combination of some metals with air elements (very often producing oxides such as copper oxides) in cases of over cleaning of metal objects [58].

2.3 Femtosecond Photo-Excitation

Although being aware that several phenomena occur between laser photon absorption and material removal, in the description of previous primary phenomena there was no real need to consider the temporal interrelationship between them.

However, and concerning laser material irradiation with femtosecond laser pulses, laser photo-excitation must be considered separately from thermalization and material removal phenomena due to the fact that they take place in time scales that are different for each process and in the order of magnitude of the laser pulse duration.

As wrote by Von Allmen, "The interaction of light with matter results from the forces of Coulomb and Lorentz, exerted by the electromagnetic radiation field on the charged particles in the material, mostly electrons" [59].

Initial interaction, the excitation of electrons due to laser energy absorption, takes place during the pulse duration, that is, in the range of femtoseconds [60]. The forces exerted by the electromagnetic field associated with laser radiation induce electron oscillation, increasing electron energy.

Free electrons in the metal surface, also named the electron gas, absorb laser photons with intraband transitions, increasing their kinetic energy [61, 62]. In semiconductors, the absorption of laser energy may change electrons from the valence band to the more energetic conduction band and in dielectric materials, where covalent electrons bind atoms or ions to each other, the absorption of laser photons results in the transition of molecules energy to higher vibrational states, or at high enough radiation

intensity multi-photon absorption (a non-linear process) and ionization (dielectric breakdown) take place uploading bond electrons from the valence band to the conduction band.

According to Gamaly *et al.* [61, 62] at this high intensity, the ionization time of dielectrics is of the order of a few femtoseconds, occurring at the initial stage of the laser pulse, and consequently further laser-matter interaction is independent of the type of absorbing material.

The energy of excited electrons, in a non-equilibrium distribution, is locally transferred. This redistribution of electron's energy proceeds via elastic collisions with surrounding electrons and, in the case of non-radiative energy transitions, is transferred by inelastic collisions to the lattice phonons. The increase of local lattice vibrational energy due to the excited electrons relaxation takes place in a time range of a few to tens of picoseconds [59, 60, 61].

However, in this time range the material volume in the increased energy state is not limited to the photon excitation volume; transport of energy out of the optical excitation volume is due to the excited electrons, which diffuse much farther (in metals) [63] than the optical penetration depth, enlarging the affected volume.

At this stage, the excited electrons and lattice are in a non equilibrium thermodynamic state, that can be described by a "Two Temperature Model" and is characterized by a temperature much higher than the material boiling point, leading to a superheated metastable state at a solid [64, 65, 66] or liquid density [67].

When the load of thermal energy in the microvolume is much faster than the time needed for mechanical expansion and relaxation, a local high tensile pressure builds up along the optical penetration depth or the non-equilibrium electron diffusion length, whichever is the larger, which propagates in every direction [63, 68]. Simultaneously, due to the superheated state of this volume, the tensile strength of the material decreases [67]. If the tensile force is larger than the strength of the material at the surface, the pressure originates material fracture and

defects [68], or bubble nucleation [67] in fast expansion (phase explosion) and material ejection and removal takes place in a range of sub or few nanoseconds, much later after the end of the laser pulse [70].

Perez and Lewis [64, 65, 66], using a molecular dynamics model to study the expansion of solids, proposed four stages, between the lattice excitation and the final material ejection: material expansion due to lattice thermal relaxation, with creation of sporadic voids near the surface; next, the coalescence and increasing volume of voids originating a fast surface expansion and the onset of evaporation; third, a faster expansion stage with ejection of solid clusters and vapour and a final stage, with a strong expansion rate typical of a free expansion gas and removal of material by vaporization.

Another model for material removal with sub-picosecond laser pulses, proposed by Gamaly *et al.* [61, 62], is based on the electric attraction forces. In the case of material irradiation with very short pulses, in the femto or picosecond range, and with very high fluencies and intensities, overall ionization of the surface material, occurs during the pulselength. Ionization can take place via single-photon or multi-photon absorption or else via electron impact (avalanche ionisation). If electrons gain enough energy, metal or bonding electrons can escape from the surface, dragging along lattice surface "parent" ions, by coulombic attraction.

At very high intensity irradiation with femtosecond laser pulses a plasma can also be generated after the vaporized material but, according Zeng *et al.* [68] the laser pulse (~100 fs) terminates before material ablation or plasma plume formation takes place.

After the surface layer material ejection and removal, due to the irradiation of femtosecond laser pulses, the energy is randomized in the irradiated microvolume in which excitation was not enough to promote ablation, in the range of a few nanoseconds. After laser thermalization, a new local thermal equilibrium is established, characterized by a new set of temperature (increased), density and pressure values, in the local microvolume, in a fluid state of solid density and high temperature and

the equilibrium with surrounding material takes place by thermal transfer.

In addition, material removal due to short pulse laser irradiation, also designated by laser ablation, might also be in consequence of changes in physical and chemical properties of the material that results in changes of the aggregation state of the material.

Several other physical and chemical phenomena of laser interaction with materials have been described [43] and many other designations of these phenomena can be found in the literature. However the set of previously referred and succinctly described phenomena are the most usually found in literature, associated with laser cleaning mechanisms.

3. MECHANISMS OF LASER CLEANING

In the mid 70's when back to the University of California, after using different laser sources for the divestment of various materials, Asmus [1] had already identified different laser cleaning mechanisms based on thermal, mechanical or chemical phenomena resulting from the absorption of the laser radiation incident at the object surface.

According to Watkins [38], the mechanisms present in laser cleaning can be divided into three main groups, depending on the predominant phenomena:

- Thermal phenomena, inducing mechanisms such as selective vaporization, sublimation, combustion and thermo-chemical decomposition

- Mechanical impact phenomena, as basis for cleaning mechanisms such as explosive vaporization and plasma detonation, steam or vapour pressure cleaning, laser shock cleaning

- Transient heating phenomena leading to cleaning mechanisms such as thermoelastic vibration, cold spallation and angular laser cleaning.

And yet, ahead in the referenced text,

- Cold ablation (or bond breaking), photon pressure and femtosecond pulse ablation based on non-thermal interaction phenomena of laser photons with materials.

Siano *et al* [40], in agreement with Watkins work [59], clearly identified and probed the first two referred mechanisms, using Nd:YAG lasers with different pulse lengths: normal free running (hundreds of micro seconds) and Q-Switched (nanosecond pulses). Still, they identified an intermediate regime designated by "Laser Sustained Combustion", using a short free running Nd:YAG laser with a pulse length of tens of micro seconds.

3.1 Selective Vaporization and Sublimation

The selective vaporization mechanism was one of the first mechanisms for laser cleaning identified by John Asmus [72, 1] during his work in Venice.

The primary phenomenon present in this mechanism is photo-thermal, leading to temperature increase and vaporization of the contamination layer and stopping at the absorbing contamination - non-absorbing substrate interface. But also secondary phenomena such as thermal conduction and vapour pressure are there, contributing to the material removal.

In the selective vaporization mechanism, the laser radiation incident on the object interacts mostly with the contamination, because this layer has high absortivity to the incident wavelength and beam direction, or else because the layer is optically thick*. In this situation the interaction of the laser radiation with the substrate is minimal, resulting often in a limited

* Optical thickness is the thickness of an object or layer when compared with the optical penetration depth of the same material or medium..

temperature increase, because the contamination layer, while present and optically thick, shields the substrate to the incoming laser radiation, and latter because the substrate has a small absorptivity to the incident wavelength, either because is reflecting or transmitting it.

The selective vaporization mechanism can also be present when the contamination is optically thin and a significant part of the incident laser radiation is transmitted to the substrate but thermal properties of contamination and substrate are clearly distinct. This is the case when the boiling temperature of the contamination is much lower than that of the substrate [59] or when the thermal conductivity of the substrate is much higher than that of the contamination, slowing the temperature raise of the substrate.

Watkins [71], summarizing the work of J. Asmus [72], refers three different conditions for selective/non-selective vaporization:

(1) non-selectivity due to similar absorbance and vaporization temperatures of contamination and substrate,

(2) selectivity due to clearly different absorbance values of contamination and substrate,

(3) selectivity due to clearly different vaporization values of contamination and substrate,

Side effects of the selective vaporization mechanism are due to thermal conduction from the heated contamination to the substrate and vapour pressure acting beyond the volume intended to be removed, causing potential harm to heat or pressure sensitive substrates.

Practical applications of laser selective vaporization is, for example, paint layers removal from metallic substrates [7]. In this example, the paint layer to be removed is much more absorptive to laser radiation than the metallic substrate that is essentially reflective. Moreover, the vaporization temperature of most industrial paints is much lower than the melting temperature of the metal, and the local temperature increase in the paint

layer is much faster than in the metal substrate due to its high thermal conductivity.

Selective vaporization mechanism occurs [59] mainly with laser pulse length in the range of 1 μs to 1 ms, and moderate power densities from 10^3 to 10^5 W cm^{-2}.

Salimbeni, Siano, Pini *et al* [40] have distinguished in this mechanism of selective vaporization two different regimes. At long pulse lengths, 0.1 to 1 ms, a slow vaporization regime occurs with vapour expansion in turbulent flux, and at shorter laser pulse lengths between 1 to 10 μs, a regime of fast vaporization, with possible formation of rarefied plasma and a quasi-sonic vapour expansion.

Laser sublimation was referred by Kautek *et al* [75], when cleaning parchment and paper with a XeCl excimer laser. The mechanism described is once more based on a photo-thermal process, in which the selective absorption of the UV (308 nm) laser radiation leads to the sublimation of the carbonaceous contamination.

3.2 Explosive Vaporization and Plasma Detonation or Hot Spallation

The initial process in explosive vaporization and plasma detonation mechanisms is again the photo-thermal phenomena followed by thermo-dynamic or hydro-dynamic phenomena. These thermodynamic phenomena include the impact pressure caused by vapour and plasma expansion, and subsequent recoil pressure associated with surface relaxation at the end of the laser interaction time, when the plasma expands away from the contamination-substrate interface [38].

For high energy densities on the surface, the plasma attains high electronic density and strongly absorbs the incident laser energy, acting like a shield between the laser pulse and the absorbing surface. The surface vaporization stops, before the end of the laser pulse and the

shock or blast wave is then built by up the detonation dynamics of the laser absorbing plasma [56].

The microscopic compression exerted during the laser pulse on the material surface by the fast expanding ionised vapour decreases suddenly when the pulse ends and the plasma expands away. At this time the material surface relaxes and a thin surface layer is removed, resulting in (hot) spallation.

Siano, Pini and Salimbeni [40, 57, 76], referring to this mechanism by "Photodisruption"*, obtained shadowgraph images showing simultaneously the vaporized material and the shock wavefronts produced when a Q-Switched Nd:YAG laser was incident on a solid mineral target simulating the black crust usually found on stone.

The explosive vaporization and plasma detonation mechanisms for laser cleaning require high intensity and short duration laser pulses [59], typical of Q-Switch lasers that can achieve 10^7 to 10^{10} W cm^{-2}, with pulses of 5 to 50 ns.

Side effects of this mechanism, also termed spallation or hot spallation mechanism by many authors are mainly due to mechanical forces exerted by the shock wave on the cleaned surface, possibly originating local roughness or cracking. Thermal conduction from the hot plasma might also cause damage on temperature sensitive materials.

3.3 Steam/ Vapour Pressure Cleaning

Steam laser cleaning is the mechanism mainly associated with the removal of microscopic particles, but also used to remove porous or water absorbent contamination crusts in the presence of a thin liquid film over or imbibed on a solid surface.

The basic physical phenomenon in this mechanism is photo-thermal, leading to the evaporation or superheating boiling of the deposited liquid

* Photodisruption is a term mostly found in medical and biology papers to designate biological tissues rupture after intense laser absorption.

film and the generation of vapour pressure acting on particles and surfaces.

Imen, Lee and Allen, early in 1991 [77], have reported a novel laser assisted particle removal technique, that they named LAPR. In this technique, a water film on the contaminated surface was irradiated by laser, removing safely the contaminant particles due to the forces generated by the explosive evaporation of the water, namely the vapour pressure. The authors also identified as a possible liquid layer the atmospheric water condensed on the surface, for the ejection of the contaminant particles.

In order to increase the cleaning efficiency, Zapka, Ziemlich and Tam [3] have intentionally applied a thin liquid film on the surface of a silicon substrate and verified that the cleaning mechanism depends on the laser wavelength. To explain such a dependence they proposed that, for the IR laser used (Er:YAG), laser irradiation absorption occurred at the liquid layer top surface while for UV, the liquid film is almost transparent and the KrF laser radiation was absorbed by the solid surface. The absorption of the laser radiation caused the temperature increase at the solid liquid interface and the commencement of boiling from the bottom of the liquid layer, increasing in this way the laser cleaning efficiency.

Yavas *et al* [78] reported the experimental study of bubble nucleation and growth at the liquid solid interface and the consequent pressure pulse, using a high-resolution optical probe.

Siano *et al* [79] used wet laser cleaning to remove the encrustation from gilded bronze panels. They consider that the cleaning mechanism is again the vapour pressure generated by the water evaporation. Although the water is fairly transparent to the wavelength of the Nd:YAG laser used, the water temperature increases due to thermal conduction from the laser absorbing constituents on the encrustation that increase in temperature and size.

The vaporization temperature (T_{vap}) and the water thermal diffusion length (δ_w) limit respectively, the temperature rise and depth of the heated water:

$$T_{w\,Max} \leq T_{vap} \qquad \text{and} \qquad \delta_w = \sqrt{4\kappa_w.\tau_p} \approx 100 \text{ nm}$$

where T_w is the liquid water temperature, κ_w, the thermal diffusivity of the water and τ_p, the temporal pulse length or pulse duration.

According to the referred authors, the particle thermal expansion and fast vapour expansion generate a compression wave propagating both into the incrustation material and water layer that reflects at the water-air interface turning into a tensile pressure wave towards the incrustation surface. Both these pressure waves contribute to the fragmentation of the incrustation and water vapour cavitation expansion, resulting in local projection of fragments of the crust layer. However, it was also noticed that a thick water layer can inhibit the material removal.

3.4 LASER SHOCK CLEANING

Another technique of laser cleaning based on the mechanism of plasma detonation, and named by Lee *et al* "Laser Shock Cleaning" [45, 80], is based on the physical process of photodisruption or electrical breakdown of the air by a high intensity focused laser pulse, very near the surface to be cleaned.

The shock wavefront resulting from the expansion of the plasma generated by laser sparking in air, with omnidirectional propagation, might exert on the surface and contaminants much higher pressure than the total adhesion forces to the substrate. In this situation, the contaminant layer or particles adherent on the surface are detached and accelerated at high speed away from the surface. This technique has the advantages of being independent of the optical properties of the contamination and the substrate and safer for optically absorbing substrates.

Moreover, in laser shock cleaning, the laser beam propagation axis is parallel to the surface to be cleaned, avoiding any damage caused by direct irradiation of the substrate surface.

C. Cetinkaya and M. Peri [81] also reported this technique, with the name of LIP – laser induced plasma, for the removal of nanoparticles. They measured the transient pressure exerted by the laser-induced plasma on the surface of a pressure transducer, at a variable distance (1.3 mm to 4.5 mm) from the laser focal spot. The measured peak pressure, in the referred experimental conditions, was of the order of tens of KPa, insufficient to cause any damage to the silicon substrate, and decreased when increasing the "firing" distance.

H. Lim and D. Kim [82] have also studied this laser cleaning technique, using different noble gases to cover the surface of a contaminated silicon surface. Photoacoustic beam deflection was used to analyse and measure the shock wave dynamics, pressure and speed, and the experimental results were in good agreement with calculated values based on the blast wave theory. In the referred study the authors report shock wave propagation speeds of several Km s^{-1} and pressures of few MPa.

3.5 Dry Laser Cleaning of Particles

This mechanism is a sequence of physical phenomena such as photo-thermal, transient heating and thermal expansion, and is mainly applied for dry laser cleaning of small particles (micron or sub-micron dimension) from surfaces. It can be considered in two different ideal situations, whether the radiation absorption takes place at the particle or substrate surface; in none of these situations is the intentional addition of a covering fluid considered.

The relative importance of the different phenomena contributing to the adhesion force of small particles on a substrate depends on several parameters including geometrical aspects- the particle shape and dimensions and roughness of the substrate, environmental- presence of

atmospheric moisture, and materials properties of particle and substrate, such as electrical parameters.

The laser radiation absorbed at the particle or the substrate surface, results in thermal expansion and displacement of the absorbing surface (or surfaces). In the situation of laser cleaning, the active or inertia forces applied to the particles must exceed the adhesion forces.

Song and Lu [83] schematically imaged this cleaning process by a spring connecting a contaminant particle to the substrate. This spring, representing the equilibrium adhesion forces, mainly van der Walls forces, is "depressed" by the thermal expansion of the substrate, the thermal expansion of the particle and by photon pressure. At the end of the laser pulse, the spring is released and the potential energy is transferred into particle kinetic energy leading to particle ejection if it overcomes the adhesion forces.

The nature and range of forces creating adhesion of micron or submicron sized particles to the underneath substrate have been widely accepted and reported in literature of laser cleaning (e.g. Lee *et al*, 2000 [45]). However, the mechanisms for the removal of these particles from the substrate are still under discussion and investigation [84, 85], as well as the removal motion: lifting, sliding, rolling or "saltation".

3.5.1 Angular laser cleaning

Another technique based on dry laser and the transient heating cleaning mechanism was described by Lee *at al* [45, 86, 87]. In this technique, the angle between the laser propagation axis and the surface to be cleaned is reduced, producing a larger irradiated area per pulse and so the cleaning speed is greatly increased.

Moreover, for incidence angles below the Brewster angle of the material, the reflectivity decreases and so the absorptivity increases when decreasing the angle between the laser axis and the surface, increasing in consequence the cleaning efficiency.

The physical phenomena involved are basically the same, with photo-thermal process increasing the temperature and expansion of contaminants and surface during the short laser pulse, creating a thermoelastic force that expels the contaminants when it overcomes the adhesion forces.

3.5.2 Verso laser cleaning

It is interesting to notice that Lu *et al*, when applying dry laser cleaning on a transparent quartz plate contaminated with aluminium particles [88], reported a large increase in cleaning efficiency (from 24% to 100%) if the contaminated object was irradiated from the back side. The reason for this was said to be that the temperature at the interface between absorbing particle and transparent substrate would be much higher, due to the optical properties of these materials.

Barone, Bloisi and Vicari [53, 89] more recently presented a technique for laser cleaning of thin sensitive substrates, which uses the laser incident in the *verso* face of a thin object, and takes profit of the thermo elastic stress waves propagating trough the substrate to remove particles from the front face.

In this technique is the photoacoustic mechanism that provides the particles with the kinetic energy necessary to escape the adhesion forces, through momentum transfer from the substrate to the particles.

According to the authors this technique may prove especially useful for light sensitive objects, like ancient textiles and manuscripts, due to the fact that the laser radiation does not impinge on the more important face of the object, such as the exposed side of a textile or the written face of a manuscript.

Another advantage pointed out is that the cleaned area is usually larger than the irradiated area, due to the spread of the acoustic stress wave from the verso irradiated surface to the front surface to be cleaned.

However, this technique is only applicable to mechanically thin samples, because the intensity of the propagating stress wave decreases with the distance, and also the cleaning efficiency of this technique.

3.6 THERMOELASTIC OR COLD SPALLATION

In this mechanism, a short laser pulse incident on the absorptive surface, either the contamination surface or the substrate surface, causes transient heating below the boiling point, and thermoelastic expansion and subsequent contraction of a thin absorbing volume.

The volume expansion causes pressure on adjacent material and creates a thermoelastic compressive stress pulse that propagates into substrate and contamination layer and that is reflected at the free boundary as a tensile stress pulse.

The magnitude of this thermoelastic stress may be sufficient, to lead to acoustic waves propagating in the material and surrounding media. This effect is usually known as photo-acoustical or opto-acoustic effect.

Because the amplitude of these stress waves depend not only on the absorbed laser energy and material characteristics, but also increase with the elastic constraints on the heated surface, this could be the mechanism in pulsed laser cleaning, where the stress waves propagating in the substrates are amplified due to the constraint exerted by the contamination layer [86].

The reflected tensile pulse can result in nucleation, growth and coalescence of new voids [90]. At the contamination – substrate interface, already existing defects, voids generated by laser absorption and thermal buckling of the contamination, and eventual thermal softening decrease the mechanical stability and adhesion forces.

If the magnitude of these stress pulses exceeds the shear stress of the contamination-substrate interface, it will cause the unwanted layer to peel off, without or with negligible vaporization or plasma detonation, unlike the mechanism described in § 2.3.

Because the visual perception of this mechanism in laser cleaning is the spallation of the superficial layer it is termed in the literature as laser induced spallation* or cold spallation.

Oltra *et al* [91] identified this mechanism, referred as "Thermoelastic Stress", when cleaning oxide layers from metallic substrates. If the oxide layer is optically thin, the energy of the laser pulse is mainly absorbed at the substrate film interface, generating an acoustic wave. At the oxide – air interface, the acoustic wave propagating in the oxide layer is reflected and converted into a tensile wave, and reaches back to the oxide-metal substrate interface, causing the lift off of the oxide film. In this situation, Oltra observed a damage-free oxide film removal.

Strzelec and Marczak [92] and Jezersek *et al* [93], used a Michelson interferometer to monitor the vibration of the rear surface of different types of stone when the front surfaces were irradiated with Q-Switched Nd:YAG laser pulses at IR wavelength and different fluencies.

Bregar and Mozina [94], using a laser beam deflection probe technique noticed that the optoacoustic wave in the air, near the front face of the sample, changes from shock wave to sonic wave when the surface is cleaned.

Fotakis *et al* [44] identified two main types of mechanical effects in the interface of thin polymer films annealed on quartz substrates; these effects might have a structure of a flaw or detachment, and cracks breaking the film continuity, depending among other parameters, on the annealing quality and consequent film-substrate adhesion.

3.7 UV Photo-chemical Ablation

Laser ablation by ultra violet radiation is also named cold ablation, non-thermal ablation or bond-breaking because the absorption of laser radiation can break molecular chemical bonds and cause strong

* Laser induced spallation is also the designation of an experimental technique used to study the adhesion of a thin film with the substrate.

expansion forces releasing the dissociation products. In this mechanism the increase of thermal energy of the irradiated area or volume is usually insignificant or with no meaningful intervention in the cleaning mechanism.

So, laser ablation cleaning is mainly based on a photodissociation (or photolysis) chemical process in which a more or less complex molecule is decomposed into its constituents due the absorption of laser photons. Photodissociation requires photons with enough energy to break the bonds of the molecules, that is, the photon is likely to have the wavelength in the visible or UV.

In polymeric materials like varnish epoxy or resin, the UV laser photons have enough energy (§ 2.1.4) to break C-H bounds of the monomer chain, resulting in shorter chains easily removable by soft mechanical action [59].

3.8 Photon Pressure

This is an example of a photo-mechanical phenomenon, in which the laser cleaning is achieved as a result of the pressure exerted on particulate contaminants in consequence of the momentum of the arriving photons of the laser beam [38, 55, 59]. This mechanism occurs simultaneously with other mechanisms, usually involving photo-thermal phenomena.

G. Vereecke *et al* [95] referred the photon pressure mechanism for laser cleaning of small particles from Si wafers. In this paper, the authors report a remarkable increase in cleaning efficiency at constant fluence, when increasing the incidence angle.

Pointing out that thermal expansion of particles or substrate, keeping constant the fluence on the surface, was not expected to depend on the beam incidence angle, the authors propose to explain the results obtained considering the influence of the force f_{beam}, exerted by the

reflected laser beam on the particle surface, and consequently proportional to the exposed area of the particle (πr^2).

In accordance with the authors and equation 21:

$$f_{beam} = p_{rbeam} \times \pi r^2 = 2R\frac{F}{c\tau_p}\ \pi r^2 \qquad \text{(Eq. 34)}$$

where $p_{r\ beam}$ is the beam radiation pressure, R the surface reflectance to the laser pulse, F is the fluence per pulse and τ_p is the pulse duration.

Decomposing the laser radiation pressure in two components, normal and parallel to the surface, Vereecke *et al* [95] deduced that it is the parallel component of the force that increases with the incidence angle. Consequently, the authors proposed that the laser radiation pressure at grazing incidence causes a rolling movement contributing to the removal of submicron particles from flat surfaces.

3.9 FEMTOSECOND PULSED ABLATION

Laser cleaning with femtosecond pulses has the advantage of allowing a better control of the area and depth of removed contamination [96]. Indeed the absence of an absorbing plasma and thermal conduction losses during the laser pulse interaction allow for a more efficient allocation of the absorbed laser energy to the removal or cleaning process.

Perez and Lewis [65, 66], proposed four different removal mechanisms associated to femtosecond pulses laser ablation: spallation associated to a phase of creation and expansion of voids or defects; homogeneous nucleation associated with the phase of subsurface material nucleation, with the expulsion of liquid droplets and vapour simultaneously; fragmentation, associated to the stage of fast expansion and solid clusters ejection and finally evaporation.

PART II LASER CLEANING - EXPERIMENTAL

"Since the invention of laser in 1960, industry has had a tool for generating large and controllable quantities of optical energy. This is a new form of industrial energy yet it is more versatile and adaptable than any previous one. We have just spent a century exploring the possibilities of electricity following the invention of the dynamo in the late 19th century; we may now reasonably expect to spend the next century exploring the possibilities of innovating with optical energy" [97]

1. INITIAL EXPERIMENTS

In order to determine the laser cleaning thresholds and cleaning parameters for precious metals, several samples of silver and gold, with different contaminations were irradiated by laser and further analysed.

Since cleaning and damage threshold depend on laser characteristics other than pulse energy, and since the reviewed literature on laser cleaning of precious metals reported mainly the use of Q-switched Nd:YAG lasers [17 - 20], different laser systems were used with several wavelengths and pulse length regimes to evaluate the influence of laser pulse characteristics.

It is well known that the optical parameters of the contamination and substrate depend* on the incident laser radiation wavelength; the pulse length has influence on the temperature variation [39, 79], and consequently on the occurrence of melting, vaporization and eventually on the formation of a more or less dense plasma.

Varying the incident laser wavelength and pulse duration was done with the aim of identifying the type of laser more efficient and with safer characteristics, that is, larger selectivity in cleaning precious metals.

Laser sources such as pulsed CO_2 Diamond from Coherent, free running Nd:YAG QY-50, from Quanta Systems or short free-running YAG laser Smart Clean from El.En., with pulse length in the microsecond range were used in this initial stage to irradiate and evaluate the effects on the material surface

Also, laser sources emitting short laser pulses of the order of tens of nanoseconds, such as Nd:YAG long Q-Switch DEKA 10 from El.En., Nd:YAG Q-Switch 5012 D, from BMI, KrF laser COMPEX, from Lambda

* Optical propoerties depend on spectral band and so, occurring optical phenomena depend on incident wavelength

Physics or the new femtosecond lasers by Clark-MXR Inc. were used, evaluating the effects of these systems.

Experiments of laser cleaning were also realised in single pulse mode or repetition mode with scanning with variable overlap, mostly without assistance medium and in a single case with sprayed water on the surface.

1.1 IR AND NEAR IR LONG PULSE IRRADIATION

The viability of cleaning precious metals with infrared and long pulsed irradiation was studied using both CO_2 and free or short-running YAG lasers.

The CO_2 laser used was a sealed-off Coherent Diamond model, with RF excitation of the active media, emitting pulsed laser radiation with wavelength in mid-infrared (λ = 10600 nm) and pulse duration adjustable from 10 μs to few milliseconds at a selectable repetition rate, in the range of KHz. The maximum average output power of this system was P_{av} = 150 W.

The silver samples, tarnished or with oil contamination were irradiated by this CO_2 laser using a convergent beam with spot size diameter of 5 mm on the sample surface. Laser pulses of short duration (for this laser system) of τ_p = 10 to 100 μs were used, aiming to reduce the effect of thermal conduction to the substrate, with energy per pulse from E_{pulse} = 1 to 50 mJ corresponding to incident fluence range from F = 6 to 300 mJ cm^{-2}.

The contaminated surfaces were irradiated in scanning mode, but no noticeable effect on the surface was detected in this fluence range.

With wavelength in the near infrared (λ = 1064 nm) and pulses with tens of microseconds, both the acousto-optic Q-switched laser (Quanta Systems) and the Short-Free Running Nd:YAG laser (Smart Clean) where used to irradiate the contaminated surfaces.

Although emitting pulsed laser radiation with average power (P_{av} =1 to 10 W) and pulse duration (τ_p = 10 and 20 μs) in the same range, the main difference between the pulsed emission is that the acousto-optic Q-Switched Nd:YAG laser pulses are low energy (E_{pulse} = 0.5 to 20 mJ) at high repetition rates (f_p = 1 to 45 kHz) while the Short-Free Running Nd:YAG laser pulses are high energy (E_{pulse} = 200 to 1000 mJ) at low repetition rates (f_p = 1 to 10 Hz).

The contaminated samples were irradiated in repetitive pulsed mode pointing at a single site at the surface, but no noticeable effect on the contaminated surfaces were detected no matter the irradiation time.

Therefore, the laser radiation with long (τ_p = 10 to 100 μs) IR laser pulses, in the conditions here described, was not adequate for cleaning precious metals covered by thin contamination layers, because no alteration in the contamination was detected.

1.2 Near IR and Visible Short Pulse Irradiation

Short laser pulses of the order of nanoseconds, such as the long Q-Switched Nd:YAG DEKA 10 from El.En. or the electro-optic Q-Switched Nd:YAG 5012 D, from BMI, both emitting pulses at low repetition rate, were also used to clean contaminated surfaces.

The long Q-Switched Nd:YAG laser pulses with a wavelength of λ = 1064 nm, pulse duration τ_p = 70 ns and energy per pulse E_{pulse} = 70 to 150 mJ were applied trough an optical fibre and collimator on the sample surface with a repetition rate of 5 Hz. In the spot size of 2 to 3 mm, depending on the distance from the fibre output, the laser fluence was varied from F= 1 to 4 J cm^{-2}; irradiating different positions in the sample surface when varying the incident fluence.

The electro-optic Q-Switched Nd:YAG laser pulses with pulse duration τ_p = 7 ns were converged trough a focusing lens on the sample surface in single pulse irradiation; the near infrared wavelength (λ = 1064 nm) and

the visible wavelength of the second harmonic (λ = 532 nm) were used*, and the incident fluence was varied from F = 0.1 to 1.2 J cm^{-2} in the IR and F = 0.05 to 1.0 J cm^{-2} in the visible.

In any of these experiments, a fluence threshold was found, depending on pulse duration, above which signs of melting were observed in the irradiated positions, without achieving the cleaning effect. Below these threshold values no other effect was noticed in the tarnished silver, sometimes being impossible to locate the laser irradiated area, after removing the sample from the irradiation set-up; in the samples with organic contamination, the irradiated contamination appeared more yellow and opaque to daylight, but still not cleaned.

Therefore, the laser radiation with short (τ_p = 7 and 70 ns) near IR or visible wavelength laser pulses, in the conditions here described, was not adequate for cleaning precious metals covered by thin contamination layers, because damage of metal sample or (chemical) deterioration of the organic contamination was achieved without the aimed cleaning effect.

1.3 UV Short Pulses Irradiation

The viability of cleaning precious metals with UV laser radiation was also experimentally studied. A few experiments** took place with stained or greased silver samples, with a KrF excimer laser COMPEX, emitting short pulses of τ_p = 20 ns and λ = 248 nm with 1 Hz in a fluence range of F= 0.1 to 0.6 J cm^{-2}.

In these initial experiments with UV radiation, it was visible at the naked eye a more or less pronounced cleaning effect (depending on the irradiation conditions) on the contaminated surface. This cleaning effect consisted in a lightning of the yellow-brown coloration of the tarnished samples or in a reflectivity increase of oiled surfaces; other than that, when observed at optical microscope, no damage was visible in the metal surface.

* A more detailed description of these experiments and results can be found in chapter 3 and 4, of this Part II

** Few experiments because no excimer laser was available at our laboratory

These encouraging results directed the experimental work to the use of the third harmonic wavelength of the Q-Switched Nd:YAG laser pulses with duration τ_p = 7 ns and UV wavelength of λ = 355 nm. The maximum energy of these UV pulses at the sample surface (E_{pulse} = 20 mJ), after passing the beam delivery optical components, had been previously considered a serious limitation for the use of this 3rd harmonic radiation for laser cleaning.

A systematic analysis of the effects of laser irradiation on tarnished and oiled silver surfaces with the 3rd harmonic radiation of the BMI Nd:YAG laser took place, and very satisfactory results were obtained *.

Therefore, the laser radiation with short (τ_p = 7 and 20 ns) UV wavelength laser pulses, in the conditions here described, was considered adequate for cleaning precious metals covered by thin contamination layers.

1.4 Ultra Short Pulses Irradiation

The source of femtosecond laser pulses was a mode locked fibre laser with a Titanium-Sapphire (Ti-Sa) regenerative amplifier, model CPA-2010 by Clark-MXR Inc; the laser pulses with maximum energy E_{pulse} = 20 μJ, duration of τ_p =180 fs and central wavelength λ_0 =775 nm were emitted at a repetition rate f_p =1 KHz and focused on the sample surface in a spot of 25 μm diameter, corresponding to a maximum incident fluence of F = 0.5 to 4 J cm^{-2}

The samples, contaminated gold and silver objects, were scanned by the focused pulses in parallel lines, at variable overlap and scanning speed.

Again a cleaning effect without substrate damage was achieved, in a limited range of parameters, but the same parameters could cause substrate damage if the substrate is scanned in multiple superposed scans.

Therefore, the laser radiation with ultra short (τ_p = 180 fs) laser pulses, in the conditions described, was considered adequate for cleaning

* This experimental work is described in chapter 5 of this Part II

precious metals covered by thin contamination layers. However, laser cleaning with these ultra short laser pulses was found not to be a self limited process, and material removal can proceed farther, keeping the same fluence for laser irradiation scanning, creating undesired microstructures in the irradiated metal surface*.

2. EXPERIMENTAL SET-UP AND GENERAL PROCEDURE

2.1 LASER BEAM HOMOGENISATION

The laser system mostly used for the experimental work was a Q-Switched Nd:YAG laser BMI- 5012 D, emitting pulses with 7 ns (according manufacturer specifications) in single pulse or repeated pulses with repetition rates from 1 to 10 Hz. Besides the fundamental laser wavelength (λ = 1064 nm), the laser system was equipped non-linear crystals emitting laser radiation in the second and third harmonic of fundamental wavelength, allowing the use of green laser radiation (λ = 532 nm), as well as ultra-violet (λ =355 nm) laser radiation.

During the work undertaken at the beginning of the experimental activity, one of the problems experienced was the non uniformity of the energy distribution across a transverse section of the laser beam, due to the fact of the laser cavity being an unstable resonator.

The cross section of the laser beam presented a pattern formed by concentric rings of maxima and minima (Fig. 8) energy distribution. This same pattern was marked and observed on the sample surface, making very difficult the evaluation of the effect of the laser irradiation on the sample, and to relate this effect with a calculated average energy density.

Therefore, one of the first tasks was to attempt to homogenize the energy distribution on the cross section of the laser beam.

Having in mind the optical characteristics of commercial glass and the wavelengths to be used (Nd: YAG laser fundamental wavelength and 2nd and 3rd harmonics), a commercial quality diffusing glass was used as a homogenizer a few millimetres from the laser output aperture, when using direct laser beam irradiation of the surfaces, or placed parallel to principal plane of the beam shaping lens.

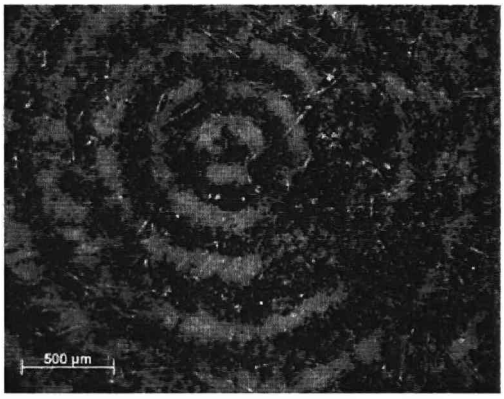

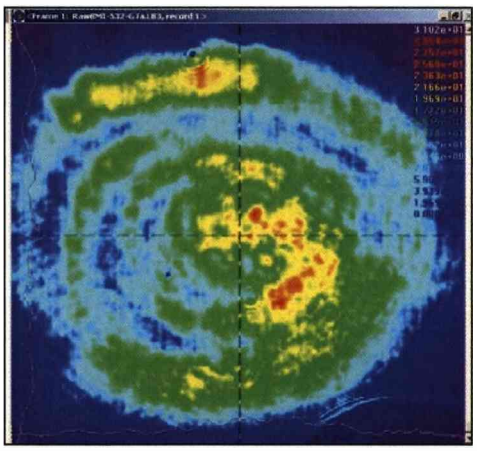

Fig. 8. Laser beam cross section obtained by laser irradiation on xeroxed paper (upper) and CCD camera (lower)

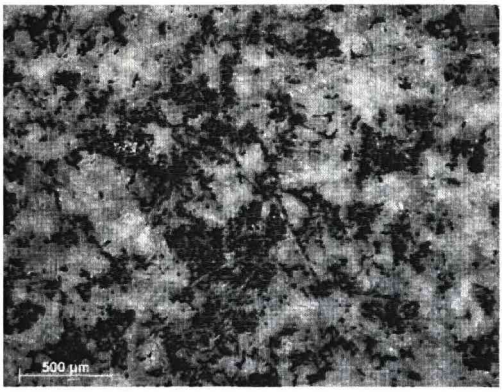

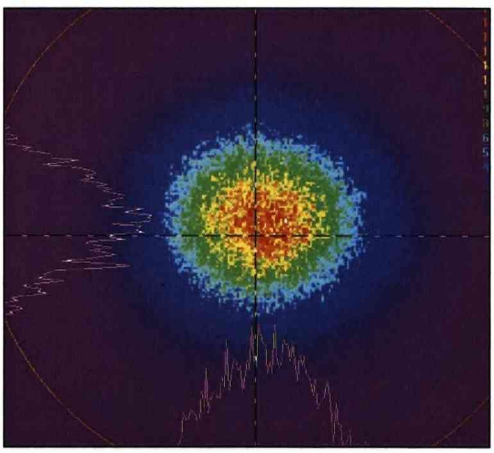

Fig. 9. Laser beam cross section after homogenisation obtained on xeroxed paper (upper) and CCD camera (lower)

The energy distribution obtained at the beam cross section after the insertion of this homogenizer was more uniform as can be seen comparing figure 8 and 9, where the upper images were obtained by irradiation of a single laser pulse on xeroxed paper and the lower images were obtained with a CCD Cohu digital camera associated with Spiricon software.

The lower picture in Fig. 9 shows that after homogenisation, the laser beam energy distribution in a transversal plane (multi-coloured areas) or the beam energy profile in two perpendicular directions (white lines) still present an irregular distribution, but in average this approaches the gaussian distribution characteristic of a good quality beam. This is important due to the absence of strong "hot spots" (visible as red dots in Fig. 8), able to cause punctual damage on the irradiated surface even at low laser fluence and because the cleaning effect is more uniform, as can be seen in the upper image of Fig. 9.

However a certain amount of energy of the incoming beam was lost by reflection and absorption at the diffuser plate and the spatial coherence of the beam was also decreased by the introduction of the diffusing homogenizer, causing an increase in the output beam divergence and also an increase of the dimensions of the beam waist after the focusing lens.

2.2 LASER BEAM CHARACTERIZATION – SINGLE PULSE

The BMI Nd:YAG laser system, according manufacturer specifications, emitted laser pulses with maximum energy at the laser output aperture, of E_p = 600 mJ at 1064 nm, E_p = 280 mJ at 532 nm and E_p = 100 mJ at 355 nm; however lower values of energy per pulse where available at the sample surface, due to ageing of laser system, to the presence of harmonic generation crystals and to the presence of diverse optical components for beam guiding and shaping. So the characterization f the laser beam and pulses at the sample surface plan was carried on.

The characterization of the energy content and geometry of the laser beam was performed as much as possible according with the international standards ISO 11554 (15-12-1998): Optics and optical instruments – Lasers and laser-related equipment – Test methods for laser beam power, energy and temporal characteristics and ISO 11146 (15-12-1999): Lasers and laser-related equipment –Test methods for

laser beam parameters – Beam widths, divergence angle and beam propagation factor.

The output of the equipment used for beam energy and spatial characterization was set in agreement with these standards, by the manufacturer or during experimental work.

Direct or divergent laser beam section diameters were larger than the sensitive area of the Laser Beam Analyser, and so these diameters were measured by the print left on thermal paper, more clearly defined for IR than for UV pulses, having also lower fluence.

A larger range and higher values of energy density or fluence, were achieved not only by adjustment of the laser power supply, but also by decreasing the beam spot area on the sample surface; in this situation the beam spatial characterization was performed by the Spiricon Laser Beam Analyser and software.

At a first stage of direct beam geometric characterization and in order to locate the raw beam waist and measure beam divergence, a piece of laser sensitive paper (ZAP-IT® Paper Z-25*) was used. After the emission of each pulse a laser affected circle, referred as the beam print, was obtained on the paper surface. The diameter of this print was taken as the diameter of the laser beam at the distance where the sensitive paper was standing.

To obtain a decrease of the spot size a converging lens (OFR LLQ-25-80) was used at a distance of 5 mm from the diffusing plate, placed in the path of the laser beam and aligned with the beam propagation axis. In this situation the spatial characterization was performed directly by the Laser Beam Analyser equipment. The laser beam was incident on the CCD sensor of a Cohu camera and the information of the camera was analysed and displayed in the computer monitor by the Spiricon software.

*ZAP-IT® paper (www.zap-it.com) is a commercial product specially conceived to document laser beam characteristics, in a pulse length range from 1 ns to 30 ms and fluence range from 5 mJ cm^{-2} to 20 J cm^{-2}; this paper is sensitive from ultraviolet to infrared.

The energy beam characteristics were measured at various distances from the lens, using a Coherent LMP10i pyroelectric detector (Fig. 10).

The characterization of the energy content and geometry of the BMI Nd:YAG laser beam was performed near the plane of laser interaction with the test surface. This procedure allowed the information about the actual values of the energy density interacting with the material, having in account the energy losses by diffusion or absorption on the optical interfaces.

Experimental conditions:

1. The laser output energy was manually adjusted on a thumbwheel (G) on the laser power supply, graduated from 1 to 8 (further represented by G1 to G8).

2. The energy of the pulses and the distance to the sensor were varied in order to characterize the focused beam diameter and fluence along the propagation axis.

3. The sensor (pyroelectric sensor, sensitive black paper or CCD) was placed perpendicular to the laser propagation axis at various positions with increasing distance; the distance is referred to the laser output, when characterizing the direct raw beam, or to the focusing lens, for the converged beam.

4. The value of energy/pulse was determined as an average over 50 measured values, for each irradiation conditions.

5. To measure the raw beam diameter in each position, a single pulse was shut on sensitive paper leaving a grey print on the paper surface. For lower fluence, several superposed pulses (usually 5) were shut, in order to reinforce and increase the definition of the print on the paper.

6. This procedure of taking the beam print in sensitive paper at various distances from the focusing lens was repeated 10 times for each distance, providing an average value. With the Spiricon the number of acquisitions to average was defined by software.

7. The spot size was measured after laser irradiation on the sensitive paper or measured by the Spiricon software based on the Cohu pixel image. The beam presented a roughly circular shape and the diameter was taken as an average of 10 measured values for the same irradiation conditions, this is at the same distance from the lens and for the same energy per pulse.

8. The value of energy density or fluence was computed for each energy level (G) and distance from the lens, as the ratio from the average energy per pulse at that level, by the average beam print area at each position (distance). It was determined as an average value, not only because the energy per pulse and the spot size have some fluctuations from pulse to pulse, but also because, even using the homogenizer, the energy distribution was not constant across the section of the laser beam.

After measuring and averaging the energy per pulse for each position of the graduated thumbwheel (G=1 corresponding to the minimum energy and G=8 to the maximum energy), and the beam spot size along the propagation path, for a set of positions with increasing distance to the focusing lens, a graphic was built of the computed laser fluence (Fig. 10) versus the position of the graduated thumbwheel and the beam spot size along the propagation path, for each laser wavelength.

These measurements and corresponding plots were made independently for the fundamental wavelength (λ = 1064 nm) and for the second (λ = 532 nm) and third harmonic wavelength (λ = 355 nm) of the Nd:YAG laser,

The use of these charts for each wavelength, allowed for rapid information of the laser fluence incident on the sample surface placed at known distance from the lens, without the need of measuring the parameters before each experiment. More than that, because this information is depicted in a graphic mode, the charts allowed also for a fast evaluation of the position where to put the sample, in order to be irradiated with certain fluence.

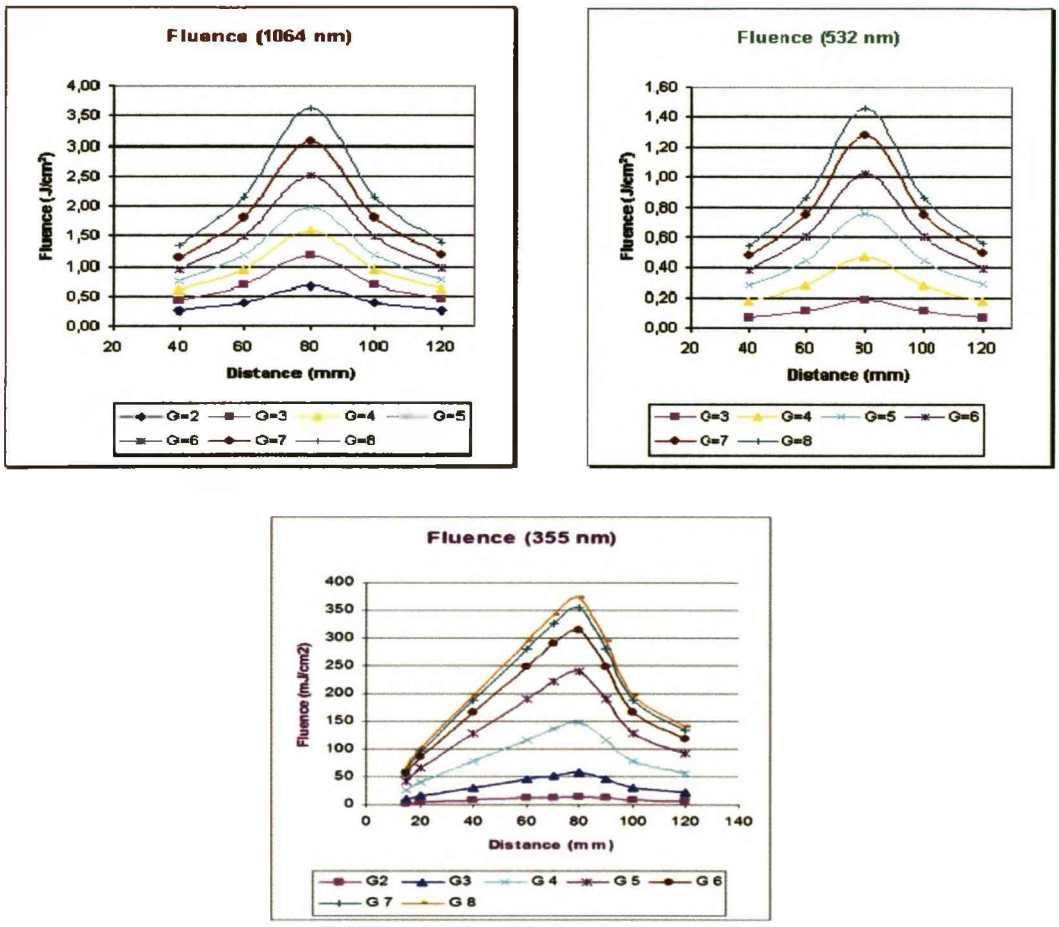

Fig. 10. Laser beam energy density after homogenizer and converging lens associated with a short term energi fluctuation of ± 10%

The values of fluence presented in these charts were checked and updated when necessary; mostly, the values of energy per pulse were checked on a time basis due to the fact that the ageing of the pumping lamp and eventual degradation of the optical components resulted in a decrease of the laser output energy. Verification and eventual correction of the energy and spot size values was also performed each time a modification in the set-up took place. The referred modifications could be a maintenance intervention in the laser source, the realignment of the laser mirrors or the non-linear crystals used for harmonic generation, or simply the replacement or cleaning of the optical components directing the laser beam.

2.3 LASER BEAM CHARACTERIZATION - SCANNING

In order to be able to laser cleaning a surface with an area larger than the spot size, it is necessary to scan the beam with respect to the surface.

Since the laser emission is pulsed, different situations can occur during the scanning, concerning the irradiated area. The laser irradiated surface areas, corresponding to two followed pulses can be:

separated, if $v_{scan}/f_p > d_\sigma$ adjacent, if $v_{scan} / f_p = d_\sigma$

and overlapping, if $v_{scan} / f_p < d_\sigma$

where: v_{scan} is the scanning speed, f_p the pulse repetition rate, and d_σ the beam diameter, at the surface plane.

The situation required for surface cleaning is the last one, and it is pertinent to quantify, in this situation, the number of pulses incident upon the same elemental area; this was called the (amount of) overlap (*OL*), defined by:

$$OL \equiv \frac{f_p \times d_\sigma}{v_{scan}},$$

The value of *OL*, determines the number of pulses, irradiating the elementary surface area along the scanning direction and on the irradiated area parallel diameter.

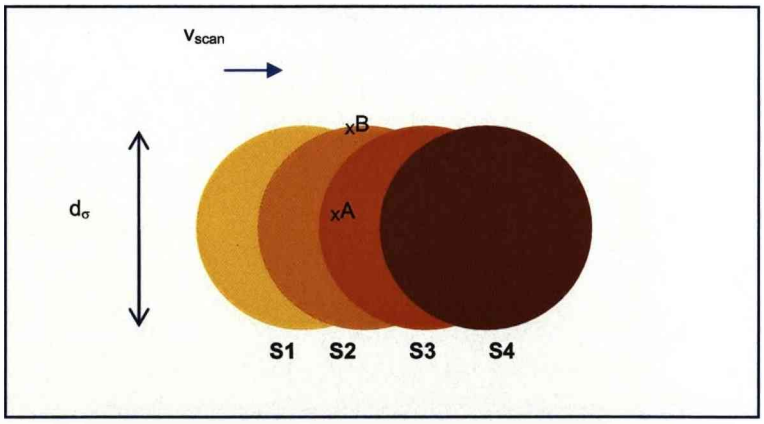

Fig. 11 Overlap of laser pulsed irradiation
depending on the position of the considered point on the irradiated circle

The scheme (Fig. 11) aims to illustrate the sample surface being irradiated with finite overlap by a scanning pulsed laser; each coloured circle (Sn) corresponds to the single area on the sample surface irradiated by each pulse.

As a matter of fact, since the beam section is approximately circular, the number of pulses hitting a surface point located on the circle diameter parallel to the scanning direction, v_{scan}, (point A, Fig. 11) is a maximum while the number of pulses hitting the surface point located on the circle diameter, $d\sigma$, perpendicular to the movement direction (point B, Fig. 11) is a minimum.

In the exemplificative figure above, point A is included in areas S1, S2, ... Sn, so this single point, would be irradiated by n consecutive pulses. However, point B on sampled surface (in the depicted situation) would be irradiated by only one single pulse. So, the number of pulses received by each point within the scanned track is not constant, and it is maximal along the central area of the scanned line.

2.4 THE ENERGY THRESHOLDS FOR GLEANING AND DAMAGE

Laser cleaning threshold, is the minimum value of energy density for which the contamination starts to be removed due to laser irradiation with single pulse at a given wavelength. In order to achieve laser cleaning without damaging the substrate it is beneficial if the cleaning threshold of contamination is lower than the damage threshold of the substrate, the energy density minimum value for which the substrate starts to present undesirable permanent modifications. These undesirable modifications or damages might be due to laser direct irradiation on the substrate or due to interaction with the altered contamination layer, such as heat transmission or material migration from the contamination layer to the underlying object surface.

Bearing in mind that the materials to be cleaned are precious metals, often used for decoration purposes, it was important to preserve the

characteristic appearance of these surfaces, mainly colour and shine. Changes in surface colour or shine after laser cleaning, like those reported by Degrigny, Lee, Sokhan, Siatou *et al* [17-20], were considered damages along this work.

When studying laser cleaning usually the first step is to determine the cleaning and damage thresholds that define the operative window, that is the fluence range between both thresholds that allow for a safe laser cleaning procedure, and that depend on the properties of the laser radiation, such as the wavelength and pulse duration, on the properties (optical, physical, chemical, geometry and morphology) of the contamination and the substrate material in respect of the laser wavelength, and on the presence or not of an assistance medium, such as a liquid or vapour.

2.5 Experimental set-up and General Procedure

If nothing is stated in contrary, the set-up in Fig. 12 was mostly used. The sample surface was place with a small angular deviation (< 5º) to the plane perpendicular to the laser beam axis, and at a variable distance to the converging lens, in order to adjust the size of the laser irradiated area and so, the energy density of the surface irradiation. The sample mount was fixed on a linear translation stage, moving at variable speed controlled by computer.

Besides the energy density, the laser wavelength, the pulse repetition rate and the number of pulses or the scanning speed (in scanning operation) were varied.

The actual set of experimental conditions and process parameters, such as energy and energy density range, laser wavelength and pulse repetition rate, number of superposed pulses and scanning speed, have been varied and adapted to the different samples and in consequence have been varied with the specific contamination – substrate to be cleaned and is described in more detail in respective sections.

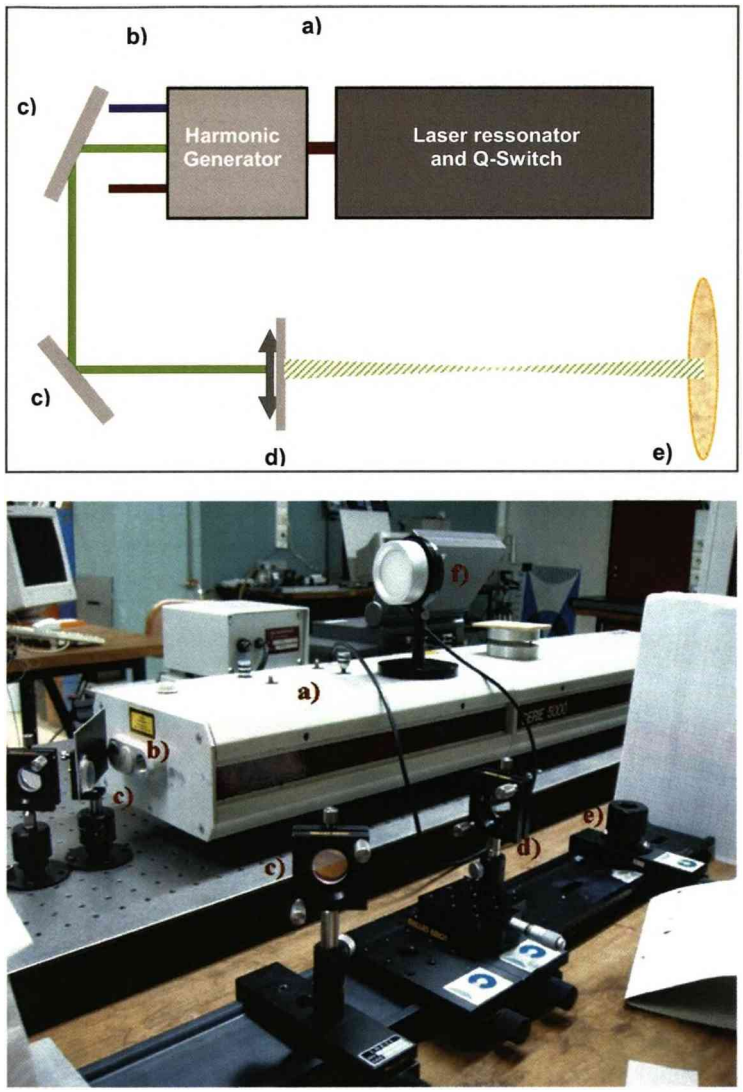

Fig. 12. Experimental set-up: (schematic and photo)
a) Nd:YAG Laser, b) laser beam(s) outputs, c) deflecting mirrors, d) lens + diffusing screen, e) sample and post-holder, f) detector

Each sample started to be irradiated in single pulse with high energy density, aiming to locate easily the irradiated site and observe the effects caused by the laser irradiation; the laser fluence was then successively decreased, either by decreasing the pulse energy or the distance to the focusing lens, and the sample was displaced without removing it from the irradiation set-up, receiving aagain a single pulse. Taking in consideration the effects of single pulse irradiation, the sample was next irradiated in scanning mode, with laser parameters considered of interest for laser cleaning. In this way several sites on the test surface (fig. 13) were obtained due to laser irradiation.

A jet of compressed air at low flux was directed towards the sample surface, in order to avoid redeposition of ablated material

After a set of experiments on a sample for different irradiation conditions (Fig. 13), the surface was analysed in order to detect chemical alterations, indicative of decomposition or removal of the contamination layer, surface topographic alterations, e. g. craters or resolified melted material, causing dulling of the surface, and colour alterations giving possible indications of the cleaning achieved, or possible chemical degradation of the substrate.

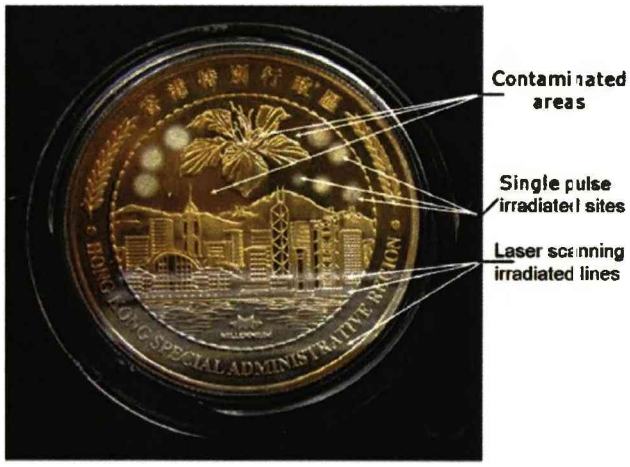

Fig. 13. Silver coin with tarnished surface after laser irradiation

single pulse (top) and scanning mode (bottom)

The cleaning or damage thresholds were identified as the lowest irradiation fluence to which the effect -cleaning or damage- was still detected, within the irradiation conditions used and the sensitivity of the analysis methods available.

2.6 SURFACE ANALYSIS TECHNIQUES

After irradiation within a given set of laser parameters, the sample surface was analysed in order to identify any permanent change in the surface, indicative of the type of laser interaction phenomena taking place during irradiation. These interactions phenomena could be, among

others, photo-thermal, causing phase change, thermo-dynamic causing liquid phase explosive ejection, and photo-chemical or thermo-chemical degradation, causing decomposition of the surface contaminants.

Moreover, as a consequence of the effect of laser cleaning mechanisms, a change in visual appearance should occur, manifesting in the present work with precious metals, as brightness increase and surface colour modification towards grey (for silver samples) or yellow (gold samples).

With the objective of identifying the referred transformations, the irradiated surfaces were analysed by means of different techniques and equipments:

COM (Computer aided Optical Microscopy): ZEISS Axiovert 200 MAT with Software Axiovision 4.0.

SEM-EDX (Scanning Electron Microscopy with electron dispersive X-Ray analysis): Philips XL30 FEG, equipped with a EDAX X-ray spectrometer for EDX

Roughness meter: Mahr Perthometer S2, equipped with a PGK sensor head

Colour meter: Avantes, Avamouse with Avasoftware

Interferometric surface profilometer WYCO NT 3300.

A fist level analysis of the surface after laser irradiation was done by direct visual inspection and optical microscopy observation, aiming to detect any surface modification induced by laser. Not only expected modifications related to the cleaning effect, such as whitening in tarnished silver coins, increased shine in greased silver blanks or colour and shine of overpainted gold surfaces, but also to detect other modifications at the substrate metal surface, such as dulling, charring or others.

A more detailed analysis was performed next, in order to confirm, quantify or explain the observed modifications. The specific techniques used to evaluate or measure the modifications of the surface after laser

irradiation, were primarily dependent on the type of modifications detected visually or at the optical microscope but also on the available equipment, whenever this one was considered enough to describe the surface modification.

SEM, roughness meter and surface profilometry allowed for qualitative and quantitative analysis of alterations on the surface structure or morphology; with this objective, SEM observations were mainly done using secondary electrons, which detection is very sensitive to surface morphology. SEM-EDX was used to make comparative analysis of elemental chemical composition of particular small areas of the surface; colorimetry was used to characterize the optical properties of the surfaces in the visible wavelength range, not only colour but also spectral diffuse reflectance. FTIR – Fourier Transform Infrared spectroscopy, not available in our laboratory, was used because EDX analysis did not show clearly the chemical changes in the organic contamination on silver samples after laser irradiation.

Using the referred analysis techniques, the surfaces were characterized after and before laser irradiation, and the detected alterations were the basis for the proposed laser interaction phenomena and cleaning mechanisms.

3. LASER CLEANING BY SELECTIVE EVAPORATION

Tarnished Coins

These samples, Fig. 14,"The Year of the Horse" coins, referred as YHC, were tarnished at The Royal Mint by enclosuring the pieces in a sulphurous environment for different time duration, being the detailed conditions not known.

Fig. 14. The Year of the Horse Coins (YHC)

3.1 SUBSTRATE CHARACTERIZATION

The silver coins, made of silver-copper alloy with a minimum content of 92.5% silver and the remaining being copper, with no other material being detected in representative amount; these coins consisted of metal disks, 38.5 mm diameter, 3 mm thickness, with a polished base surface-average roughness of 52 nm and non-polished figures and digits on both sides (Fig. 15).

At the optical and electron microscopes, it was also noticed the presence of copper grains sitting on or embedded on the alloy matrix (Fig. 16).

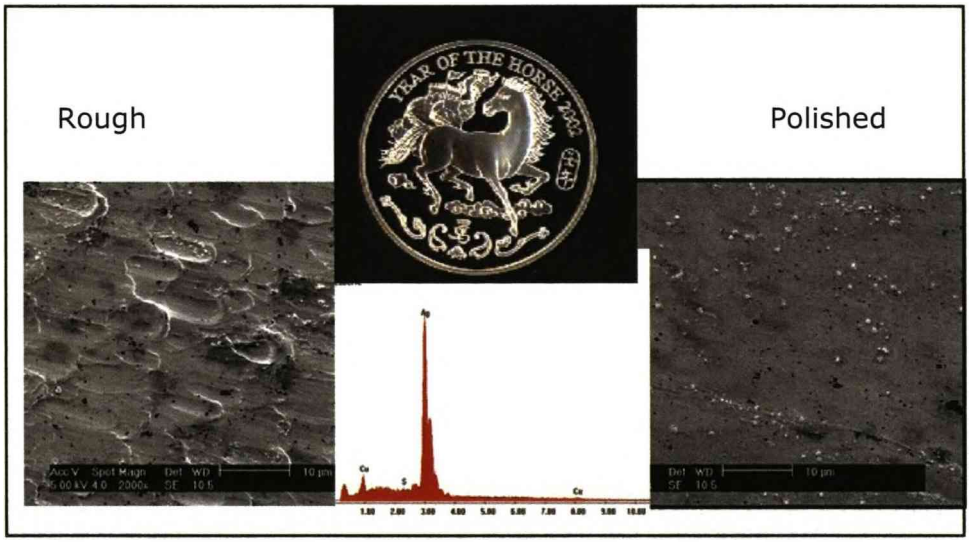

Fig. 15. SEM micrographs of carved (left) and polished (right) areas on the substrate of the coin. EDX analysis of surface composition

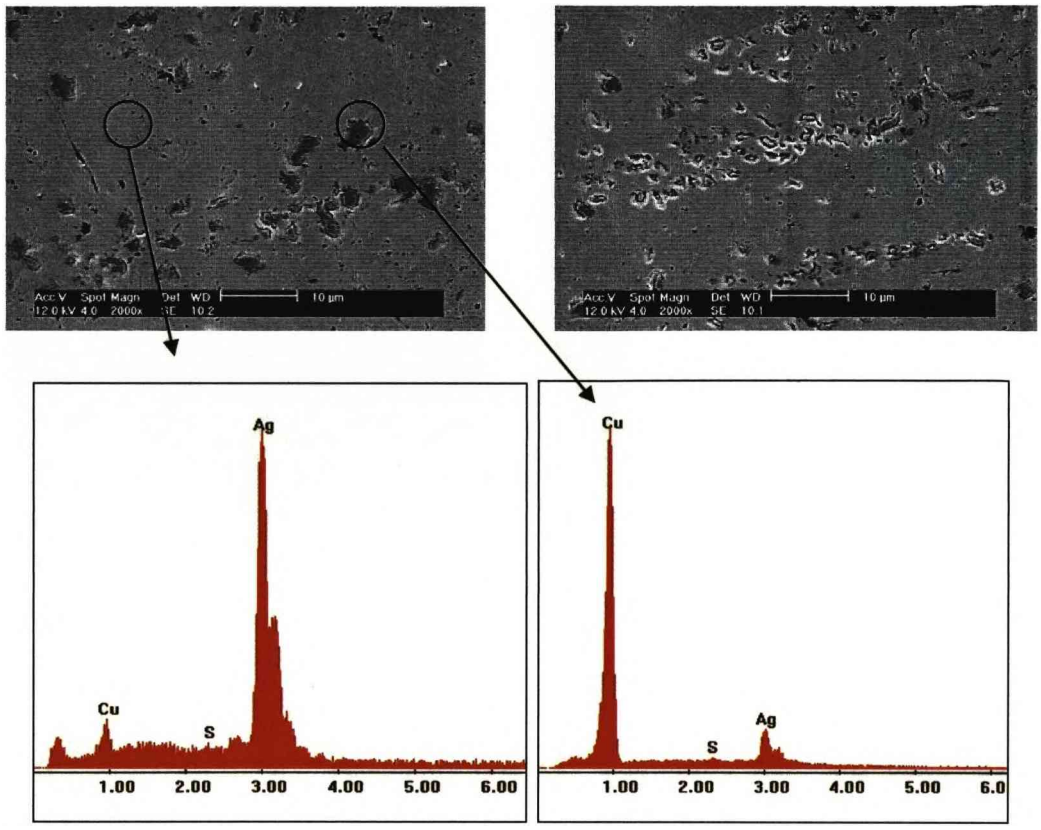

Fig. 16. SEM micrographs of copper grains embedded on the alloy. EDX analysis on homogeneous alloy area (left) and an embedded copper rich grain (right)

3.2 CONTAMINATION CHARACTERIZATION

Silver tarnishing takes place by the combination of metallic silver with sulphur existent in several atmospheric gases such as hydrogen sulphide or even carbonyl sulphide [98]. In this study the samples have been deliberately tarnished by sulphur vapour, in a controlled environment, originating a sub-micron thin layer of silver sulphide (Ag_2S) on the coin surface.

The chemical composition, as obtained by EDX analysis of an homogeneous area of the substrate alloy (Fig. 17) showed the expected presence of silver and copper, a small peak for sulphur, but also the presence of other elements such as carbon and oxygen, as it is usual for unprotected [19] silver surfaces.

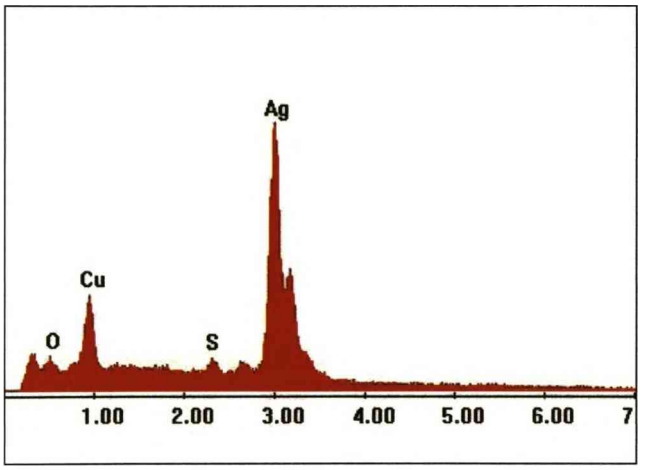

Fig. 17 EDX analysis of a homogeneous area of the silver alloy

The artificial tarnishing of the silver surfaces allowed not only the study of the cleaning process, but also to cover the test sample with a thin coloured (yellow/brown) layer (Fig. 17) that made simple to the naked eye the observation and localization of irradiated area, based on the colour change.

Since the tarnished surfaces presented a yellow-brown coloration, clearly distinguishable from the white silver surface by naked eye, the measurement of colour and colour alteration was the main technique used for the evaluation of the cleaning state of these samples. Due to the fact that the contamination layer, the silver sulphide film, was very thin, it was rather difficult to track the alterations of the surface conditions based on microscope observations or elemental analysis.

The measurement of the surface colour was performed with a spectrometer based colorimeter, and the colour information, processed by Avasoftware was presented in the CIE Lab colour measurement system. The colour information is given by 3 coordinates, namely luminance or luminosity (L), red-green saturation (a) and yellow-blue saturation (b).

As can be seen in Fig. 18 the surface contaminated with silver sulphide presented, prior to laser irradiation, a yellow brownish colour quantified by the coordinates a=+12.07, b=+39.99, much higher than the values of the white reference.

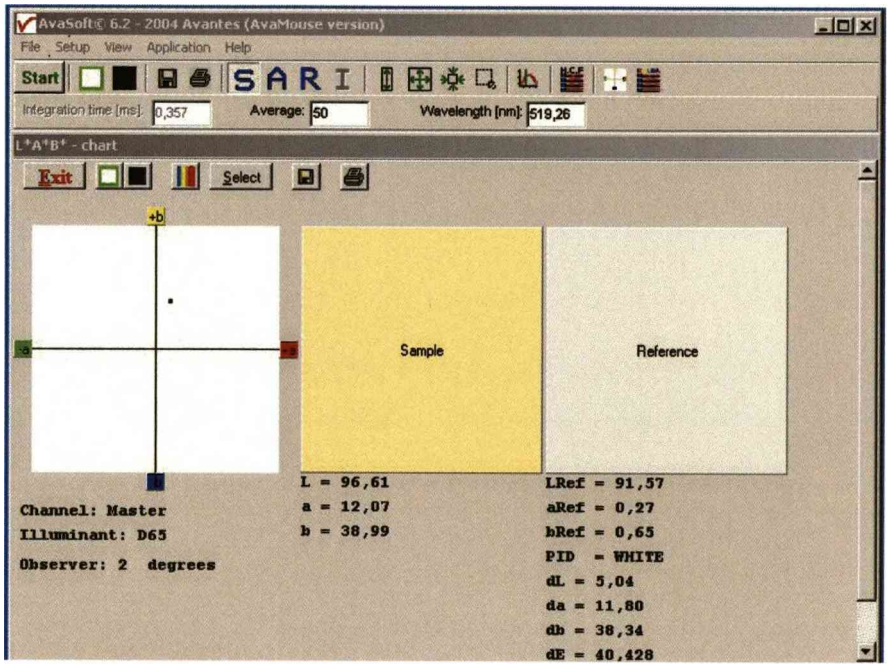

Fig. 18. Optical characterization of the contaminated sample referred to a non-contaminated one

3.3 IRRADIATION OF SAMPLES

3.3.1 Irradiation with Fundamental and Visible Laser Wavelength

The tarnished coins have been irradiated with the Nd:YAG laser beam (diameter at laser output ≅ 7 mm) in single pulse mode (Fig. 19), with two different wavelengths:

- Sample YHC-06→ infrared wavelength (1064 nm) varying the pulse energy from 0.04 J to 0.24 J.
- Sample YHC-05→ visible wavelength (532 nm) with energy per pulse up to 0.09 J.

At this time the beam energy distribution was already homogenised and the raw beam profile was as that in Fig. 9.

For both samples the laser energy density on the sample surface was varied to a maximum of 1.2 J cm^{-2} for the IR and up to 1.0 J cm^{-2}, for the 2^{nd} harmonic.

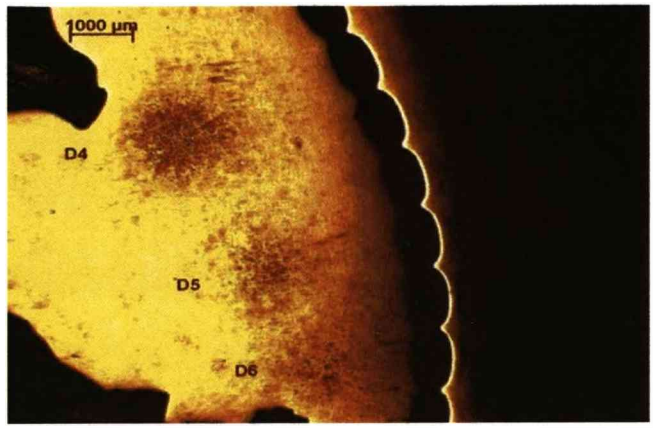

Fig. 19. Sites obtained by laser irradiation on YHC06
(Image at optical microscope)

3.3.2 Evaluation of the Interaction Effects

A preliminary evaluation of the surface modifications due to laser irradiation was done by direct and optical microscopy observation, aiming to detect any surface change induced by laser.

In the case of tarnished surfaces, the cleaning effect upon laser intervention, should bring the colour of the surface (yellow-brownish when tarnished) to the typical "silver" colour. Moreover, the original polished or carved substrate should not suffer surface topographic alterations, causing surface dulling.

A more detailed analysis was performed next, using specific techniques, depending on the detected modification, in order to confirm, quantify or explain the observed modifications.

Therefore, after visual and optical microscopy observations, also SEM and EDX elemental analysis, corroborated that, for these wavelengths (1064nm and 532 nm) it could not be found a cleaning threshold without damaging the substrate.

As can be seen in the colour micrographsof Fig. 20 and Fig. 21, the remaining silver sulphide coating coexisted with damaged (melted) underlying silver surface in the irradiated area. Therefore a cleaned area was not achieved

a) Optical microscope 100X

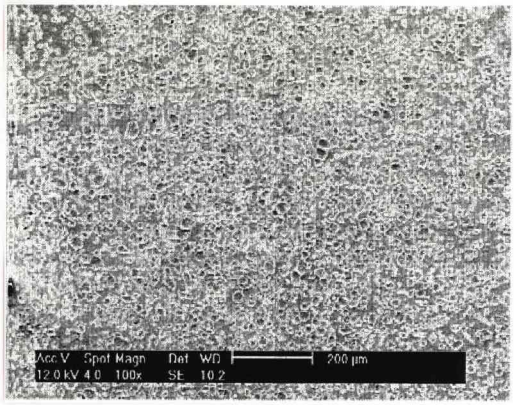

d) SEM 100X

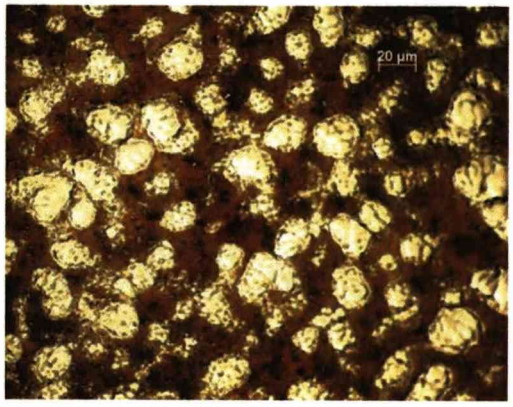

b) Optical microscope 500X

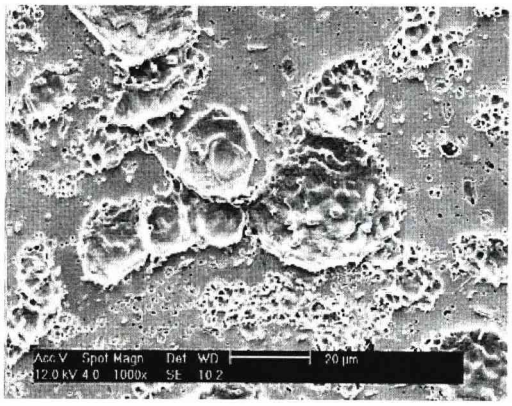

e) SEM 1000X

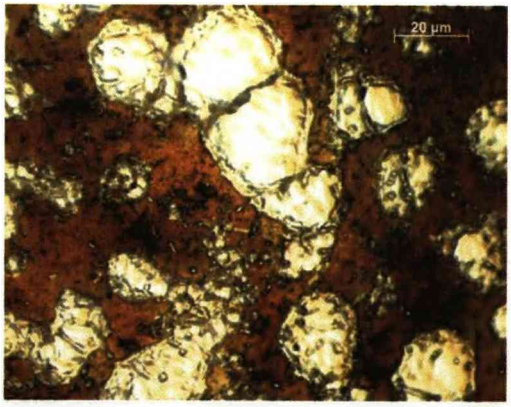

c) Optical microscope 1000X

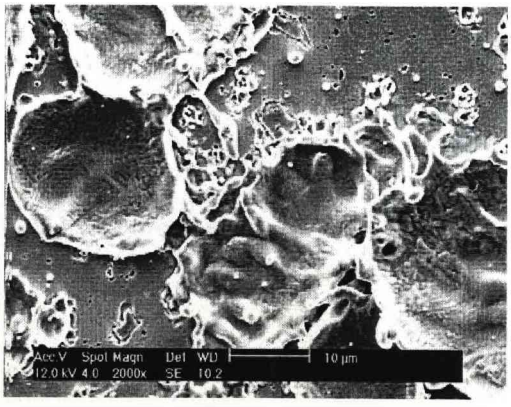

f) SEM 2000X

Fig. 20. Laser irradiated area 1 on YHC-06 surface
single pulse 1.2 J cm^{-2}, at IR wavelength

For higher energy density values the irradiated area was covered by overlapping melt (and re-solidified) pools surrounded by the still coated surface as shown in pictures on Fig. 20 a) to f).

As the energy density incident on the tarnished surface was decreased, the laser irradiated zone was formed by defects of smaller dimension and more separated, as can be observed in pictures on Fig. 21 a) to d), though the EDX elemental spectrum obtained in the laser affected area, did not show a meaningful decrease of sulphur content (Fig. 22).

For laser irradiation with single pulses at fundamental wavelength with energy densities lower than 0.2 J cm^{-2}, no visible mark was produced on the surface, and the irradiated area could not be localized, either with naked eye or by microscope.

a) Optical microscope 100X

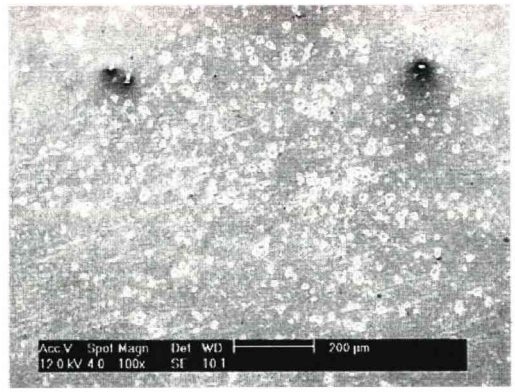

c) SEM 100X

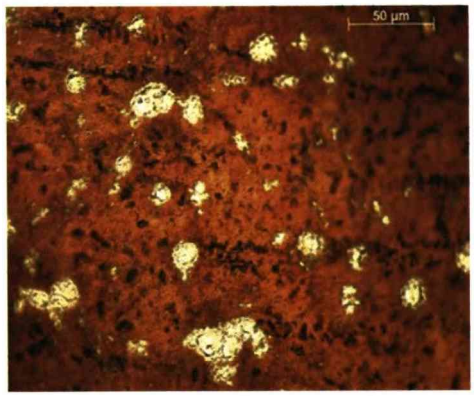

b) Optical microscope 500X

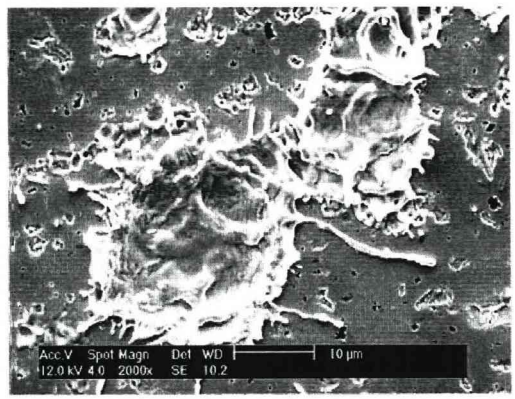

d) SEM 2000X

Fig. 21. Site 6 on YHC06
single pulse 0.2 J cm^{-2}, at fundamental wavelength

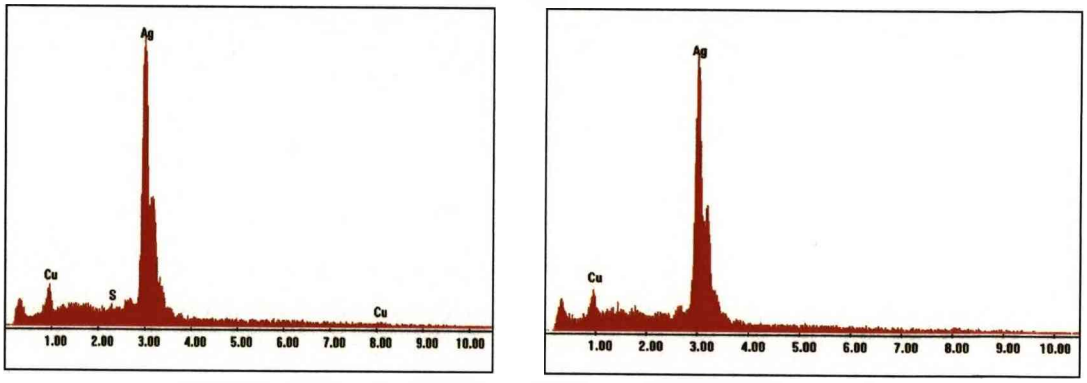

Fig. 22. EDX spectra obtained in a non irradiated area
(left) and an irradiated site (right) on YHC06

The damaged was caused by melting resulted in an increased roughness of the polished surface and consequently in the decrease of the specular reflectivity of the surface. This visual appearance of the laser affected area has been previously reported [17, 18, 19, 20], and named a whitening or a dulling effect.

a) Optical microscope 100X

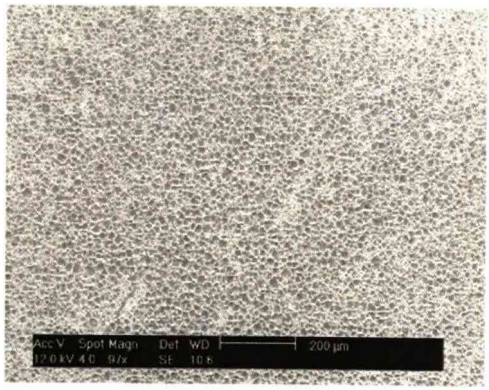

c) SEM 100X

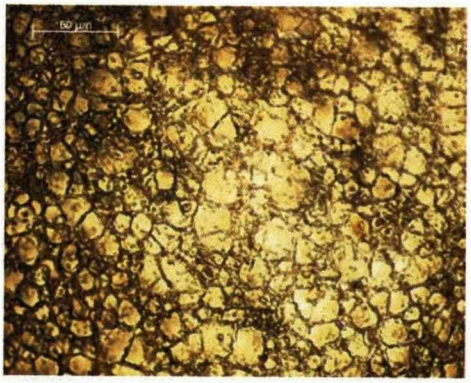

b) Optical microscope 500X

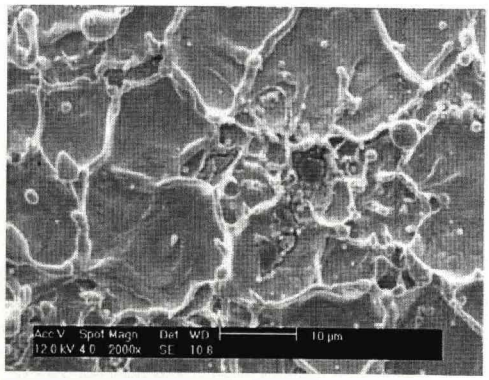

d) SEM 2000X

Fig. 23. Irradiated site 1 on YHC05
single pulse 0.9 J cm^{-2}, at 532 nm

The other sample (ref. YHC05) was irradiated in the same conditions described above but with the Nd:YAG second harmonic wavelength (532 nm), with energy densities up to 1 J cm^{-2}.

The irradiated sites produced in the sample surface (Fig. 23) appeared similar to those produced with the IR wavelength. However, for comparable energy densities, the irradiated site presented larger dimensions and the pools appeared to be less deep.

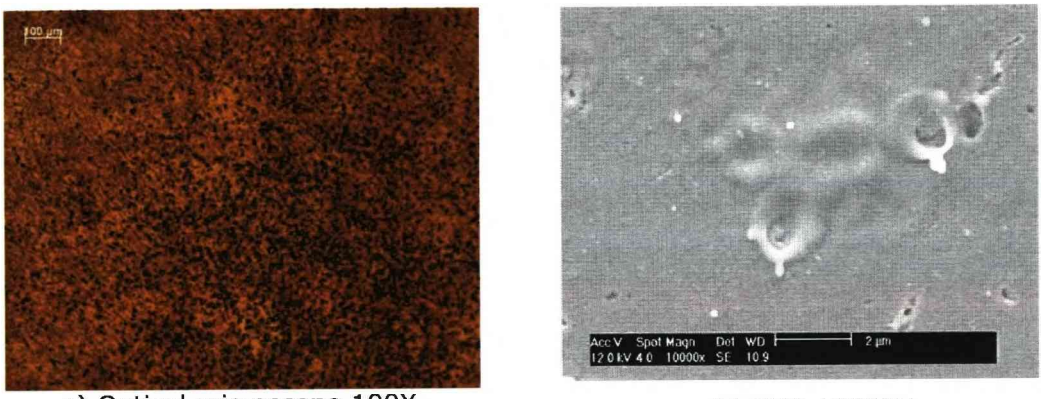

a) Optical microscope 100X

b) SEM 10000X

Fig. 24. Irradiated site 8 on YHC05
single pulse of 0.05 J cm^{-2}, at 532 nm

It was also noticed that the energy density threshold for damaging the surface for this wavelength (532 nm) was 0.1 J cm^{-2}, lower than the threshold value for the IR wavelength, which was found at 0.2 J cm^{-2}, what is in agreement with the decreasing of silver and copper reflectance with decreasing wavelengths.

The micrographs of Fig. 24 show the surface of the tarnished silver irradiated at 532 nm by a single pulse with energy density less than 0.1 J cm^{-2}; the irradiated area was undetectable by naked eye and very difficult to localize on the optical or electron microscope.

3.3.3 Irradiation with Wet Surface

Since it was not possible to remove the coating without damaging the originally flat surface and trying to limit the temperature increase of the

substrate, other two samples (ref. YHC04 and YHC03) were wetted by means of a deionised water spray, and after that irradiated in the same set up and conditions described previously. It could be immediately seen by naked eye that the water layer didn't spread uniformly, but on contrary formed small droplets on the surface.

The samples were irradiated again with the laser infrared wavelength (1064 nm) and the visible harmonic wavelength (532 nm) at various fluence levels.

After the irradiation the samples were observed by COM and SEM. It could be seen that the water droplets, although evaporated after irradiation, stained the sample surface. Moreover, during the irradiation these droplets acted like small positive lenses, concentrating the energy towards their optical axes and diminishing the uniformity of the irradiated area as it is clearly visible in the photos of Fig. 25 and Fig. 26.

No improvement in the cleaning action was noticed, either by the naked eye or by microscopy. Yet, it was observed that the melting process of material covered by the water droplets was much more "explosive" than what is usually observed in wet laser cleaning, showing deep craters with porous re-solidified walls and larger amounts of droplets, as shown in the micrographs of Fig. 27.

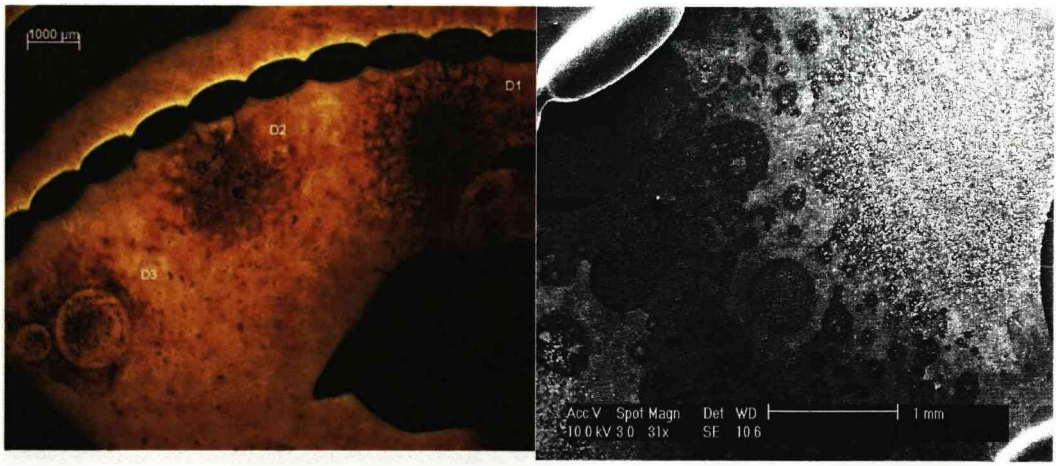

Fig. 25. Stains produced on the water spayed surface of YHC04 after laser irradiation at 1064 nm and fluence of 2.4 J cm^{-2} (site D1, also imaged with SEM on the right), 1.9 J cm^{-2} (site D2), 1.4 cm^{-2} (site D3)

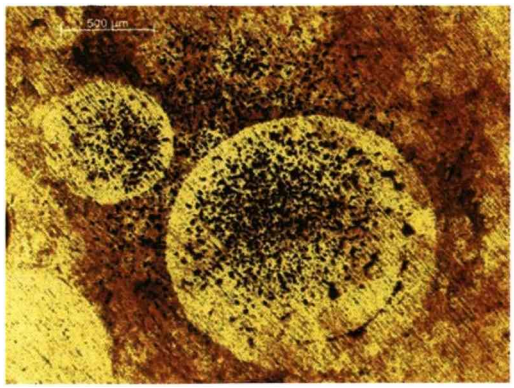

a) YHC04; single pulse 0.7 J cm^{-2}, at 1064 nm. Optical microscope 50X

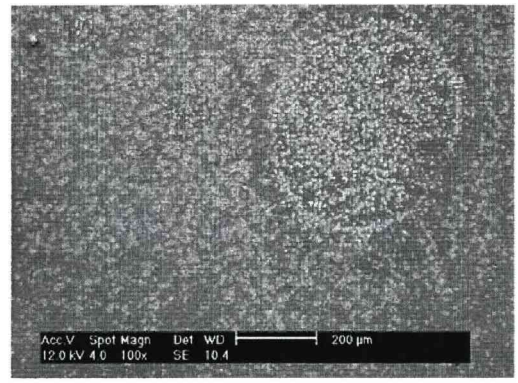

b) YHC03; single pulse 0.3 J cm^{-2}, at 532 nm. SEM 100X

Fig. 26. Lensing effect produced by the water sprayed surfaces of YHC04 and YHC03

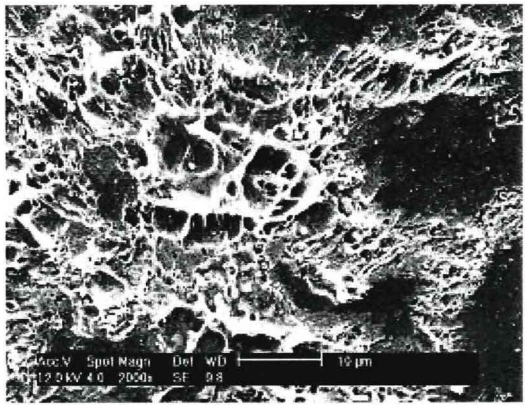

a) YHC04, irradiation with 1.2 J cm^{-2}, at 1064 nm. SEM 2000X

b) YHC04, irradiation with 1.2 J cm^{-2}, at 1064 nm. SEM 5000X

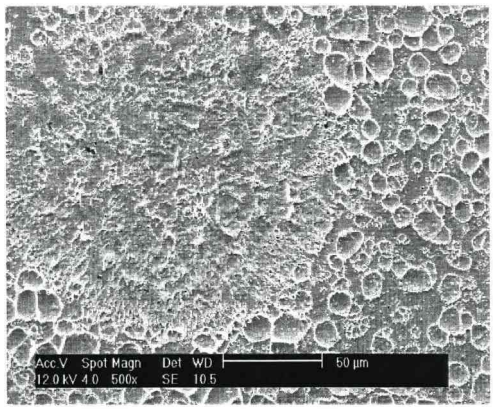

d) YHC03, irradiation with 0.6 J cm^{-2}, at 532 nm. SEM 500X

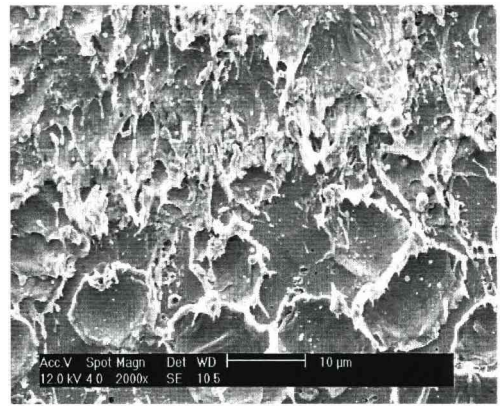

c) YHC03, irradiation with 0.6 J cm^{-2}, at 532 nm. SEM 2000X

Fig. 27. "Explosive" effect produced by laser irradiation on the wet surface

3.3.4 Irradiation with Scanning

In order to avoid the heating and damaging the substrate of the irradiated samples, some experiments in scanning mode were done on the same type of samples described above.

The laser beam, after redirected by the deflecting mirrors was homogenized by the diffusing screen, and incident upon the sample surface, without using any focusing optics.

The tarnished silver coin was mounted with a small angle relative to normal incidence, on a linear translation stage by Spindler & Hoyer. The sample was placed at little distance (40 mm) from the homogenizer in order to avoid an undesirable contamination of the homogenizer surface, and an also undesirable increase of the spot size due to diffusion. At this distance the irradiated area had approximately 7 mm diameter.

The energy density per pulse incident on the sample surface was varied by changing the energy per pulse. The sample translation speed was adjusted in agreement with the pulse repetition rate in order to get the intended pulse overlap.

Along next experiments the sample was irradiated at λ=532 nm, the single pulse average energy was 0.06 J and the laser energy density was set at a constant (average) value of 0.12 J cm^{-2}. It has been noted before, that for this wavelength and these low energy density values there was still an interaction of the laser radiation with the silver surface, although a very superficial one.

With an overlap of 1, that means that the irradiated circular areas on the surface were adjacent but not superposed, the laser track could not be visualised, even if the same track was scanned several times.

Increasing the overlapping, the laser track on the surface could be observed (Fig. 28) with a slightly lighter coloration, but also less shining when compared with the tarnished surface.

a) Non-irradiated surface

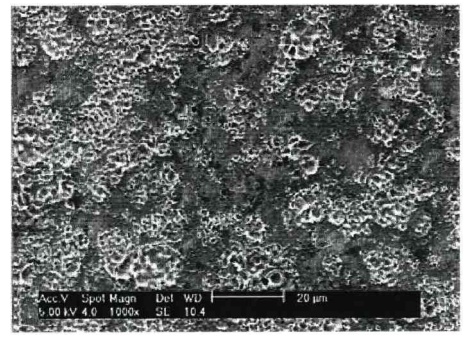

b) Scanned laser irradiation, OL= 8

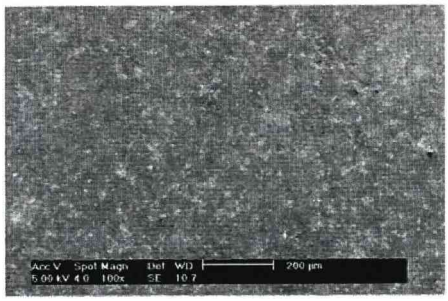

c) Scanned laser irradiation, OL= 4

Fig. 28. Scanned laser irradiation of flat area

YHC02 0.12 J cm^{-2}, 532 nm

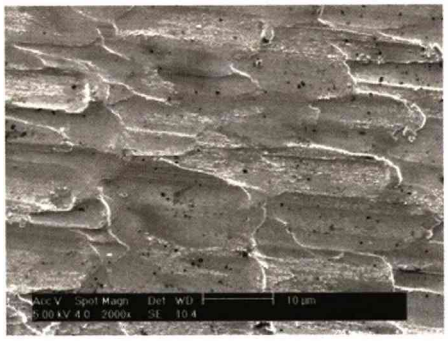

a) Non-irradiated sample surface

b) Scanned laser irradiation, OL=

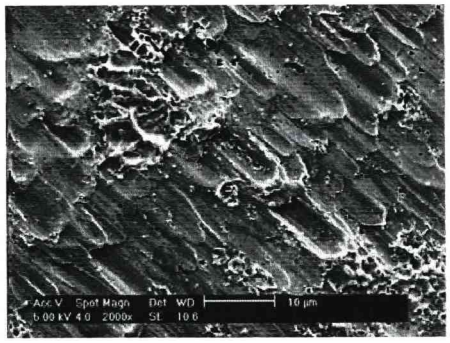

c) Scanned laser irradiation, OL= 4

Fig. 29. Scanned laser irradiation of sample rough area

YHC02, 0.12 J cm^{-2}, 532 nm

In these experiments, with wavelength of 1064 and 532 nm, surface melting (Fig. 28, Fig. 29) was a permanent and unavoidable effect whenever the discoloration of the surface was obtained. Even if attempts were made to limit surface temperature, by wetting the surface or scanning the laser beam on the surface, still some signs of melt were observable.

3.4 IRRADIATION WITH UV 3RD HARMONIC

Using the 3rd harmonic of the Nd:YAG laser, the surface of these samples was irradiated with short pulses at 355 nm, in single pulse, several pulses incident in the same spot or in scanning mode (Fig. 30). The set up for irradiation was the one in Fig. 12.

Fig. 30. The Year of the Horse Coin (YHC04) after irradiation with UV pulses

Varying the energy per pulse from 10 mJ to 16 mJ as well as the distance between the silver surface and the positive lens, the fluence range of irradiation was from 0.05 J cm^{-2} to 0.37 J cm^{-2}.

The cleaning threshold was found at 0.1 J cm^{-2}, but the irradiated site was only visible after 10 superposed pulses at low pulse repetition frequency (1 Hz). At this low fluence the yellow-brown contamination become greyish (Fig. 31 top and bottom), but no damage was observed on the substrate surface, indicating that for this UV wavelength and surface contamination, the cleaning threshold was below the damage

threshold. The colour change can be understood as a diminishing of the yellow-brown contamination layer and consequent approach to the "silver" colour of the metal substrate.

At higher fluence some melting and damage of the surface occurs. This damage threshold was found to be 0.25 J cm^{-2}. The irradiated area was visually detected by a decrease in the yellow/brown coloration and a greyish appearance, as can be observed in Fig. 30.

However for a satisfactory cleaning a number of overscans were needed, usually more than 10, depending on the laser fluence and scanning overlap.

3.5 Assessment of the Cleaning Effect

After the removal of the silver sulphide film, achieved by scanning the UV laser beam on the sample surface, the more obvious change on the surface was the colour modification. The yellow/brown colouration of the contaminated surface became progressively more greyish after each scan superposed on the same stripe area and, after a few overscans a "silver" colour appeared on the surface.

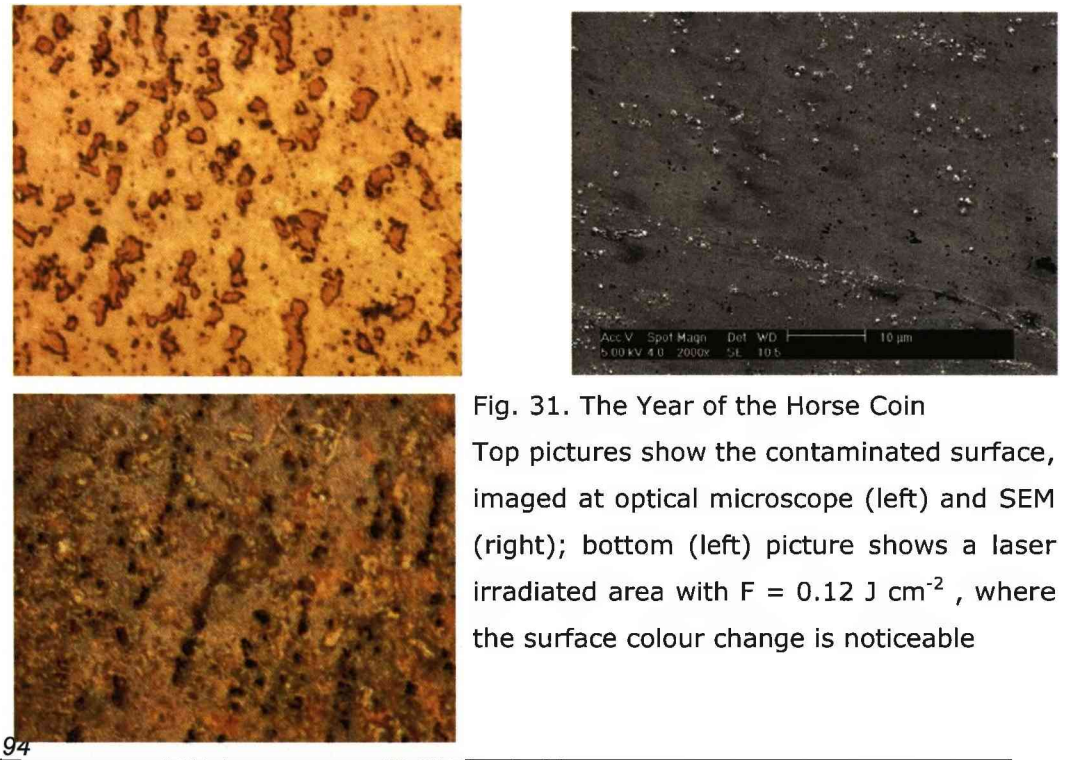

Fig. 31. The Year of the Horse Coin
Top pictures show the contaminated surface, imaged at optical microscope (left) and SEM (right); bottom (left) picture shows a laser irradiated area with F = 0.12 J cm^{-2} , where the surface colour change is noticeable

However it is to be noticed that no change in the brightness of the surface was observed at the naked eye, for low and moderate laser irradiation, meaning that the surface roughness was not altered.

To detect any other alterations on the surface, caused by laser irradiation, the observation of the sample at the optical and electron microscope was performed (Fig. 31 and Fig. 32).

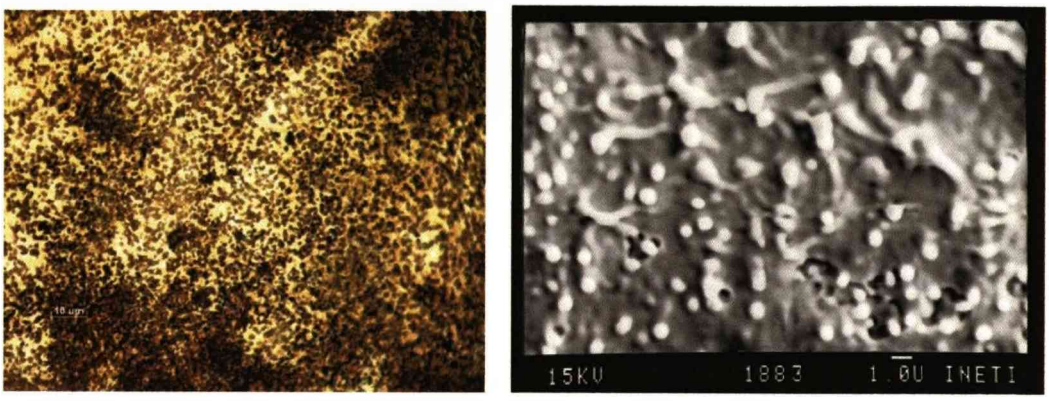

Fig. 32. The Year of the Horse Coin (YHC06)
showing modifications on the surface, after irradiation with 0.37 J cm^{-2}

When no damage occurred on the surface the irradiated area could not be distinguished in SEM and some mark must be used to indicate the irradiated area. This fact corroborates the visual appreciation showing that no permanent modifications or damages have occurred in the substrate.

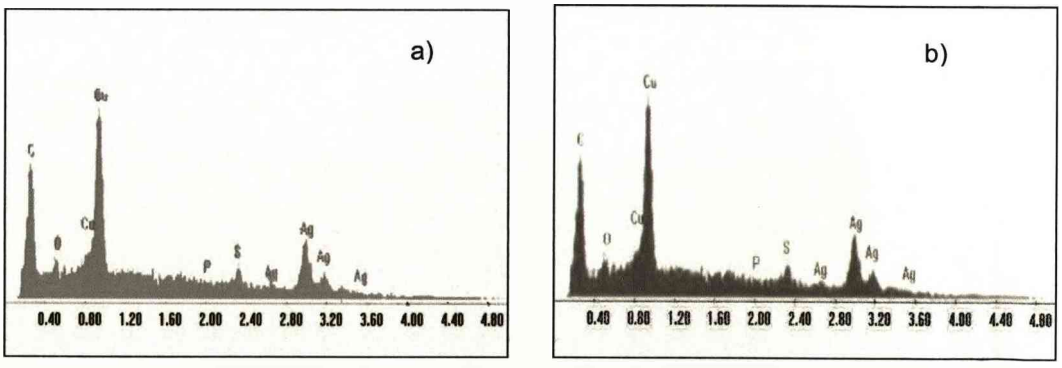

Fig. 33. EDX spectra obtained on the surface of YHC04
before and after UV laser irradiation
a) Spectra of contaminated surface b) spectra of partial cleaned surface

The elemental analysis provided by EDX is not very meaningful as can be seen comparing both spectra in Fig. 33; due to the reduced thickness of the silver sulphide layer, the decrease of the peak of sulphur in EDX spectra is not appreciable, even if a reduced value for the electron acceleration voltage (5 kV) is used in the SEM.

Although the electron microscope used was a high resolution system, it is known that X-rays generated by the de-excitation of atoms heated by primary electrons, are generated from a greater volume of the specimen than would be expected simply from consideration of probe spot size, due principally to the lateral spread of the incident electron; this can explain the small height of S peaks in the thin contamination layer of the tarnished coins when compared with the bulk Ag peaks.

The assessment of the cleaning effect was done by means of the visible spectra of the reflected light and by the measurement of the surface colour using the AvaMouse spectrophotometer.

With this system it was possible to acquire successive reflection spectra and compare the position of the dominant maxima on the spectra or to quantify the surface colour of the cleaned silver surface based on the CIE Lab colour system.

A first record of the reflection spectra for carved (rough) and polished (shining) non irradiated areas was obtained in sample YHC01, as depicted on Fig. 34. It shows that the "pure", non corroded silver presents a fairly homogeneous spectrum in the visible range, while the tarnished areas (referred TARN in the figure) show an increase of intensity in the yellow-red side of the visible spectrum.

It was also visible the intensity decrease of the spectra of the polished (shining) areas when compared with the carved (rough) ones. This was due to the fact that the specular reflected light from the polished areas was not so intense at the detector, as opposed to the diffuse reflected light received from the rough areas.

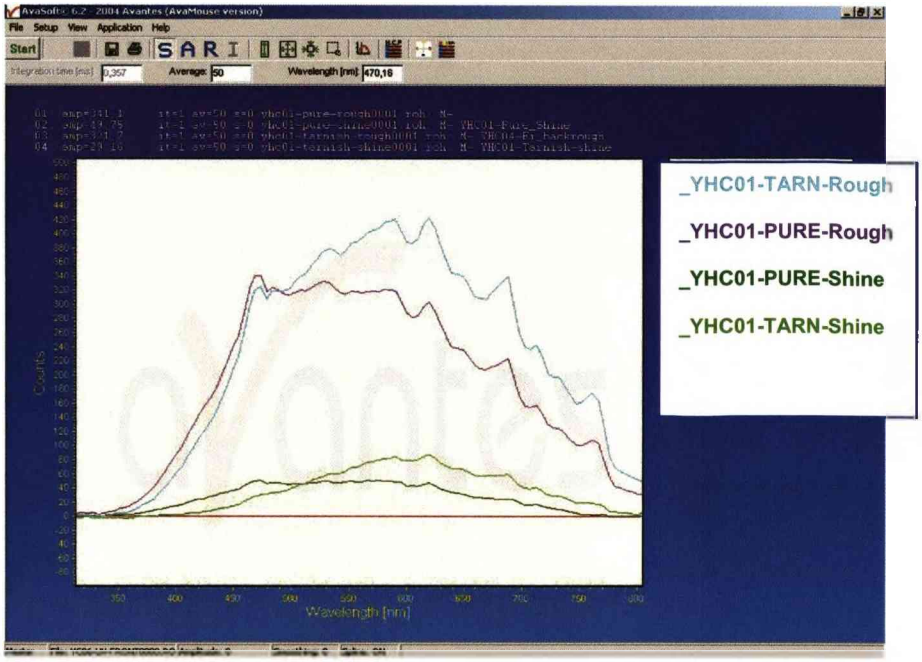

Fig. 34. Visible reflection spectra of original surfaces of sample YHC01 obtained in both non-contaminated and tarnished sides

A set of spectra that has been recorded for different cleaning parameters with the UV radiation is presented on Fig. 35 and Fig. 36; process parameters such as fluence (F), pulse repetition frequency (fp), pulse overlap (OL) and number of overscans (OS) are indicated in the figures.

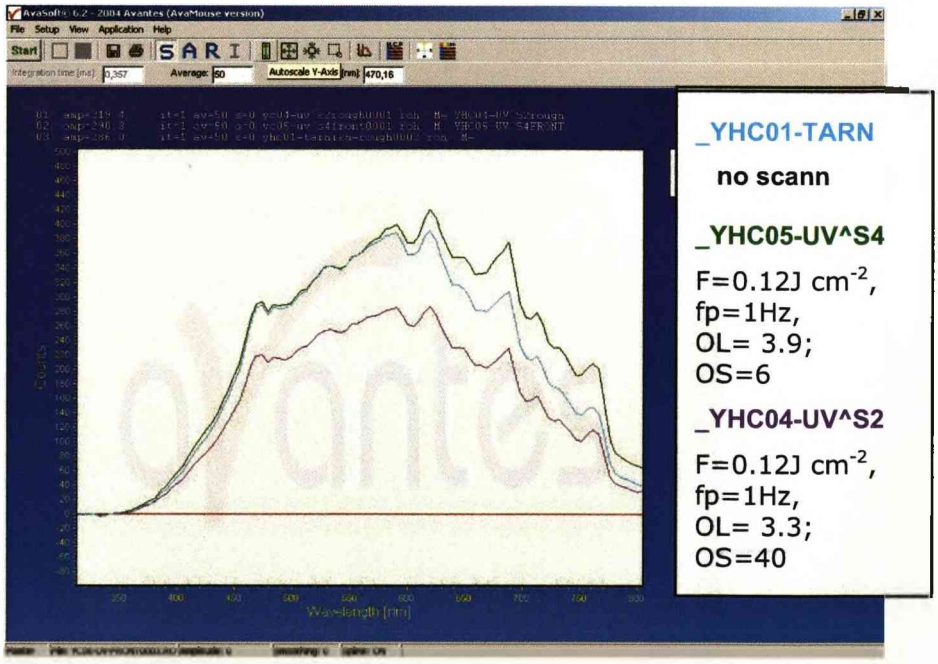

Fig. 35. Visible reflection spectra of tarnished surfaces (YHC01) and under-cleaned areas (YHC04 and YHC05)

Fig. 35 shows the less succeeded cleaning cases of tarnished surface cleaning by a scanned UV laser beam (refs YHC05-UV^Scan and YHC04-UV^S2), together with the spectrum obtained for un-corroded silver (ref. YC01).

The colour spectra of the best succeeded cleaning cases (refs YHC05-UV^Scan and YHC04-UV^S2) are shown in Fig. 36, together with the spectrum obtained for un-corroded silver (ref. YC01).

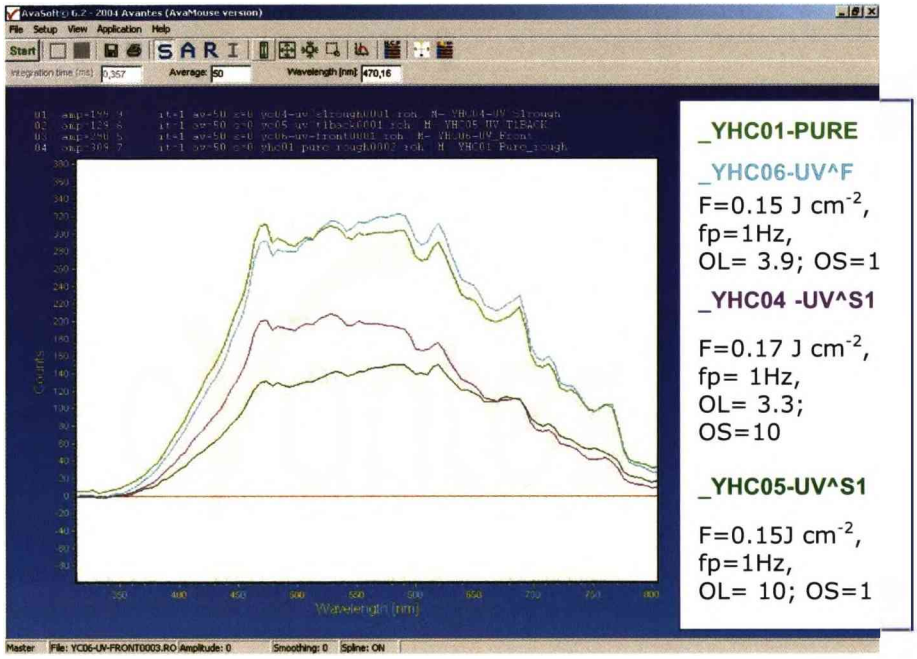

Fig. 36. Visible spectra of original silver surface (YHC01) and cleaned areas

For a more precise quantification of the surface colour modification, the colours obtained are depicted in the CIE colour space (Fig. 37):

The quantitative information related with the colour change of the cleaned area related to the contaminated one can be associated with the cleaning efficiency. It might be expressed by the deviation of the most meaningful coordinate of the colour space, *db* or *da*, or most generally it is expressed in terms of the overall colour change:

$$\Delta E = \sqrt{\partial L^2 + \partial a^2 + \partial b^2}$$

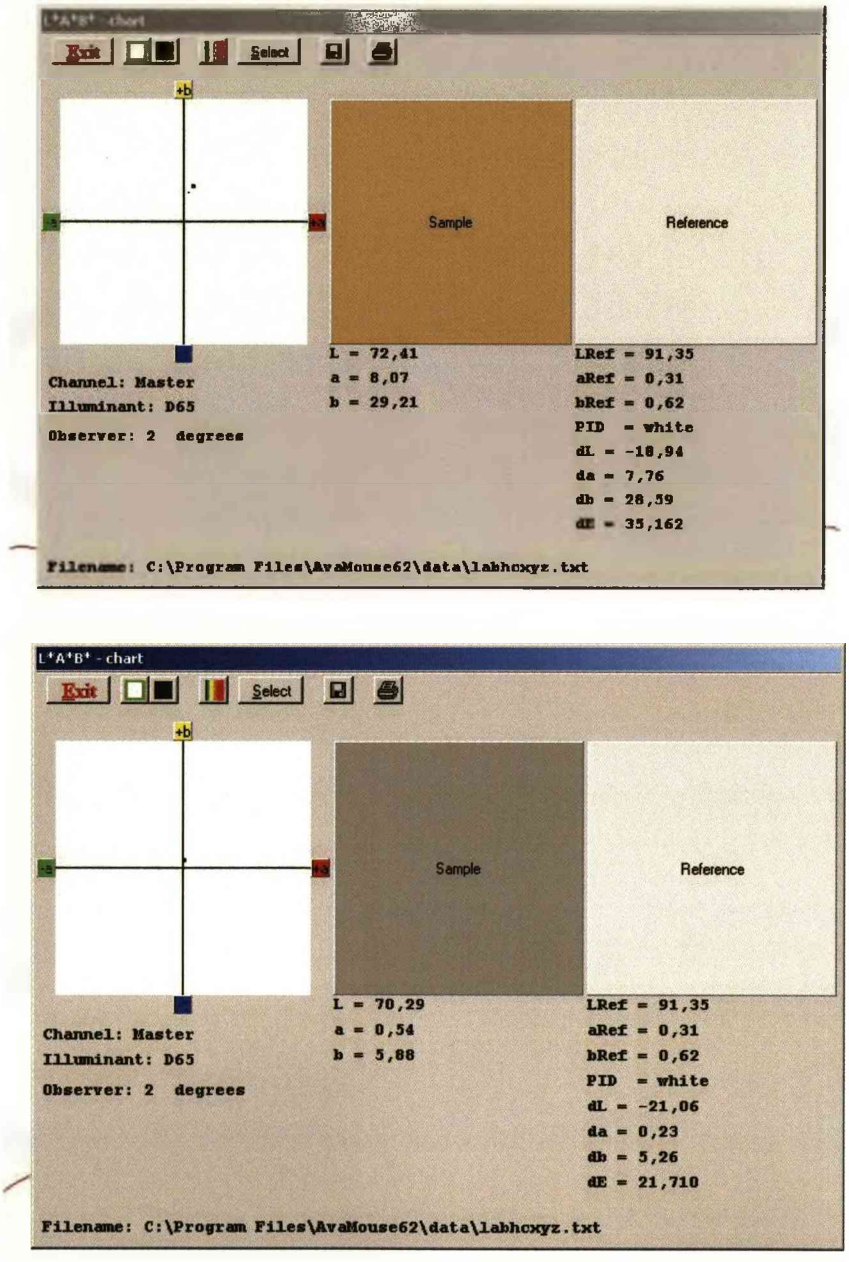

Fig. 37. The Year of the Horse Coin (YHC06), colour measurement tarnished surface (above) and after irradiation with 0.17 J cm^{-2}

The qualitative information obtained in the registered spectra together with the surface colour quantification show the cleaning effect of the UV laser irradiation of the tarnished samples and allow for the assessment of the surface cleaning.

3.6 Discussion of Results and Cleaning Mechanism: Selective Vaporization

Along the experimental tests with the Q-Switched Nd:YAG laser infrared radiation or its 2nd harmonic, it was verified that the coloured silver sulphide layer was not significantly removed without melting of the silver substrate, as could be observed by Optical Microscopy, SEM and EDX analysis (Fig. 20 to 24). For lower fluence no modification was observed on the irradiated surface, but increasing the fluence for higher values ($F \geq 0.2$ J cm^{-2} at $\lambda = 1064$ nm or $F \geq 0.1$ J cm^{-2} at $\lambda = 532$ nm, single pulse) the irradiated surfaces displayed obvious signs of punctual surface melting, such as shallow craters possibly generated by molten material ejection and resolidified material droplets.

In none of these conditions, independently of irradiation conditions, a cleaning effect, this is a removal of tarnished layer, easily detected by its yellow/brown colouration (Fig. 19 and Fig. 37) was observed. Possible cause is that the silver sulphide layer thickness of the order of 0.1 μm, is less than the optical penetration depth of IR and visible laser radiation in this material and so it has not optical thickness enough to absorb the incident energy or to shield the silver substrate from the incident laser radiation.

When comparing the reflection spectrum of the tarnished surface (Fig. 38, pink line) with that of the original pure silver (Fig. 38, green line), it is observed the decrease of the of the tarnished surface reflectivity for wavelengths larger than 500 nm, denoting an little increase in absorption due to the presence of the silver sulphide contamination film on the surface.

Moreover it was found that the damage threshold for these silver surfaces irradiated by the Q-Switched Nd:YAG laser, in the conditions that were mentioned – quasi normal incidence and homogenised laser beam, it was circa 0.2 J cm^{-2}, for the fundamental wavelength of 1064 nm, and lower than 0.1 J cm^{-2}, for the second harmonic at 532 nm but higher, about 0.25 J cm^{-2} for UV radiation at 355 nm, although silver reflectivity decreases from visible to near UV. These values are also pointing an

"optical shielding" effect of the silver sulphide layer concerning the UV laser radiation.

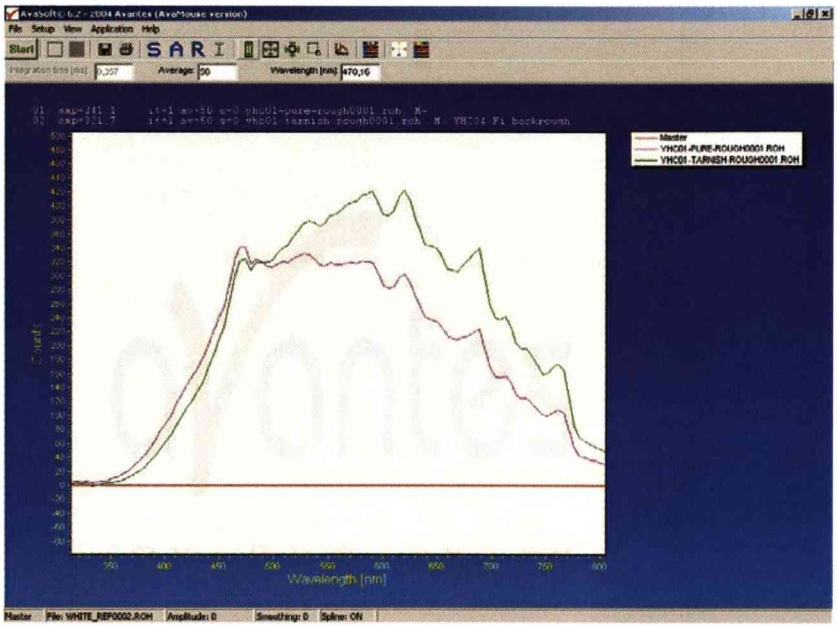

Fig. 38. The Year of the Horse Coin (YHC01&6), optical characterization

The damage threshold fluence is the energy density minimum value for which the substrate starts to present undesirable permanent modifications. Although this fluence level varies with the wavelength, for both IR (λ = 1064 nm) and visible wavelength (λ = 532 nm) this damage took the form of punctual surface melting associated to the photo-thermal primary interaction phenomena (§2.1.2) followed by thermal phase change (§2.2.2).

Being polished silver surfaces, as those found in these samples, highly reflective for visible and IR radiation, direct absorption of incident laser radiation is not a plausible explanation for the observed surface melting of the alloy (around 1050 K, depending on alloy composition). But copper grains imbibed or laying on the surface of the samples (Fig 16) can undergo oxidation in ambient atmosphere due to temperature increase and so acting as absorption centres, this is small inhomogeneities with high absorptivity to these incident wavelengths, leading to local high thermal gradients (photo-thermal mechanism as described in §2.1.2), that in turn generate high pressure centres due to secondary

thermodynamic effects (§2.2.3), that can explain the "explosive" aspect of the surface damages (Fig. 20 to Fig. 23). This "explosive" appearance was increased for water assisted laser irradiation (Fig. 27), due to cooperative action of water vapour.

It is also visible at optical microscope that the melted and resolidified areas on the sample surface (Fig. and Fig. 21) have a white shining appearance typical of silver; the explanation of this appearance might be associated to the silver sulphide chemical decomposition at 473 K, not directly due to laser radiation absorption, but due to a thermo-chemical effect promoted by heat conduction from silver substrate.

From Near IR to the visible, the decrease of silver reflectance with the wavelength (Fig. 39) and inherent increase of absorption is in agreement of lower damage threshold values and shallower micro melt pools for samples irradiated with the visible instead of IR wavelength.

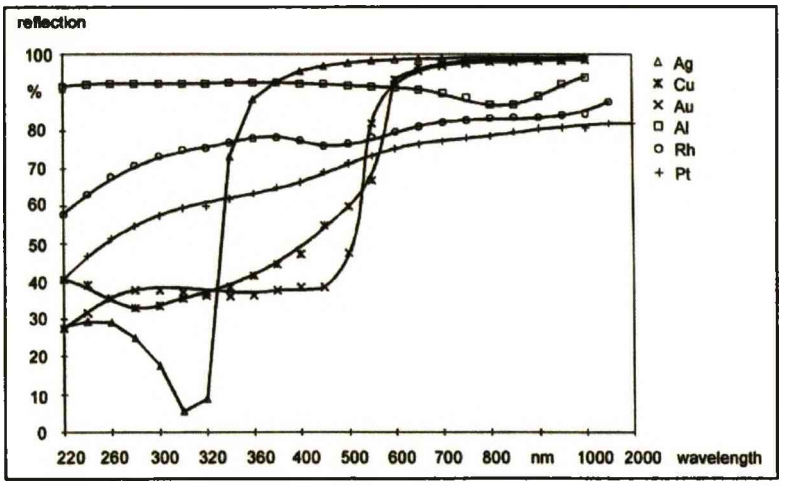

Fig. 39. Spectral reflectance of metals to UV, Visible and IR [99]

When irradiating the tarnished coins YHC with the 3rd harmonic UV wavelength (λ = 355 nm) of the Q-switched Nd:YAG laser with fluence F $\geq$ 0.1 J cm^{-2} it was easily detected by the naked eye a decrease in the yellow/brown colouration without visible loss of shine (Fig. 31) understood as a cleaning effect, this is a removal (partial) of the tarnished layer.

This cleaning effect was further confirmed by optical measurements on the cleaned surface, such as spectral reflection intensity and colorimetric measurements.

The spectral reflection measurements (Fig. 35 and Fig. 36) show a decrease in the reflection intensity of the UV laser cleaned areas; similarly to what happened in the original sample characterization (Fig. 34), the decrease in intensity is associated to a more specular reflection or shinning surface. This is due to the fact that the specular reflected light from the polished areas has a preferential direction for reflection and so is not so intense at the detector, as opposed to what happens with the diffuse reflected light received from all directions from the rough areas of the analysed surface.

The colorimetric measurements, made in agreement with CIE Lab Standards (1976) also gave clear indication of the cleaning effect based on colour characteristics, approaching of the colour components of the laser irradiated areas to the colour of the clean silver reference (Fig. 37). In fact, comparison of the colour measurements made upon a tarnished surface and a laser irradiated surface show a decrease in the "+a" value associated with the red colour component (from 8 to 0.5, in the depicted situation) together with a decrease in the "+b" value associated with the yellow colour component (from 29 to 6).

A decrease in the sulphur content of the surface, before and after laser irradiation would also be a confirmation of the cleaning effect in the chemistry of the surface; however comparison of the EDX spectra obtained in the contaminated surface and in the irradiated surface (Fig. 33) was not clear about this alteration due to the small intensity of the sulphur (S) peaks in the spectra. This might be owed to the reduced thickness of the contamination layer (of the order of few hundreds of nanometres) over a bulk silver and cooper alloy.

Observing the surfaces irradiated with the UV laser irradiation by optical or electron microscopy no thermal damages were detected (Fig. 31) except for much higher fluence (Fig. 32); in this situation micrometric

droplets appeared in the irradiated surface, originating a dull silver surface, as reported by other authors.

When cleaning the tarnished coins YHC with nanosecond 1064 nm or 532 nm laser pulses, laser interaction with the surface gave rise to a light emitting plasma plume and associated "snap" sound, characteristic of laser explosive vaporization (§3.2) or laser shock cleaning (§3.4) mechanisms.

However, during laser cleaning by UV, no plasma plume or sound from the target surface was detected, what is considered indicative of the presence of weak plasma resulting from selective (and non-explosive) vaporization. Yet, possibly a low absorbing plasma was formed, since the energy density used in the experiments was above the threshold for plasma formation at ambient pressure and temperature, that is about 10^7 W cm^{-2} [59] equivalent to 0.07 J cm^{-2} for 7 nanosecond laser pulses. Moreover there were no visible signs of peeling produced by hot or cold spallation.

Knowing that the bonding energy of sulphur to silver ions (2.25 eV) does not match the energy of laser photons at 355 nm (3.49 eV), what sets aside a possible UV photochemical cleaning mechanism (§3.7), the proposed mechanism associated with laser cleaning of silver sulphide contamination from silver surfaces is selective vaporization (§3.1) by UV laser radiation.

Increased absorption of UV laser radiation in the silver sulphide layer gives rise to temperature increase in the contamination layer, leading to material thermal decomposition and vaporization.

The increased absorption of UV laser radiation in the contamination layer, allowing for laser cleaning at lower fluence, together with the high reflectivity values of silver alloy substrate to 355 nm radiation (Fig. 39) allow for a selective or self limited cleaning process, in which the contamination is removed without laser damaging of the substrate.

4. LASER CLEANING BY UV ABLATION

Large Blanks with Organic Contamination

These samples provided by The Royal Mint were contaminated with industrial oil proceeding from the production plant. They consisted on large silver blanks (referred in general as LBC) used to be stamped for medals and coin production.

Similarly to what was described before for the silver coins, the contaminated blanks were analysed in order to characterize the substrate and contamination.

4.1. SUBSTRATE CHARACTERIZATION

The substrate of these large blank coins was 958 silver, a silver alloy formed by 95.8 % silver and the remaining being copper, with no other material being detected in representative amount. They consist of silver disks having 38.5 mm diameter and 3 mm thickness, with non-polished surfaces with an average roughness of 0.10 μm, grey colour and isotropic diffuse reflectance.

Observed at the optical and electron microscope, it was also noticed the presence of darker copper grains embedded or salient over the silver alloy matrix, as noticed previously in the case of the YHC coins (Fig. 16).

4.2. CONTAMINATION CHARACTERIZATION

These samples have been deliberately contaminated with rolling oil before annealing, with specific chemical composition not known *a priori* and presenting a heterogeneous distribution of this contamination on the surfaces.

In some areas of the silver surface, the oil formed a continuous transparent or diffusive thin layer with variable thickness only noticed by the yellowish hue. Since a clean silver surface should be grey, and in order to analyse the cleaning effect in what concerns colour alterations, the oil contaminated surface was characterized by colorimetry (Fig. 40).

The colorimetric results provided by the Ava software show that, in the contaminated sample surface the "b" component related with the yellow colour by the CIE Lab standards (1976), has an increased value (+b ≅ 5) when compared with the reference "pure" (clean) silver surface (+b ≅ 0). Not so meaningful but also reported is an increase in the luminosity (L) of the contaminated sample surface (dL ≅ 4), and also an increase of the green component (-a) of the colour surface (da ≅ -2).

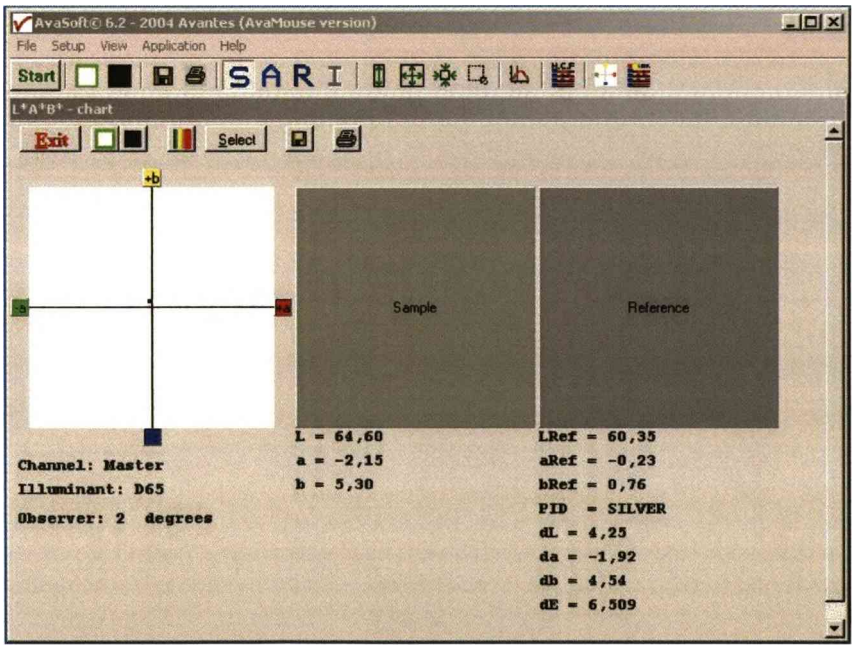

Fig. 40. Optical characterization of a contaminated sample referred to a non-contaminated one
The yellow hue is quantified by the parameter +b = 5.30

In other areas or samples the distribution of the oil on the silver surface was discontinuous, occupying millimetric or submillimetric areas; the colouration and thickness (in the range of few micrometers) was variable, not only from one sample to another, but also in the same surface.

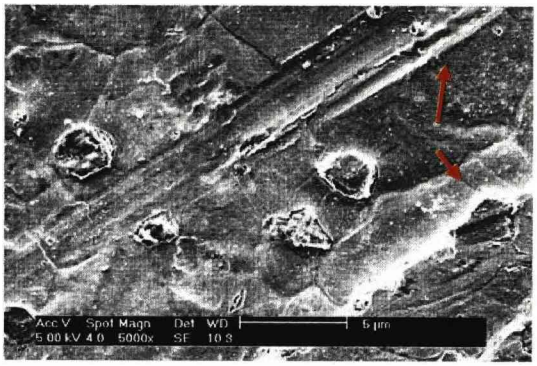

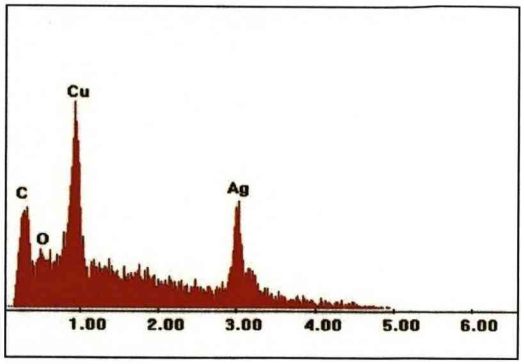

Thin film contamination. a) SEM b) EDX

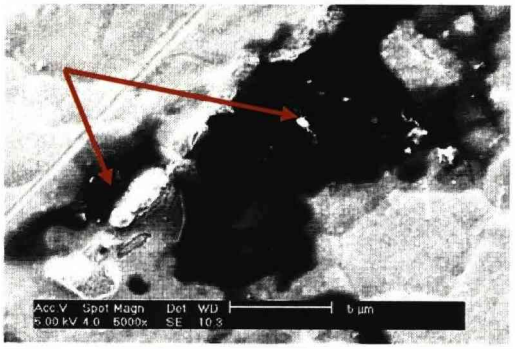

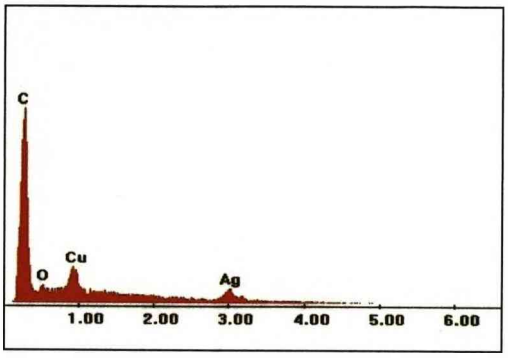

Thick contamination. c) SEM d) EDX

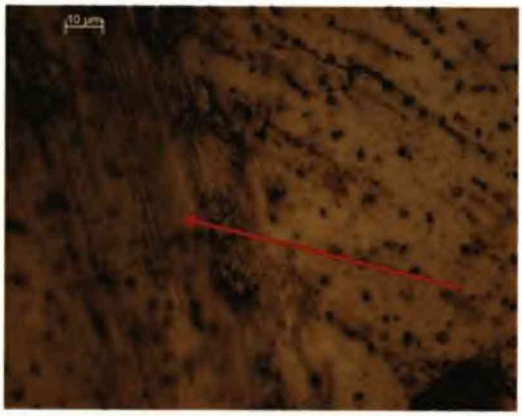

e) Other greasy contamination f) Other greasy contamination

Fig. 41. Surface of LBC-01 with several oily contaminations (pointed by arrows)

In order to have a better knowledge of the contaminant, and since some of these areas were too small for the colorimetry equipment, the samples were imaged by (Fig. 41) optical and electron microscopy and their chemical composition analysed by EDX (X-ray energy dispersive spectroscopy) and FTIR (Fourier transform infrared spectroscopy).

The main occurrence of contamination was a transparent yellowish oil layer (Fig. 40) with variable thickness, mainly distributed along lines on the

sample surface (pointed by arrows in Fig. 41 a, e). But other oil deposits (also pointed by arrows on Fig. 41 c, f) with darker colouration and different surface distribution were also detected on the sample surface.

The EDX spectra of the contamination (Fig. 41 b, d) always showed a large peak associated to carbon, as it would be expected for organic compounds found in industrial oils, together with a significative presence of Ag and Cu, originated in the silver alloy substrate.

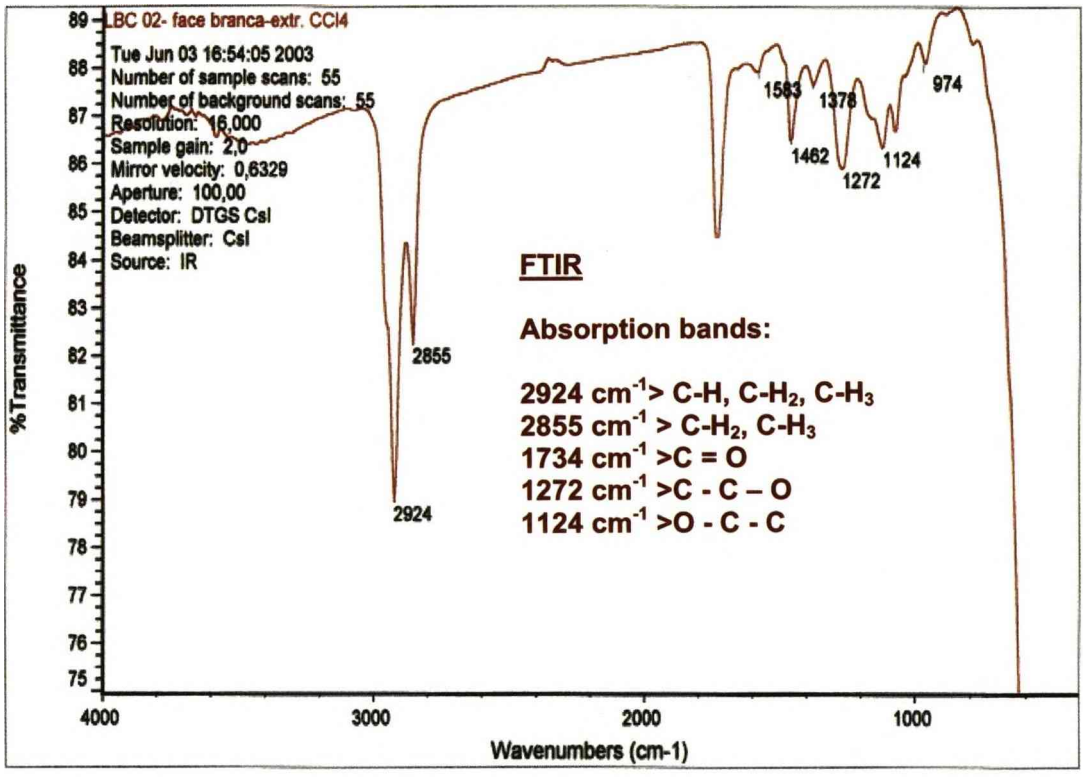

Fig. 42. FTIR spectrum of oily contamination on LBC02 surface

Due to the general complexity and wide variety of organic substances used in lubricating oils, FTIR analysis was also used to characterize this contamination. Diluting a small amount of the oily contamination in acetone, it was possible to analyse it by Fourier transform infrared spectroscopy (FTIR) and the obtained spectra (Fig. 42) shows the presence of several C-C, C-O, and C-H groups, characteristic of aliphatic hydrocarbons used in industrial lubricants.

4.3. IRRADIATION WITH IR WAVELENGTHS

The large blanks contaminated with oil (LBC) have been irradiated with IR laser pulses (λ = 10600 nm and λ =1064 nm) at low fluence ($F \leq 1$ J cm^{-2}) in the microsecond range but no alteration on the contamination or silver surface was detected.

Irradiating the oiled surface with the long Q-Switch Nd:YAG laser (τ_p = 70 ns) at low fluence no effect was observed, but at fluence values $F > 2$ J cm^{-2}, it was observed an increase of the opacity and yellow hue of the contamination layer, associated with thermal degradation.

These samples were also subjected to a few irradiation tests with low fluence ($F < 0.2$ J cm^{-1}) short pulse Q-Switch Nd:YAG laser (τ_p = 7 ns), but surface yellowing after laser irradiation was soon detected possibly due to thermal degradation of the industrial oil.

So these samples have been irradiated with short (nanosecond) laser pulses, and short wavelengths (visible and UV), aiming to avoid thermal degradation of the contamination.

4.4. IRRADIATION WITH VISIBLE WAVELENGTH

The contaminated surfaces have been irradiated as described in § 2.5 - Experimental Set-Up and Procedure. However, taking in consideration the non uniform distribution of the contamination, the surface was irradiated in scanning mode, to obtain larger irradiated areas for a more general observation of the effects.

Laser irradiation took place quasi perpendicular to the sample surface, mounted on a translation stage, with the homogenised Q-Switched Nd:YAG laser beam, in the following conditions:

1. irradiation of the sample surfaces in scanning mode, allowing the scanning speed (v_{scan}) to be varied from 1 to 10 mm s^{-1}, the pulse repetition rate was varied from 1 to 10 Hz resulting in pulse overlap (OL) values from 1 to 80,

2. use of the raw beam after homogenisation, without any focusing lens in order to increase the area covered in each scan,

3. use of short distance from samples to the diffuser (40 mm) in order to avoid simultaneously undesirable contamination of the diffuser plate and also undesirable increase of the spot size (due to diffusion),

4. in the above conditions, the beam diameter on the sample surface was measured to be 8 mm,

5. irradiation with the 2nd harmonic wavelength (λ = 532 nm); the pulse energy range was from 10 mJ to 90 mJ, that is, the energy density range from 20 mJ cm^{-2} to 180 mJ cm^{-2}.

In the first set of scans, the pulse repetition frequency was f_p = 1 Hz, originating on the surface spot overlap OL = 1.6 (for v_{scan}= 5 mm s^{-1}) to 8 (for v_{scan} =1 mm s^{-1}) with the energy densities up to 0.2 J cm^{-2}.

Almost no changes could be detected on the surface in this first set of scans, except for a slight increase in the gloss of the scanned area at the higher fluence. This was only observed at naked eye and , but the surface alteration wasn't observable on the optical microscope, nor the scanned area detectable, probably due to the strong illumination of the microscope, normal to the sample surface.

Observation by SEM (Fig. 43) revealed minor damages on the substrate caused by laser irradiation (Fig. 43 a), in the form of shallow craters possibly generated by expansion and resolidification of melted material, but also remaining contamination (oil) was detected on the irradiated area (Fig. 43 b).

Knowing that the intensity of the peaks in the EDX spectra depends on several factors such as the amount of time spent in the spectra acquisition, the surface morphology, or the sensitivity of the detector to different energy ranges, a quantitative analysis could not be done in these conditions. However a semi quantitative analysis of the EDX spectra (Fig. 44) over an

area irradiated by laser, shows a visible decrease of the relative intensity of the peak corresponding to the presence of carbon, indicating a certain removal of the organic compound, the lubricant oil.

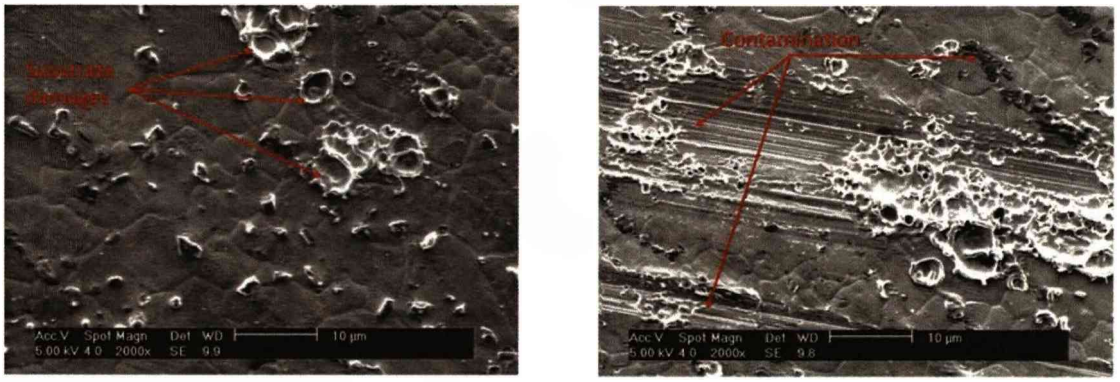

a) OL = 8, fp=1Hz, F = 0.17 J cm^{-2} b) OL = 2.7, fp=1Hz, F = 0.17 J cm^{-2}

Fig. 43. SEM images of laser scanned silver blank (LBC01) at λ = 532 nm, with different pulse overlap (OL)

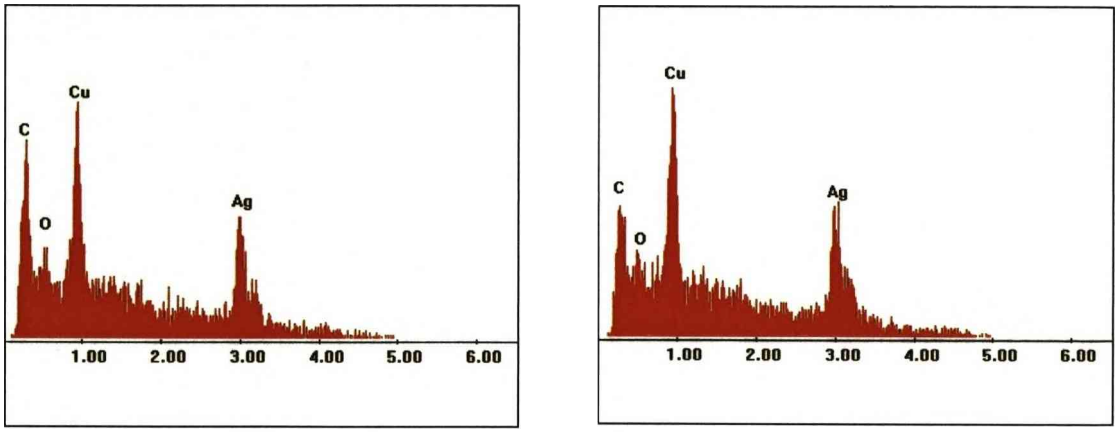

a) Contaminated surface (LBC01) b) Laser scanned zone

Fig. 44. EDX before (a) and after (b) laser irradiation (at λ = 532 nm, OL = 8, fp = 1 Hz, F = 0.17 J cm^{-2})

It was also noticed that the acquired spectra has a large component of background or Bremsstrahlung noise. This is usual when analysing the low energy part of the spectra where carbon and oxygen have their characteristic energies; moreover, the acquisition time to obtain the spectra was kept short in order to avoid the contamination of the microscope column with contamination vapours and in this case the ratio between the specific X- radiation, characteristic of each element, and the continuous radiation (Bremsstrahlung or background noise) is smaller. The eventual

presence of other impurities mixed or sticking on the oiled sample surface can also lead to a more noisy spectra.

A second set of scans of the laser beam on the contaminated sample was experimented, maintaining the values of energy per pulse (10 to 90 mJ) and the scanning speed (1 to 5 mm s^{-1}) but increasing the pulse repetition rate to 10 Hz, and consequently the pulse overlap from 16 to 80. All the other irradiation conditions remained the same.

In this situation it could be observed the fumes or vapours escaping from the contaminated blank surface LBC01, during laser scanning irradiation of the samples and the transparent oil film on the silver surface became more dense and opaque (Fig. 45) as the energy density or pulse overlap increased.

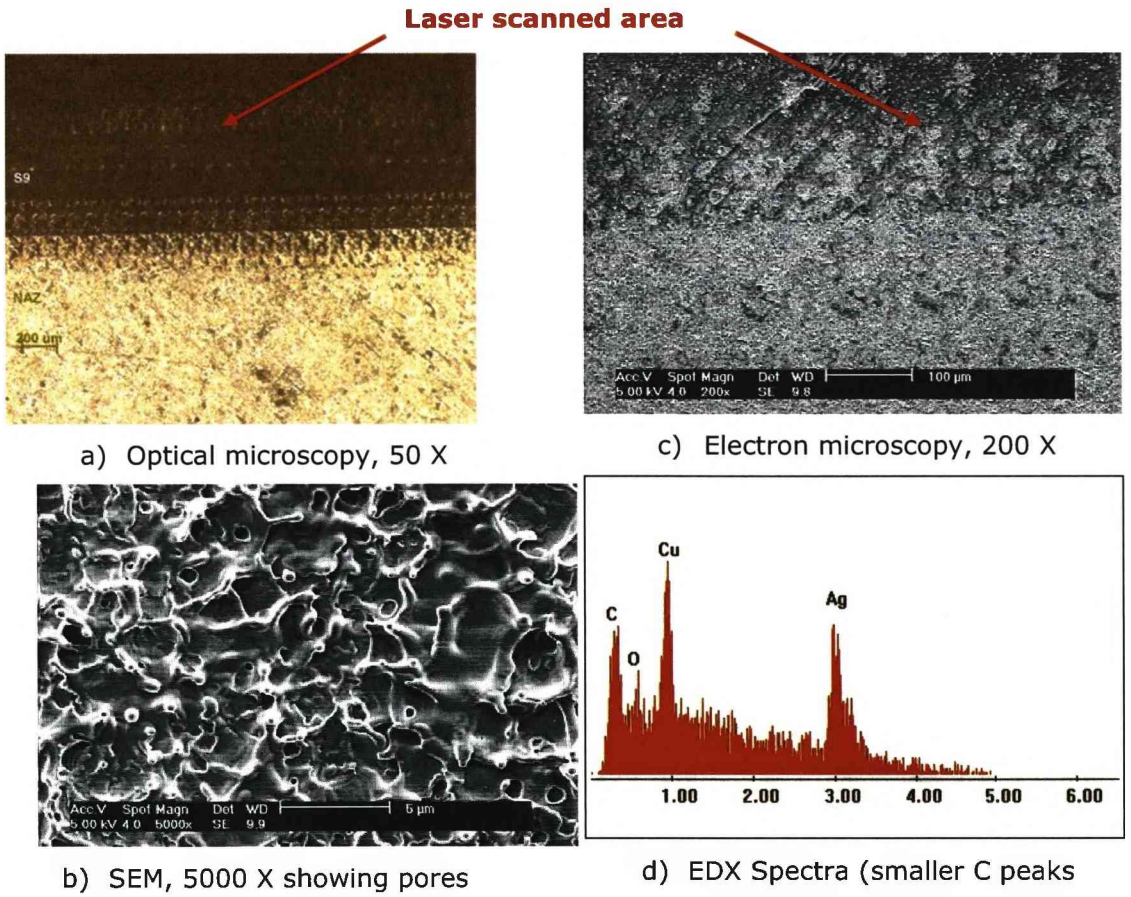

a) Optical microscopy, 50 X

c) Electron microscopy, 200 X

b) SEM, 5000 X showing pores

d) EDX Spectra (smaller C peaks

Fig. 45. Laser scanned silver contaminated coin blank (LBC01) at λ = 532 nm, F = 0.17 J cm^{-2} fp=10 Hz, vscan= 1 mm s^{-1}

Figure 45 shows the surface of the contaminated blank LBC01 after laser irradiation in the more severe conditions- high pulse repetition rate and low speed. It can be seen in the optical microscopy image (Fig. 45 a) that the transparent rolling oil became darker and more opaque on the laser irradiated area.

It can also be seen from the pictures of electron microscopy (Fig. 45 b) that the laser scanned area presents signs of melting, such as craters and droplets. On the SEM image of higher magnification (Fig. 45 c), one can also see over the surface, pores of circa 1 μm diameter (smaller than the craters) indicating the generation and escaping of vapours, eventually due to thermal decomposition of the contamination.

The EDX spectrum (Fig. 45 d), acquired on a laser irradiated area show a relative decrease in the height of the carbon peak, indicating a possible partial removal of the organic material.

The FTIR spectrum was obtained on the oil sample removed from the laser scanned area (Fig. 46) with visible wavelength (λ = 532 nm) at fluence F = 0,17 J cm^{-2}, pulse repetition rate up to 10 Hz and various scanning speed up to 5 mm s^{-1}. This spectrum shows a clear decrease of the peaks at 1736, 1272 and 1124 cm^{-1}, associated with carbon-oxygen bonds, indicating a process of thermo-chemical decomposition of the hydrocarbon oil, usually designated by "charring" what would be in agreement with the darker aspect detected by visual inspection.

With moderate irradiation conditions, that is, with the same values of energy density per pulse but lower pulse frequency or higher scanning speed, with overlap values in the range of 10 to 40, still some increase in the opacity of the oil layer was visible, as well as some yellowing on the surface.

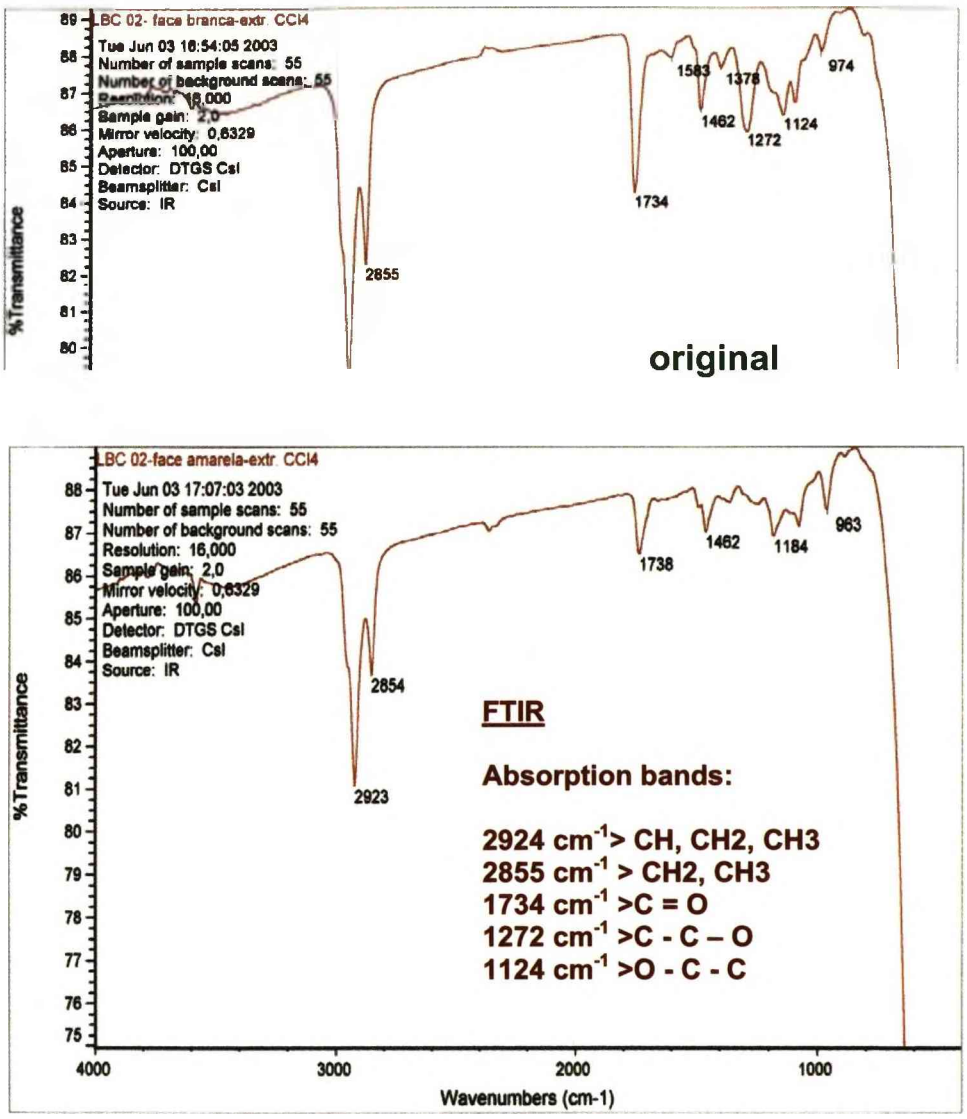

Fig. 46. FTIR spectra of oil contamination on the surface of blank LBC02
original contaminated surface (above) and
laser irradiated surface at λ = 532 nm, F = 0.17 J cm^{-2} , fp= 10 Hz, (below).

4.5. IRRADIATION WITH ULTRAVIOLET WAVELENGTH

A few initial experiments* took place with a KrF excimer laser COMPEX, emitting short pulses of τ_p = 20 ns and λ = 248 nm with 1 Hz in a fluence range of F= 0.1 to 0.7 J cm^{-2}.

* Few experiments because no excimer laser was available at our laboratory.

In these initial experiments with UV irradiation of silver blanks with organic contamination, it was visible at the naked eye a more or less pronounced cleaning effect (depending on the irradiation conditions) on the contaminated surface. This cleaning effect consisted in reflectivity increase of oiled surfaces (Fig. 47 a); other than that, when observed at optical microscope no damage was visible in the metal surface.

Once more, a systematic experimental work was done using the laser system and the optical set up depicted in Fig. 12 and described in §2.5 – Experimental Set-Up and Procedure. The surface of these silver blanks (LBC) was irradiated in scanning mode with short laser pulses (7 ns) at 355 nm (Fig. 47 b) with different irradiation parameters, such as fluence (F) and pulse overlap (OL).

When using the UV wavelength of the Q-switched Nd:YAG laser system, the number of overscans was also a variable parameter, this is the number of times that the same area on the sample surface was irradiated with laser scanning keeping the same irradiation parameters. Increasing the number of superposed scans instead of increasing the overlap or incident fluence allowed for removal of the contamination in small fractions per pulse avoiding undesired temperature increase.

Varying the energy per pulse from 2 mJ to 16 mJ as well as the distance between the silver surface and the positive lens, the fluence of laser irradiation on the sample surface was increased from 0.02 to 0.10 J cm^{-2}.

The scanning of the laser beam on the oily surface resulted in bands of visibly increased reflectivity when compared with the non-affected zones (NAZ). Fig. 47 b) shows the stripes or bands (I, II and III) produced on the surface of the oil contaminated blank LBC02 after irradiation in scanning mode at UV wavelength λ=355 nm, and pulse repetition frequency f_p=1 Hz. The three bands shown in the picture Fig. 47 b) are representative of three different cleaning conditions:

- Band I - Under cleaned surface. It was irradiated with laser fluence F=30 mJ cm^{-2} pulse scanning overlap OL=5 and the same area was overscanned 4 times (OS = 4). The result is a band on the sample

surface not so dull and not as yellow as the oily contaminated surface.

- Band II - Cleaned surface. Irradiated with a laser fluence F=60 mJ cm^{-2}, scanning overlap OL=5 and two scans over the same area (OS = 2). The result is a greyish reflective band on the sample surface, much more shining that the contaminated surface.
- Band III – Over heated surface. Irradiated with a laser fluence F=100 mJ cm^{-2}, scanning overlap OL=5 and also two scans over the same area (OS = 2). The result is a more reflective band on the sample surface, but presenting remains of the contamination.

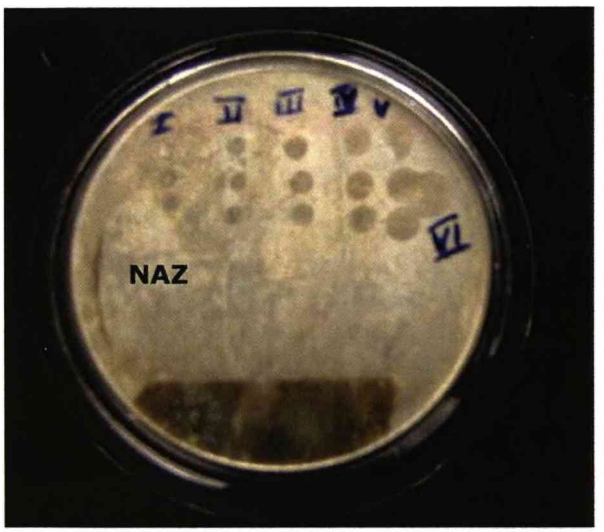

a) Silver blank (LBC03) irradiated with 248 nm laser pulses at fp = 1 Hz:

I- F= 0.7 J cm^{-2}
II- F= 0.6 J cm^{-2}
III- F= 0.5 J cm^{-2}
IV- F= 0.4 J cm^{-2}
V- F= 0.2 J cm^{-2}
VI- F= 0.1 J cm^{-2}
Bottom: scanned cleaning

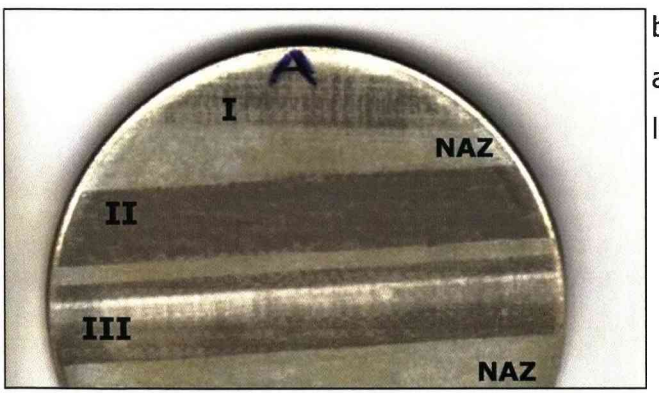

b) Silver blank after scanning with 355 nm laser pulses at fp = 1 Hz:

I- F=0,03 J cm^{-2}
II- F=0,06 J cm^{-2}
III- F=0,10 J cm^{-2}
IV- NAZ non affected zone

Fig. 47. Silver blanks contaminated (LBC02, LBCO3) after scanning with UV laser irradiation (areas marked)

In these photos is well visible the contrast of colour and shine between the UV laser irradiated areas (marked with roman numerals) and the non-affected zones (NAZ).

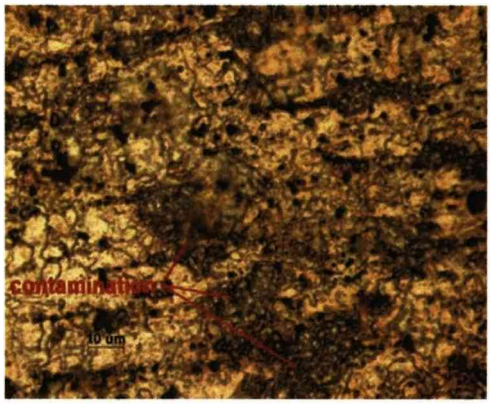

a) original contaminated surface (NAZ)

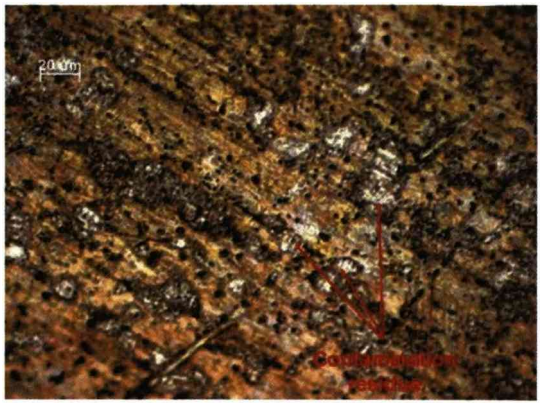

b) under cleaned surface, band I (F=30 mJ cm^{-2} OL=5, OS=4)

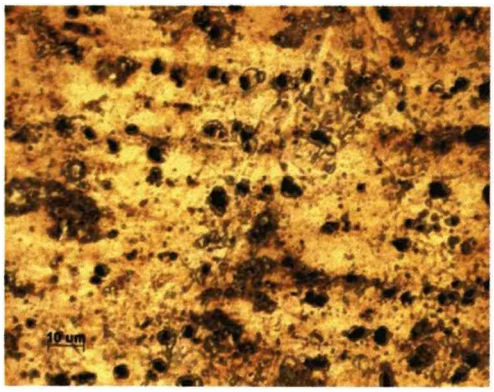

c) cleaned area band II

X10 (left), x2500 (right) (F=60 mJ cm^{-2}, OL=5, OS=2)

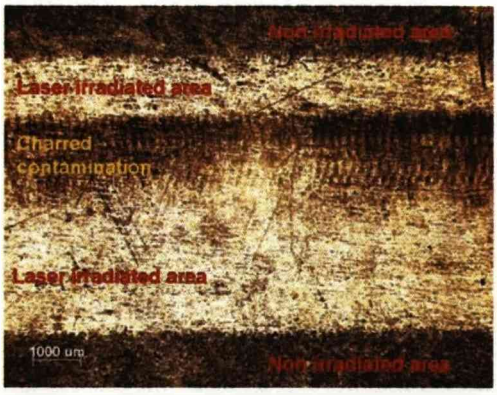

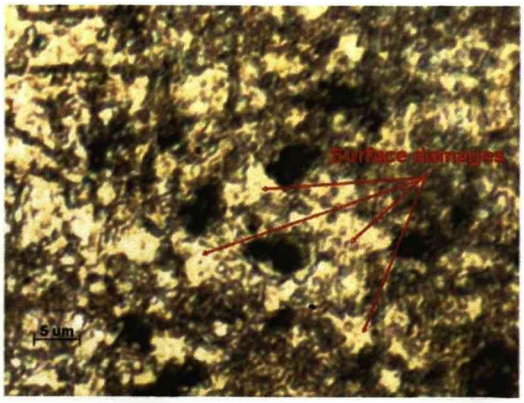

d) over cleaned area band III

X10 (left), x2500 (right) (F=100 mJ cm^{-2}, OL=5, OS=2)

Fig. 48. Large blank contaminated LBC02

scanned with UV (λ = 355 nm) laser irradiation

Optical microscope images acquired at sample LBC02 surface (Fig. 48 a) still show the presence of vestiges of original contamination in undercleaned band I (Fig. 48 b), overheated (or singed) oil residues (Fig. 48 d) in over heated band III, and more clean and undamaged area in band II (Fig. 48 c).

The cleaning threshold, as said, is the minimum value of energy density for which the surface contamination starts to be removed due to laser scanning irradiation and simultaneously, the surface characteristics such as colour and shine, start to be modified, approaching the characteristics of the cleaned precious metal substrate.

Scanning the contaminated surface with low overlap and increasing the pulse fluence, the cleaning threshold was determined, at 0.03 J cm^{-2} with incomplete removal of the contamination (Fig. 48 b), whereas the damage threshold for the silver surface substrate, irradiated by single pulse was not found for this wavelength in the fluence range available, 0.35 J cm^{-2} maximum.

It was also observed that excessive energy input due to high energy per pulse, high pulse repetition rates or to the presence of hot spots in the laser cross section could cause a visible overheating of the substrate and contaminant layer, resulting in carbonization of the organic film (Fig. 48 e), damage of the underneath silver surface (Fig. 48 f) or even both.

4.6. Assessment of the Cleaning Effect

The assessment of the cleaning effect was done comparing laser irradiated zones with a "pure" (i.e. clean) sample or with non affected zones on the surface of the same contaminated sample (LBD), since the specific characteristics of the contamination was variable from sample to sample.

Due to the yellowish hue indicative of the presence of this contamination the characterization of different areas was done by colorimetry, and the chemical composition by EDX. FTIR was also used, but seldom, because

this technique requires a significative amount of contamination material to be removed from the surface, not available when small test areas were irradiated.

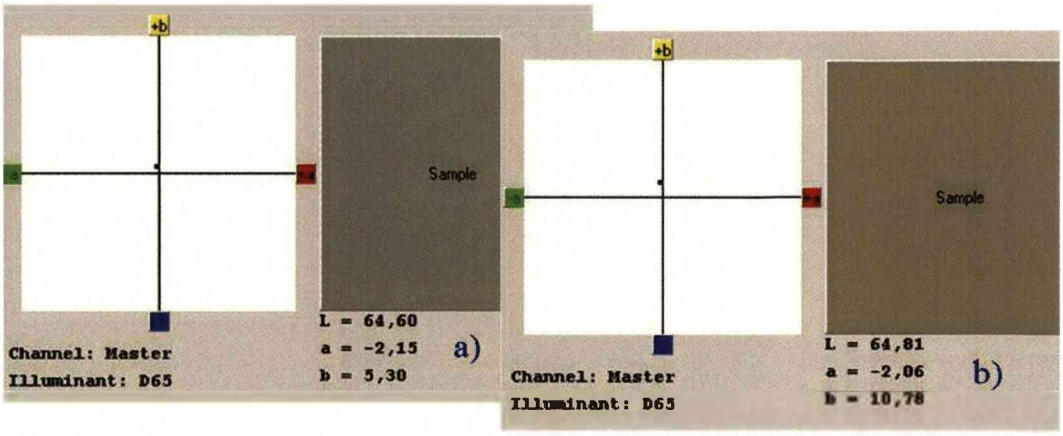

Fig. 49. Colour measurement on silver surface contaminated
a) LBC01, before irradiation; b) LBC02 irradiation at λ = 532 nm, F = 0.15 J cm^{-2}

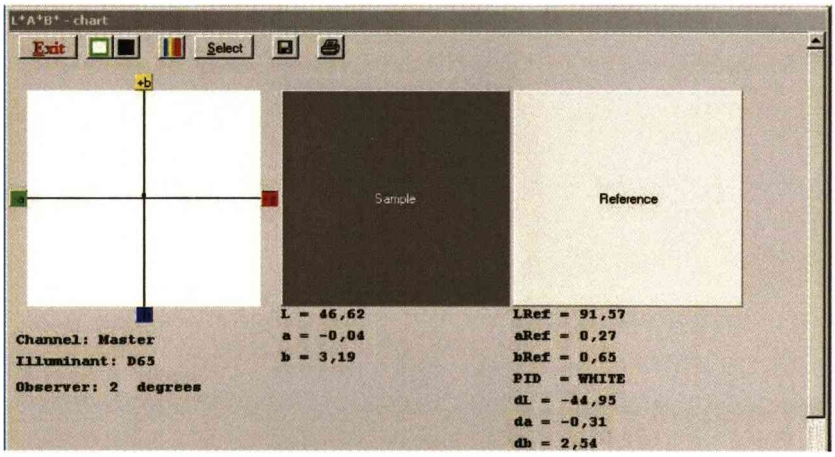

Fig. 50. Colour measurement on silver surface contaminated (LBC02)
Laser irradiated with 355 nm, F = 0.06 J cm^{-2}

Figure 49 and Fig. 50 show the values of colour measurement obtained on the contaminated surface (a), on the irradiated surface with visible 2nd harmonic-532 nm laser scanning (b), and on 3rd harmonic 355 nm laser cleaned area (Fig. 50).

These measurements, depicted on the colour space CIE Lab, show that after laser scanning with the visible radiation of the Nd:YAG 2nd harmonic, the yellow component of the colour ("+ b") in the irradiated

area was enhanced (+b ≅ 11), in respect with the initial yellow hue (+b ≅ 5) associated to the organic contaminant, confirming the visual perception obtained along the irradiation tests with this wavelength (λ = 532 nm).

The areas scanned with UV irradiation (λ = 355 nm) brought the colour coordinates (+b ≅ 3) nearer the white reference (+b < 1) (Fig. 50), but still denoting an incomplete cleaning.

The elemental analysis by EDX shows reduced size of the peaks associated with carbon and oxygen elements in comparison with the Ag peak, denoting a clear decrease of the organic contamination at the surface after laser irradiation (Fig. 51 and Fig. 52).

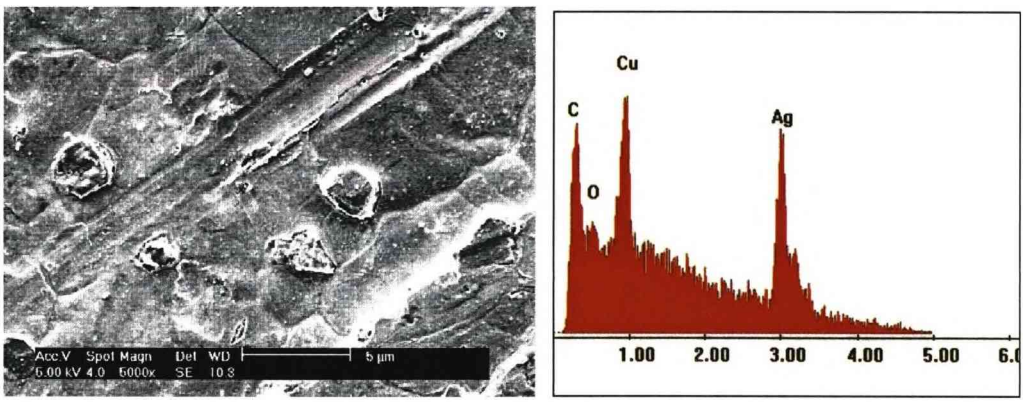

Fig. 51. Silver surface contaminated, before laser irradiation

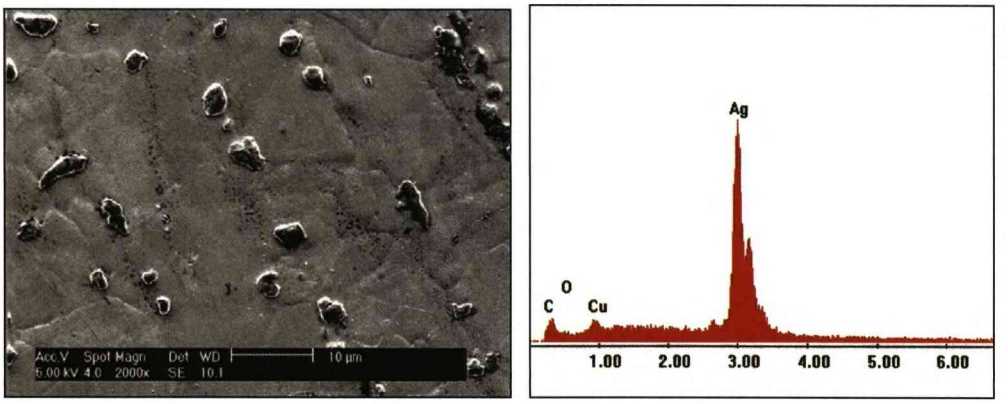

Fig. 52. Silver surface contaminated with industrial oil after irradiation with 84 mJ cm^{-2} at 355 nm (E=4.2 mJ)

It can also be observed that the spectrum in Fig. 51 is much noisy than the spectrum in Fig. 52. This is due to the fact that the acquisition time

used to obtain the EDX spectra of the contaminated surface before laser irradiation (Fig. 51) was shorter than that used for the laser cleaned surface (Fig. 52), in order to detect and identify the composition of the surface contamination but avoiding the contamination of the microscope with vapours from the sample. In this situation the continuous X-ray radiation has a higher relative contribution to the spectra, having an additive effect on the peaks specific of the elements present, increasing their height, mainly for those emitting X-rays with lower specific energy.

This fact, and the irregular distribution of copper particles in the sample surface, can also lead to the decrease of size of the peak associated the L line of copper, on the EDX spectrum obtained on the laser cleaned surface.

The decrease of organic contamination on the surface after laser irradiation is also observed on the SEM image (Fig. 52), corroborating the visual inspection and the colour measures obtained over the oiled and cleaned surface.

However, the EDX spectrum of Fig. 52 still shows the presence of carbon and oxygen after laser irradiation of the surface denoting an incomplete cleaning action.

The microscopy observations made also showed some residual grease mainly around the copper grains and other defects, as shown in Fig. 51, although the thin transparent organic contamination on the silver surface was difficult to be observed at the optical microscope.

A fume extraction system was used, but some redeposition [100] of decomposed products or vapour condensation could also take place on the silver surface.

4.7. Discussion of Results and Cleaning Mechanism: UV Photo-chemical Mechanism

Due to the small thickness and optical properties to the visible light (transparency) of the rolling oil contaminating the silver surface, the laser beam with visible or near infra-red wavelength was transmitted through

the contaminant layer, possibly with minor absorption, leading to photo-thermal heating (§2.1.2) of the silver alloy substrate.

The temperature increase of the rolling oil contamination, due to thermal conduction from the metal substrate, might originate thermal degradation such as breaking of the organic molecule in smaller species, loss of oxygen and hydrogen, leading to an increased presence of carbon (carbonization or charring) and eventually polymerization of the organic residues causing increased viscosity and opacity.

When irradiating the contaminated surfaces with long CO_2 and SFR Nd:YAG laser pulses, in the range of tens of microseconds, no effect was observed; this was probably due to the fact that the long duration of the pulses associated with the high thermal conductivity of the silver lead to significative thermal losses by conductionm [40], limiting the surface temperature increase.

Using short pulses (nanosecond regime) IR or visible wavelengths at low fluence ($F \leq 0.2$ J cm^{-2}) or low repetition rate (f_p = 1 Hz), the temperature at the substrate surface could punctually rise up to the melting point; this was evidenced by the shallow craters and ejected droplets visible at a few sites by SEM on the substrate surface (Fig. 43 a) to b); however for these irradiation parameters no significative modification was detected on the contamination layer (Fig. 44 a to b), and so no cleaning effect was observed.

Irradiating with short laser pulses with IR or visible wavelength, at higher fluence ($F \simeq 0.2$ J cm^{-2}) or higher pulse repetition rate (f_p = 5 to 10 Hz), the substrate surface temperature increase due to the absorption and thermalization of laser radiation lead to generalized surface melting (Fig. 45 b); subsequent conduction to the contaminant layer could have resulted in partial carbonisation of the organic contaminant by thermo-chemical degradation (§2.2.4). This is supported by the observation of the decrease of the peak of C = O (1734 cm^{-1}) in FTIR spectra (Fig. 46) realized on a sample of contamination removed from the coin surface LBC02 after irradiation at 532 nm.

After laser irradiation with IR or visible wavelength at moderate fluence, the surface residues become of darker or more intense yellow colour and less transparency (Fig. 45a and 49 b), giving to the silver surface an appearance "less clean" that it had prior to laser irradiation; this also point out the a thermo-chemical effect, such as thermal degradation or incomplete carbonization of the oil contaminant.

Comparing the results obtained after UV (at 248 or 355 nm) short pulse (few nanoseconds) irradiation (Fig. 52) with the results obtained with IR or visible laser wavelength, it is evident for the first case, the absence of thermal effects such as melting of the silver substrates (Fig. 43) or darkening of the organic contamination (Fig. 45).

Although some temperature increase usually takes place with UV laser irradiation, the thermal effects are only detected at higher UV fluence values, such as F = 100 mJ cm^{-2} (Fig. 48 d), in the form of slight defects on the silver surface morphology and alteration of the contamination.

Other than that, the removal of the contamination by UV laser radiation either at 248 nm or 355 nm, is demonstrated by the decrease of the dull appearance and yellow hue characteristic of oiled surfaces, detectable at the naked eye (Fig. 47) or at the optical microscope and measured with the colorimeter (Fig. 50). This cleaning effect is also pointed out by the decrease of the peak of carbon in EDX analysis taken in irradiated areas (Fig. 51 b and Fig. 52 b).

Considering that the energy of the photons (3.49 eV) at the 3^{rd} harmonic of the Nd:YAG laser matches very well the dissociation energy of C-H covalent bonds (~3.5 eV), and that no thermal damage was observed at the UV irradiated surface for moderate cleaning fluence, the proposed cleaning mechanism is UV photo-chemical ablation (§3.7) of the organic contamination, based in the primary laser photo-chemical interaction (§2.1.4) as it was verified by other authors [43, 44] and possibly accompanied by some amount of thermal vaporization (§2.2.2) or thermo-chemical decomposition (§2.2.4).

5. LASER CLEANING BY FEMTOSECOND PULSE ABLATION

Overpainted Gold

Cleaning of gold is a rare situation, possibly due to the fact that gold does not corrode in most common environments. As a matter of fact, corrosion appearing in gold objects is found to be due to the presence of other metals.

However during XIX century, several restoring campaigns overpainted the golden surfaces found in churches and decorative religious ornaments with a white layer, with the goal of covering damaged areas or just for a question of fashion. This represents a practical situation in which gold surfaces require a cleaning intervention in order to replace the original decoration.

5.1 SUBSTRATE CHARACTERIZATION

The samples used for the experimental study of laser cleaning of gold surfaces were small commercial pieces of used artefacts. The gold alloy was 18 karats, that is, an alloy with 75% gold and the remaining being copper, with no other material being detected in representative amount.

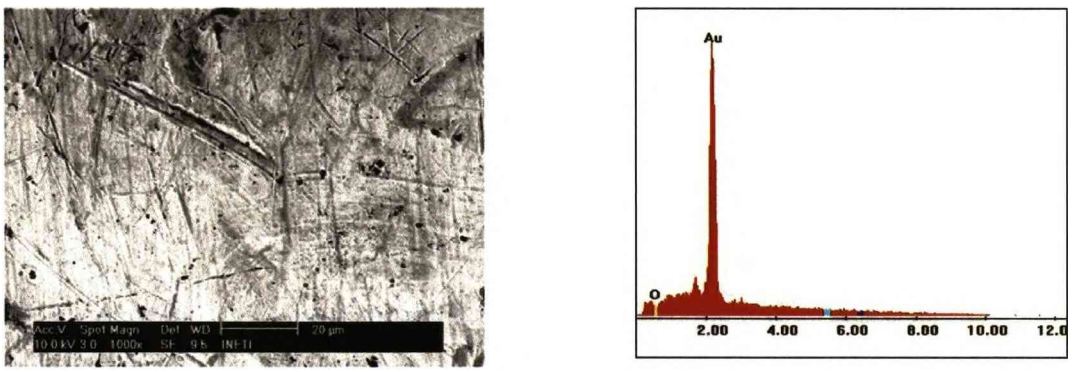

Fig. 53. Surface of gold (GM01) not contaminated
SEM micrograph (left), EDX analysis (right)

Gold is the most malleable and ductile metal and very soft, even when alloyed with copper or silver, so mechanical damage such as scratches and notches are usually found on the surface, as is visible in Fig. 53.

5.2 Contamination Characterization

To simulate conditions encountered in some monuments and religious decorations in church, where gold artefacts and gilded architectural elements were decorated with a white paint, gold samples have been intentionally covered with a co-polymer based paint layer of general used in construction works, about 2 μm thick, to study the process of laser cleaning of gold (Fig. 54).

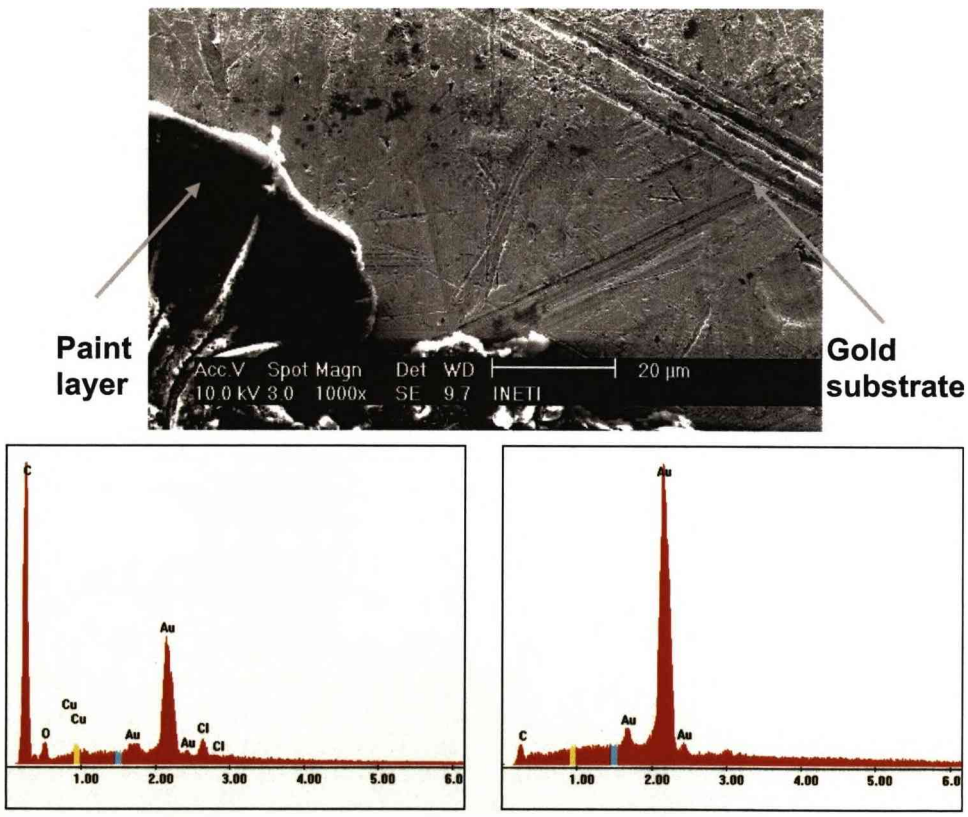

Fig. 54. Gold surface overpainted with organic paint

SEM micrograph (up)

EDX on painted layer (bottom left) EDX on gold surface (bottom right)

As in previous situations the surface sample was analysed preceding to laser irradiation, in order to allow for detection and identification of the modifications caused by laser interaction. Fig. 54 shows the analysis made by SEM and EDX, in which the polymeric paint, presenting the characteristic C and O peaks in the EDX spectrum, is seen covering the scratched gold surface (peaks Au in EDX spectra).

5.3 Experimental Procedure

The light source used in these experiments was a femtosecond pulse laser system, model CPA-2010 by Clark-MXR Inc; the experimental set-up and experimental procedure were not those used in previous cases and described in Part II- 1 and 2.

The seed laser is a mode locked fibre laser, doped with Erbium, producing short pulses at 1550; after frequency doubling and pulse stretching, the 775 nm seed pulses feed a Titanium-Sapphire (Ti-Sa) regenerative amplifier. The laser system output consists in 180 femtosecond pulses with a maximum energy content of 1 mJ per pulse with a near gaussian energy distribution in a transverse section slightly astigmatic with 4.8 X 5.2 mm axis. The all set of laser generator is thermally stabilised with a small dedicated chiller.

The system was adjusted at the beginning of the experimental work to emit pulses with maximum energy E =20 μJ with a central wavelength λ_0 =775 nm, with a fixed pulse duration of τ_p =180 fs (FWHM) at a repetition rate f_p =1 KHz.

The output beam delivery path included a beam splitter to sample the pulse temporal shape and wavelength at an APE pulsescope, a variable optical attenuator to adjust the pulse energy incident on the sample, and an optical scanning system TTI CPX 200 Dual, with galvanometric mirrors and a F-Θ lens, resulting in a laser spot with diameter d_σ = 25 μm in the working plane, set at the sample surface.

The laser scanning system was pre-programmed to sweep the laser pulse on the sample surface in parallel lines (Fig. 55), with scanning speed v_{scan} = 10 mm s^{-1}, resulting in a pulse overlap OL= 2.5. The scanned area was, in some cases, irradiated more than once in superposed scans and the number of overscans, OS, was varied from 1 to 10. Fig. 55 shows the parallel lines marked on the gold surface, after laser scanning with excessive incident energy.

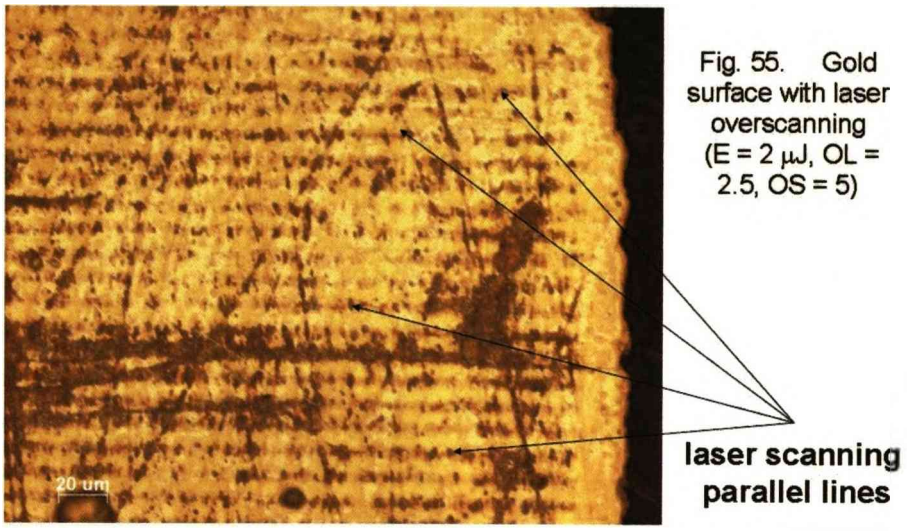

Fig. 55. Gold surface with laser overscanning (E = 2 μJ, OL = 2.5, OS = 5)

5.4 Irradiation of Samples with Femtosecond Laser Pulses

The contaminated gold surface were scanned by laser, first with a single scan (OS = 1) with increasing energy, that is to say with increasing fluence, in order to determine the cleaning threshold and the damage threshold, meaning the minimum fluence values where modifications on the organic paint layer or on the gold substrate surface could be detected.

Multiple squared areas in the bare and painted gold (Fig. 55) were irradiated with the energy per pulse incident on the surface varied from E =0.5 to 10 μJ; with the referred spot size this energy originates an energy density from F = 0.1 J cm^{-2} to 2 J cm^{-2}, equivalent to laser intensity in the range of 10^{12} W cm^{-2} to 10^{13} W cm^{-2}.

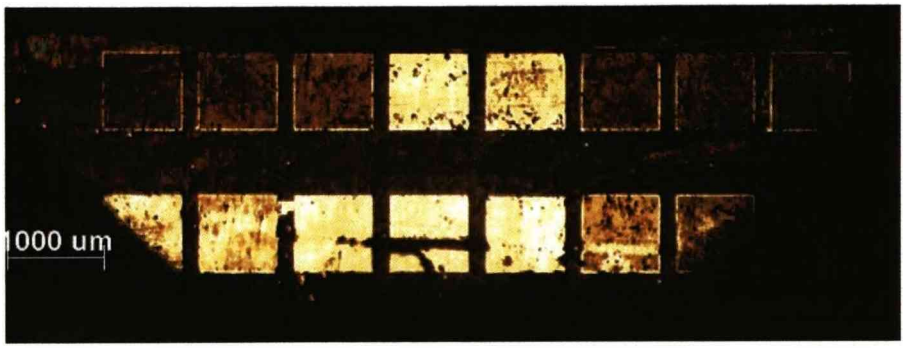

Fig. 55. Laser irradiated experimental areas on gold painted surface with variable laser parameters

The damage caused by laser irradiation on gold substrate was found to be a thermal damage, as can be observed in SEM micrographs (Fig. 57 a) showing sub-micron shallow craters indicative of local surface melting, after laser scanning irradiation with energy per pulse E = 3 μJ corresponding to F = 0.6 J cm^{-2}; though at laser energy E = 1 μJ no damage was observed (Fig. 57 b). Consequently, for a single overscan, the damage threshold in the described experimental conditions was found for pulses of 2 μJ, corresponding to F = 0.4 J cm^{-2}.

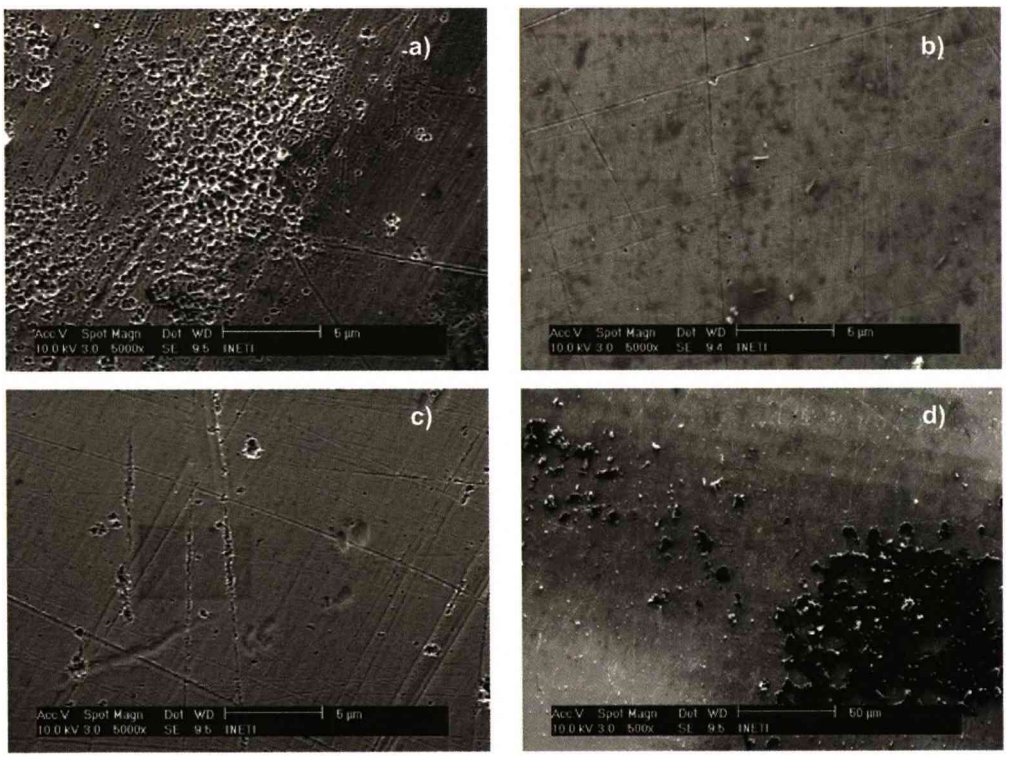

Fig. 56. Gold surface (GM04) single scanned with laser pulses
a) E = 3 μJ, b) E = 1 μJ, c) and d) E = 2 μJ; spot diameter = 25 μm

At laser fluence damage threshold, with E = 2 μJ, scarce signs of damage were observed. However, at this fluence, the cleaning was incomplete (Fig. 57 d) and the surface still display remnants of the paint leading to the need of multiple superposed scans. SEM images also show (Fig. 56 c) that some melting vestiges are mainly observed along defects on the surface.

As is well known, the absorbance and inherently the laser damage threshold depend on the surface quality. In fact for gold surfaces in the worst conditions, as in Fig. 58, laser pulses with the same fluence (2 μJ), generate increased damage on the gold surface.

Fig. 57. Bare gold surface (GM02) single scanned
E = 2 μJ, OS = 1, spot diameter = 25 μm

Paint removal from gold without damage of the substrates was achieved, but only in a narrow range of laser fluence from 0.2 to 0.4 J cm^{-2}. This fluence range was determined by the experimental conditions implemented and materials used such as pulse characteristics, paint thickness, and substrate gold surface conditions.

On a second stage of the experimental work other parameters were varied in order to evaluate their role in the cleaning effect and further in the interaction of femtosecond laser radiation with gold surface.

In the case of scanning the same area more than once (OS > 1), with laser fluence near or below the fluence for damage threshold, the damage areas increased (Fig. 58), with the number of overscans.

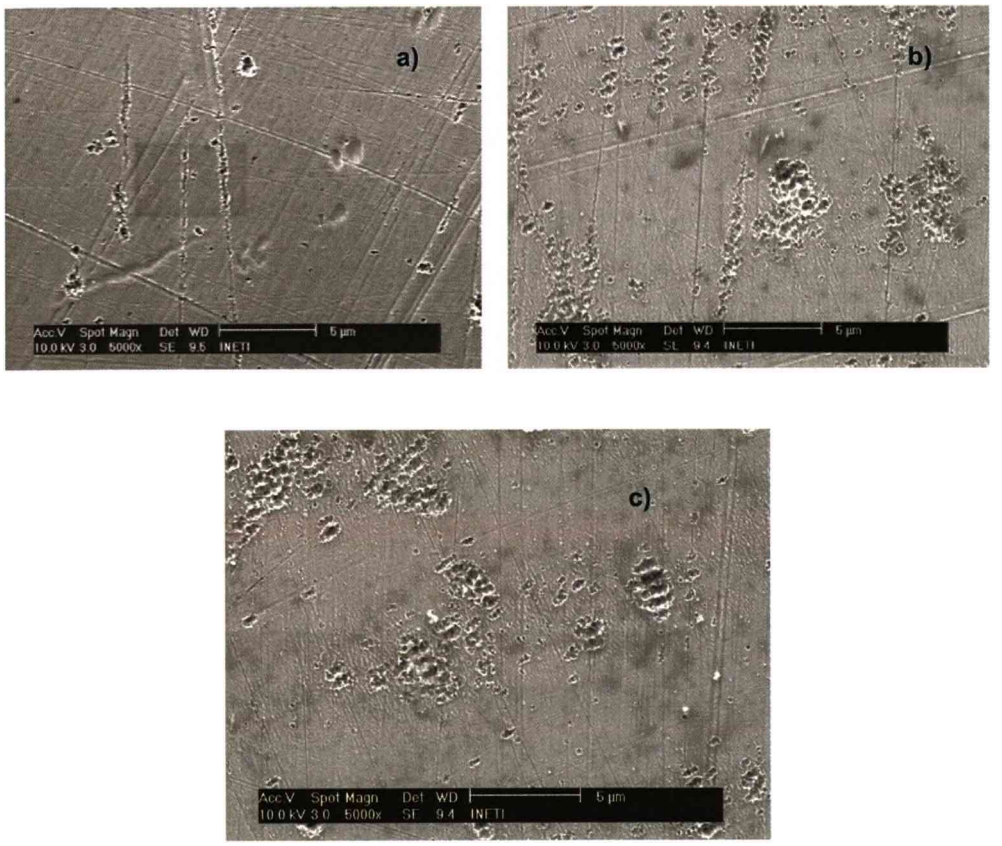

Fig. 58. Gold surface (GM04), laser irradiated with overscanning
a) OS = 1, b) OS = 3, c) OS = 5, all with E = 2 μJ and spot size = 25 μm

At soft irradiation conditions, this is with low energy per pulse and reduced number of overscans, the organic paint was total or partially removed from the surface (Fig. 60) without significative damages, except in the presence of surface defects (Fig. 60 c).

Different aspects of the surfaces after laser irradiation with diverse experimental parameters can be observed in the SEM micrographs in Fig 61 to Fig. 62.

a) E = 1 µJ, OL=2,5, OS=1

b) E = 2 µJ, OL=2,5, OS=3

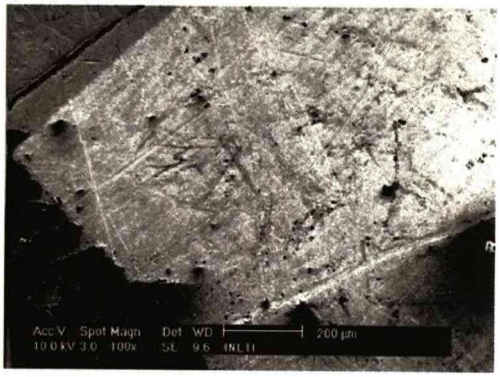

c) E = 2 µJ, OL=2,5, OS=5

Fig. 59 SEM images of laser cleaned areas
(at low energy and spot diameter = 25 µm)

Irradiating the contamination surface with energy per pulse, above the damage threshold (Fig. 61) the contamination is partially removed (Fig. 61 a), but several scans are required (OS>1) to achieve cleaning; damage of gold substrate can be observed (Fig. 61 b, c) due to the high laser fluence applied (F = 1 J cm^{-2}).

It was verified that, without multiple superposed scans (OS = 1) at moderate fluence, the irradiated area was difficult if not impossible to locate. And the number of overscans required for complete removal of the contamination depends not only on the laser pulse parameters, primarily fluence, but also on the material characteristics and thickness.

a) E = 5 μJ, OL=2,5, OS=1

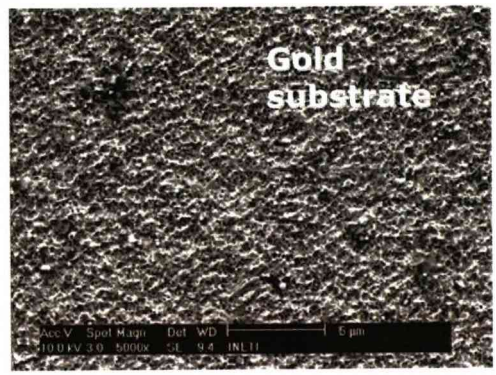

b)E = 5 μJ, OL=2,5, OS=3 c) E = 5 μJ, OL=2,5, OS=3

Fig. 60 . Laser cleaned areas by femtosecond irradiation
(E = 5 μJ, spot diameter = 25 μm)

Fig. 61 . Laser inhomogeneous cleaned areas
(E = 4 μJ, OL = 2,5, OS = 5 spot diameter = 25 μm

Fig. 62 shows another situation, often found in irradiated samples with femtosecond pulses and high laser fluence; the irradiated substrate show signs of melting due to the high fluence but looks clean and apparently unchanged near the borders of the irradiated area as it is shown in Fig.

62. This situation might be explained by the fact that the contamination on the limits of the irradiated area is not removed by direct laser interaction, but by heating and vaporization due to thermal conduction from irradiated areas.

5.5 CLEANING ASSESSMENT

In a similar way to what was done in previous work, Scanning Electron Microscopy for surface morphology analysis and X-ray Energy Dispersive spectroscopy, for compositional analysis were used, as can be observed in Fig 54 or Fig. 63, where both analyses evidence a cleaned gold surface without contamination or significative surface damage.

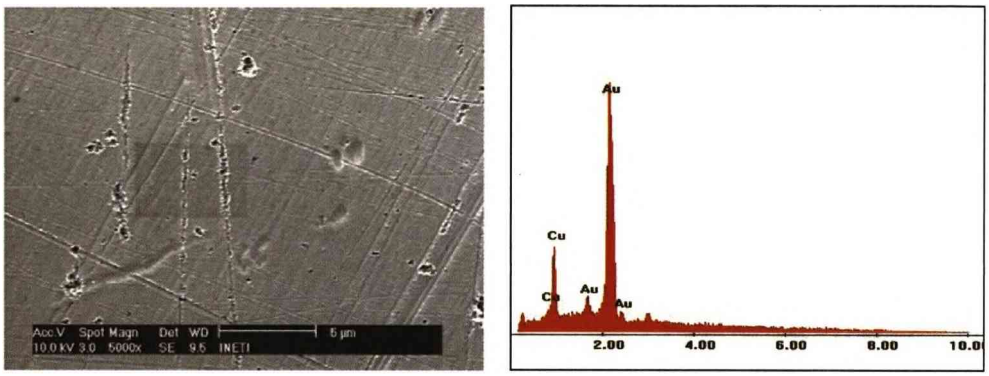

Fig. 62 . SEM and EDX images of laser cleaned gold area
E = 2 µJ, OL=2.5, OS=1

Other techniques used for other samples, such as FTIR or colorimetry were difficult to implement with the irradiated gold artefacts, due to the small area of the irradiated zones (of the order of 1 mm^2).

Besides colour, the high reflectivity for visible light is a general characteristic of precious metals; and this high reflectivity is associated with a polished surface, as the one of the test gold samples; other than that, the damages previously observed and expected, caused by laser irradiation of metals surface cause an alteration of the even metal surface morphology. So, not only SEM but also surface Micro Profilometry, using an interferometric profilometer WYCO NT 3300 was done to assess the condition of the precious metal surface after the removal of the paint.

This WYCO NT 3300 analyses the surface profile using white light interference instead of a stylus, with nanometer resolution in the direction perpendicular to the surface, what was considered adequated to sense the paint layer removal, detect any remnants of this layer on the metal surface or characterize damages in the substrate induced by laser irradiation.

With this high sensitivity optical profilometry system, it was possible to observe that irradiation with femtosecond laser pulses at laser fluence above the damage threshold, caused unexpected texturing in precious metal surface (Fig. 64) as reported previously by Perrie *et al.* [101].

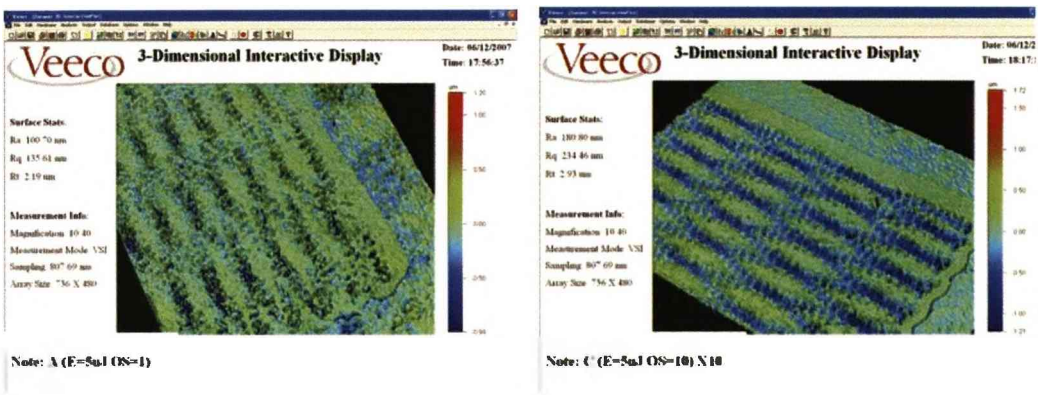

Fig. 63 . Optical profilometry of surface structures by femtosecond laser
E = 5 μJ; fp = 1 kHz, OS = 1 (left) and OS = 10 (right)

But also the irradiation of the surface with overscan (multiple superposed scans) with laser fluence within the same range of cleaning parameters also originate these surface nano structures, as shown in Fig. 65.

The structuring effect is also visible with the SEM micrographs (Fig.66), though not so evident and clear.

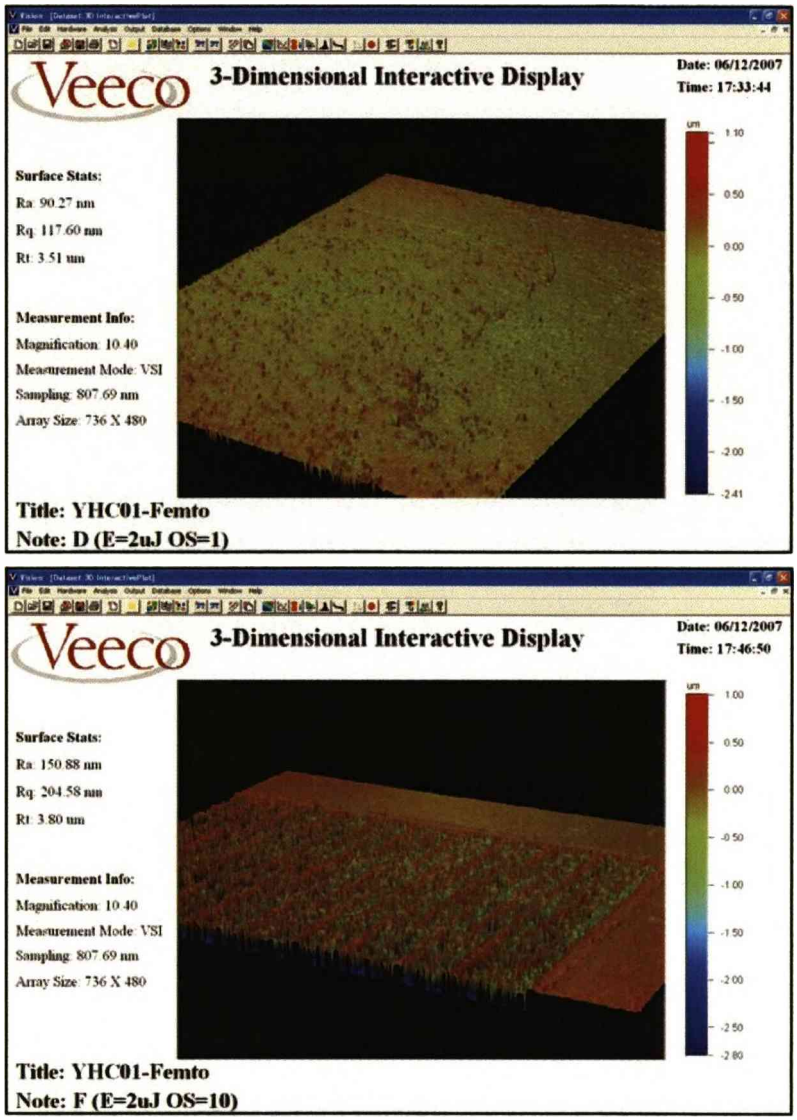

Fig. 64 . Optical profilometry of surface structures by femtosecond laser

E = 2 μJ; fp = 1 kHz, OS = 1 (left) and OS = 10 (right)

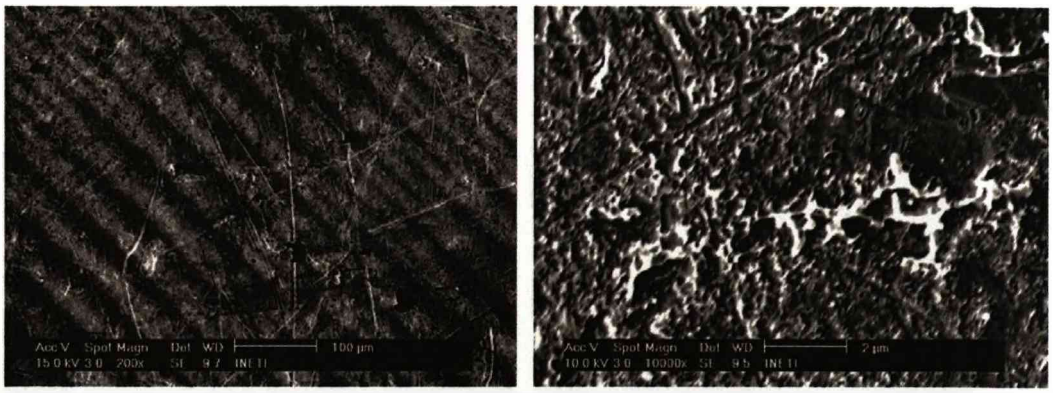

Fig. 65 . Surface SEM images of femtosecond laser cleaned surfaces

Ep = 2 μJ, fp = 1 kHz, OS = 5, different magnification

These observations may indicate a cleaning mechanism no "Self limited" for this set of experimental conditions. The "Self Limited" mechanism concept [11] consists on the ending of the material removal or modification by laser, at the interface contamination/substrate, due to the discontinuity of material properties, such as reflectivity, thermal conductivity or others.

However what was observed by optical and electron microscopy, and corroborated by optical profilometry of the metal surfaces irradiated with femtosecond lasers was that further irradiation of the surface, within the same range of laser cleaning parameters, results in further interaction with the substrate surface such as melting (Fig. 67) and other residual features on the surface as those observed by Perrie *et al.* [101].

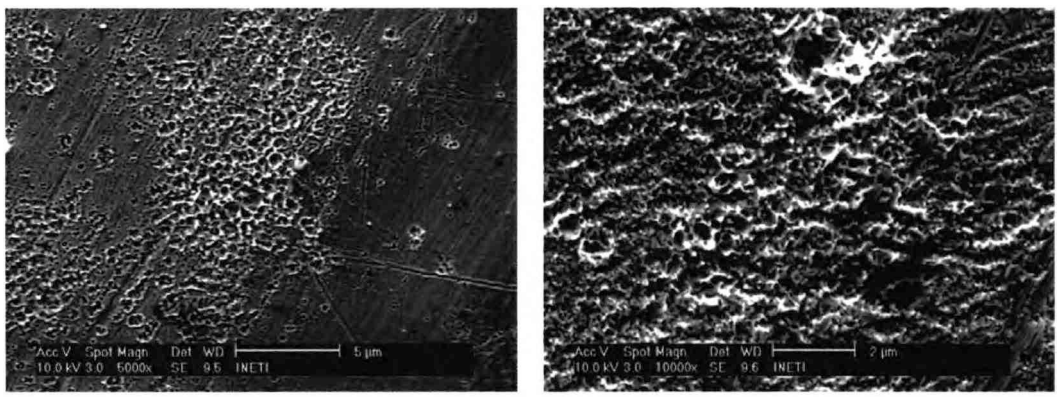

E = 5 µJ, OS = 3 E = 5 µJ, OS = 10

Fig. 66 . Signs of local surface melting on femtosecond laser cleaned surfaces

5.6 Discussion of Results and Cleaning Mechanism: Laser Ablation

Ultra-short or Femtosecond laser pulsed interaction with materials, mainly metallic surfaces is a recent research area and so the analysis of the experimental results obtained can not be well supported in the published literature. Moreover, due to the limited amount of sample

material available, the test surface areas were small, restricting the surface analysis methods adequated.

The experimental work consisted on irradiation of painted gold surfaces varying a set of parameters, but mainly the pulse energy and the number of laser scans over the same area (overscan). It was verified that laser cleaning was achieved with IR femtosecond pulse fluence in the range of 0.2 to 0.4 J cm^{-2}, but complete cleaning was only achieved with several superposed scans, depending on the thickness of the contamination layer.

It was also concluded that the fluence damage threshold for gold (0.4 J cm^{-2}) was very near or even within the cleaning parameters range, and gold surface damage was easily observed by optical profilometry or optical microscopy after a cleaning experiment, mainly over previously defective areas such as scratches, where increased absorption can probably arise. This absence of a (safety) fluence gap between the cleaning fluence and damage threshold fluence demonstrate that laser cleaning of metal surfaces with ultrashort pulses is not a self-limited process, according with the studies of S. Siano et al. [79] on the influence of pulse duration for the optimization of the laser cleaning process.

The analysis of the irradiated surfaces, by optical and electron microscopy and profilometry don't show any signs of craters or surface spallation indicative of photo-mechanical (§2.1.3) or thermodynamic (§2.2.3) interaction phenomena.

Also no evidence of chemical alteration was detected by optical microscope observation or EDX spectral analysis, keeping away the possibility of photo-chemical (§2.1.4) or thermo-chemical (§2.2.4) interactions as the main responsible for the cleaning effect.

In fact only signs of very localised melting was observed, taking place possibly after femtosecond laser pulse interaction; the localised transient heating due to thermalisation of laser photons absorption, may be a possible cause for the nano structures observed at the gold surface after laser irradiation, as well as the cause for paint removal.

Due to the characteristics of the laser pulse, of femtosecond duration, and the peak power intensities used for the removal of the paint layer, between 10^{12} and 10^{13} W cm^{-2}, the proposed mechanism for femtosecond laser cleaning is ablation by fragmentation and solid clusters ejection for lower fluence, where the gold substrate is not altered, and eventual vaporization for higher fluence or thinner contaminant films, in consequence of the observation of melted substrate material.

5.7 Comparison of Results for Different Laser Systems

In the course of this work, experimental research was done concerning the process of laser cleaning of precious metal surfaces with corrosion contamination, industrial oil or covered with a paint layer.

Among several laser sources such as pulsed CO_2 laser, long Q-switched and short free running Nd:YAG lasers, it was a Q-switched Nd:YAG laser and a Titanium Sapphire chirped pulse amplified laser that allow for the most successful cases of cleaning and so, those were more systematically studied and consequent results analysed.

The initial experiments with different laser sources have shown that laser irradiation of precious metals with surface contamination, by long pulses in the microsecond regime does not result in a cleaning effect or other permanent modification. This fact might be due to two simultaneous reasons. The first is the reduced energy absorption in the contamination layer, due to its optical transparency (such is the case of the grease layer) or small thickness (in the case of tarnish layer); the second reason is the high thermal conductivity of the precious metal substrate, impeaching a strong localized temperature increase.

In the case of irradiation with the long Q-Switch Nd:YAG laser (τ_p = 70 ns) a yellowing of the organic layer, indicative of thermal degradation, was observed at fluence values $F > 2$ J cm^{-2}, but without a cleaning effect.

The laser systems emitting short and ultra-short pulses showed an improved capacity to interact with the contaminated samples through

diverse physical and chemical processes, presenting potential capability for cleaning contaminated precious metal samples.

For each type of sample, a first stage of the experimental work was the characterization of the applied laser beam as well as the characterization of contamination and substrate; this analysis was focused on the distinctive aspects of a contaminated and a clean precious metal surface, namely the chemical composition, the colour or spectral reflectivity and the morphology. These – colour and chemical composition, were the principal aspects that were aimed to revert when cleaning with laser, avoiding significant alteration of surface morphology.

The characterization of the different samples and contaminant layer was done by optical and electron microscopy (SEM), energy dispersive X-ray spectroscopy (EDX), FTIR (Fourier transformed infrared spectroscopy), colorimetry and mechanical or interference optical profilometry.

The laser beam was delivered to the sample surface via one or more redirecting plane mirrors and converged by an appropriated positive lens. The energy distribution at a transverse section of the laser beam was quasi-gaussian on the femtosecond Ti-Sa laser, but very low quality for the Q-switched Nd:YAG laser, reason why a laser beam homogeniser was used with the raw beam or near the focusing lens.

Scanning the laser beam on the sample surface was achieved by a galvanometric mirror system associated with the femtosecond laser, and with a linear translation stage in the case where the Q-Switched Nd:YAG system was used.

The irradiation of the contaminated surfaces was performed firstly by single pulse emission on a single site of the standing sample, or multiple pulse for the femtosecond pulsed laser, with increasing energy density values; different wavelength, pulse duration and pulse repetition rate were also experiment within the limits of each laser system used.

This procedure allowed for the determination of the fluence (single pulse) for cleaning threshold and damage threshold, defining the operative cleaning window, this is, the range of operative laser parameters allowing for contamination cleaning without substrate damage.

Laser cleaning in an extended area was realized by scanning the beam over the sample with specific parameters of scanning speed, pulse repetition rate, pulse overlap, wavelength and fluence, chosen after the results of the fixed position irradiation.

After irradiation of the precious metal samples in single pulse or laser scanning, the surfaces were analysed for the identification of the alterations occurring on the irradiated areas and determination of laser cleaning and damage thresholds, for the assessment of the laser cleaning process.

The value of fluence thresholds for the referred precious metals samples in the experimented conditions implemented are presented in the final summary table.

The surface analysis undertaken in parallel with the irradiation tests in different conditions were indicative of the primary or secondary interaction effects taking place during laser irradiation of the samples.

For IR and visible (532 nm) nanosecond pulses, with fluence above a threshold, it was observed signs of fusion on the metallic surface; the temperature increase in the sample due to laser irradiation absorption was enough to cause permanent thermal effects such as melting on the substrate, though not removing the above contamination layer.

This fact can be due to the reduced laser energy absorption in the contamination layer, and consequent transmission to the substrate; the interaction of the nanosecond pulses with the precious metal is a photo-thermal phenomenon, causing a temperature increase much faster than the time required for thermal conduction on the metal substrate. The strong localized temperature increase can induce the "explosive" melting observed in the irradiated surfaces, initiated at "defects" location (inhomogeneous grains, surface scratches, etc.) where the laser absorption is enhanced.

For UV nanosecond pulses, with fluence above a threshold partial cleaning, namely decrease of the yellow component of the surface colour was observed, without damage of the metallic surface.

This cleaning effect is possibly due to specific increase of absorbance of the organic contamination materials to the UV and to low penetration depth (increase of diffusion) in the contamination layer, associated with increased absorption.

The increase of absorption of the UV laser pulses within the contamination layer, and consequent gradual temperature rise and possible phase change of the silver sulphide contamination, point towards a selective vaporization cleaning mechanism. Knowing that the bonding energy of sulphur to silver ions (2.25 eV) does not match the energy of laser photons at 355 nm (3.49 eV), a possible UV photochemical cleaning mechanism is not plausible.

Irradiation with visible and UV nanosecond pulses, due to 2^{nd} and 3^{rd} harmonic generation on a Q-switched Nd:YAG laser turned out in different results when used for laser cleaning of silver blanks contaminated by a thin layer or fine traces of lubricant oil, left on the surface after rolling the metal sheets.

At 532 nm, the irradiated surface show once more signs of surface melting even for low fluence irradiation. However irradiation with the 355 nm wavelength at moderate fluence and repetitive number of pulses or scans, produced areas in the sample surface with optical characteristics such as decreased yellow hue and decrease of diffuse reflectivity, approaching those of bare silver.

For higher fluence of UV laser pulses, thermal damage on the silver surface could be observed, but increasing the number of superposed scans, depending on contamination characteristics and thickness, allowed for removal of the contamination in small fractions per pulse avoiding undesired temperature rise.

It was expectable that, with this discontinuous and visibly transparent layer, laser radiation absorption would take place in the silver substrate, causing temperature increase in the substrate and the contamination by thermal conduction, leading to phase change in the metal substrate and thermal degradation of the industrial oil, involving both photo-thermal and thermo-chemical interaction phenomena.

But when irradiating the oil contaminated silver surface at moderate fluence no thermal effects or degradation was observed. Knowing that the dissociation energy of C-H covalent bonds (~3.5 eV) is very near the energy of the photons (3.49 eV) at the 3rd harmonic of the Nd:YAG laser, the proposed cleaning mechanism is UV photo-chemical ablation of the organic contamination, based in the primary laser photo-chemical interaction.

Femtosecond IR laser pulses were successfully used to irradiated and clean painted gold surfaces. Paint removal was observed for very low energy pulses such as 0.5 μJ. At high energy, fluence or number of superposed scans, the precious metal surface presented nano-structuring effects common in ultra-short laser material processing.

The interaction process supporting surface cleaning with femtosecond pulses is proposed to be laser ablation, although localised signs of surface melting were observed with high energy input.

SUMMARY TABLE

	CO_2 λ=10600 nm τ_p=10-50 µs	**Nd:YAG SFR** λ=1064 nm τ_p=20 µs	**Nd:YAG LQS** λ=1064 nm τ_p=70 ns	**Nd:YAG Q-S** λ=1064 nm τ_p=7 ns	**Nd:YAG Q-S** λ=532 nm τ_p=7 ns	**Nd:YAG Q-S** λ=355 nm τ_p=7 ns	**KrF** λ=248 nm τ_p=20 ns	**Ti-Sa Femtosec** λ=778 nm τ_p=180 fs
SAMPLES ↓	fp = 0.1-10 kHz	fp =5 kHz	fp =5 kHz	Single pulse to 10 Hz	Single pulse to 10 Hz	single pulse to 10 Hz	fp =1 Hz	fp =1 kHz
Silver coins with tarnished (Ag_2S) layer	No observable effect	No observable effect	Melting from 2 J/cm^2	Melting from 0.2 J/cm^2	Melting from 0.1 J/cm^2	Partial clean 0.1 J/cm^2	Partial clean 0.2-0.6 J/cm^2	
Large blanks with organic contamination	No observable effect	No observable effect	Yellowing from 2-3 J/cm^2	X	Yellowing from 0.2 J/cm^2	Partial clean 0.06-0.12 J/cm^2	Partial clean 0.2-0.6 J/cm^2	
Gold surface overpainted				Darkening from 0.3 J/cm^2	Darkening from 0.3 J/cm^2	No observable effect		Partial clean from 0.1 J/cm^2

143

6. CONCLUSIONS

In this work an experimental study on laser cleaning and interaction with precious metal samples covered with thin contamination layers was carried out.

The experimental results of this work allow for the following conclusions:

- Laser cleaning with non-homogeneous beam profile led to surface damage, even at low energy density; only homogenised beams allowed for a safe cleaning procedure.
- The efficiency of the laser cleaning process depends not only on the optical properties of the contamination layer and substrate surface, namely absorptivity, but also on other physical (such as thickness of contamination) and chemical characteristics.
- Laser cleaning of thin (submicron) layers of inorganic or organic compound contamination without precious metal substrate damage was only successfully achieved with short wavelength laser radiation or ultra-short laser pulse duration.
- The fluence values of substrate damage threshold depend, not only on the optical and thermal properties of the metal substrate, but also on the presence of defects on the surface, such as scratches, voids or other material inclusions.
- Using UV wavelength laser radiation or femtosecond duration laser pulses an operating window for laser cleaning of precious metals was determined, depending on contamination type and characteristics and precious metal properties.
- For the analysed precious metals and contaminations the laser fluence for cleaning without damage was always in the range of tenths of joules per square centimeter, as can be observed in the summary table.
- Laser cleaning of a thin layer of inorganic contamination was only achieved with UV wavelength radiation; selective vaporization is

proposed as the cleaning mechanism, based on the low laser fluence used and the increased contamination absorptance to the short wavelength radiation.

- Laser cleaning of a thin layer of organic contamination was successful with UV wavelength radiation; UV photochemical ablation is proposed as the cleaning mechanism, based on the absence of visible thermal effects on the substrate and on the proximity of the dissociation energy of C-H covalent bonds (~3.5 eV) and the energy of incoming UV photons (3.49 eV).
- Laser cleaning of precious metals with femtosecond pulses at near IR radiation was also successful within a limited range of overscans; the cleaning mechanism proposed is ultrashort laser ablation.
- Laser cleaning with moderate fluence (below damage threshold) was observed to be always partial, and a number of multiple overscans (depending on the incident laser fluence and contamination thickness) were needed to obtain a cleaned surface.
- Laser cleaning with high fluence (above damage threshold) or with moderate fluence at high repetition rate was observed to cause superficial melting on the precious metal substrate, referred to "dulling" of the surfaces by Degrigny [17].
- Laser cleaning with ultra-short laser pulses is a "non Self Limited" mechanism because irradiating the surface with laser fluence within the same range of cleaning parameters with overscan (multiple superposed scans) originates surface damage such as the observed surface nano structures.

Laser cleaning of thin layers on precious metals was ascertained to be a very delicate process, due to the fact that short or ultrashort laser pulses are required to overcome thermal losses on the substrate, but surface melting will easily occur with the corresponding high peak power, requiring fine control over the different laser and non-laser parameters involved.

7. RECOMMENDATIONS FOR FURTHER WORK

The experimental work herein described, on laser cleaning of metals, namely precious metals would be improved with a more precise adjustment of fluence values on the sample surface, using calibrated attenuators between the laser source and the surface, or larger spot size, what requires a more uniform laser beam.

Having in mind the promising results obtained with UV laser radiation on the removal of thin organic contamination on metal surfaces, further work with other laser or non laser sources with different wavelengths would be an interesting and innovative field.

Although femtosecond laser pulses were seen as too much aggressive for cleaning thin film contamination, further exploitation of the use of ultra-short femto and picosecond laser pulses in different wavelength and pulse repetition regimes for precise and accurate contamination removal seems to be also an interesting field.

References

1. Lazzarini L, Asmus J F, Marchesini M L, **Lasers for the Cleaning of Statuary- Initial Results and Potentialities**, 1st Int. Symposium on the Deterioration of Building Stone, La Rochelle (1972) 89-94.

2. Asmus J F, **Light Cleaning: Laser Technology for Surface Preparation in the Arts**, Technology and Conservation (1978) 14-18.

3. Zapka W, Ziemlich W, Tam A C, **Efficient Pulsed Laser Removal of 0.2 μm Sized Particles from a Solid Surface**, Applied Physics Letters, Vol. 58 No 20 (1991) 2217-2219

4. Lee S J, Imen K, Allen S D, **Shock Wave Analysis of Laser Assisted Particle Removal**, J. Applied Physics, Vol. 74 No 12 (1993) 7044-7047

5. Lu Y F, Takai M, Komuro S, Shiokawa T, Aoyagi Y, **Surface Cleaning of Metals by Pulsed Laser Irradiation on Air**, Applied Physics A, Vol. 59 No 3 (1994) 281-288.

6. Lu Y F, Aoyagi Y, Takai M, Namba S, **Laser Surface Cleaning in Air: Mechanisms and Applications**, Japanese J. Applied Physics, Vol. 33 (1994) 7138-7143

7. Lovoi P A; Alan M, **Method and Apparatus for the Removal of Paint and the Like from a Substrate**, U S Patent 4,588,885 (May 13, 1986)

8. Daurelio G, Chita G, Cinquepalmi M, **New Laser Surface Treatments: Cleaning, De:Rusting, De-Oiling, De-Painting, De-Oxidizing and De-Greasing**, Proc. "Lasers in Materials Processing" Munich DE, June 97, SPIE Vol. 3097 (1997) 369 – 391

9. Larson J, **EROS: The Laser Cleaning of an Aluminium Sculpture**, "From Marble to Chocolate, the Conservation of Modern Sculpture" Archetype Pub. (1995) ISBN 1873132859

10. Cottam C A, Emmony D C, Larson J, Newman S, **Laser Cleaning of Metals at Infra-Red Wavelengths**, Proc. LACONA I Heraklion, Restauratorenblatter (1995) 95-98

11. Cooper M, **Laser Cleaning in Conservation: An Introduction**, Butterworth-Heinemann ed., 1 edition (Dec 1997) 74-75

12. Oltra R, Yavas O, Kerrec O, **Pulsed Laser Cleaning of Oxidized Metallic Surfaces in Electrochemically Controlled Liquid Confinement**, Surface and Coatings Technology, No 88 (1996) 157-161

13. Yavas O, Oltra R, Kerrec O, **Enhancement of Pulsed Laser Removal of Metal Oxides by Electrochemical Control**, Applied Physics A, Vol. 64 No 4 (1996) 331-339

14. Lee J M, Watkins K G, Steen W M, Ryan J D, Russel P, **Investigation of Acoustic Monitoring in the Laser Cleaning of Copper**, Proc. "ICALEO 97", S. Diego CA 17-20 Nov. Section C (1997) 226-234

15. Kearns A, Fischer C, Watkins K G, Glasmacher M, Keyrandish H, Brown A, Steen W M, Beahan P, **Laser Removal of Oxides from a Copper Substrate, Using Q-Switch Nd:YAG Laser Radiation at 1064nm, 532 nm and 266 nm**, Applied Surface Science No 127-129 (1998) 773-780

16. Ohba M, Kuzukawa K, Sakairi K, **Experimental Study on the Process of Cleaning the Contacts of Signal Control Relays**, Proc. "34th Meeting of the IEEE Holm Conference - Electrical Contacts" (1998) 311-320

17. Degrigny C, Tanguy E, LeGall R, Zafiropulos V, Marakis G, **Laser Cleaning of Tarnished Silver and Copper Threads on Museum Textiles**, LACONA IV Proc. in J. Cultural Heritage Vol. 4 S 1 (2003) 152s-156s

18. Lee J-M., Yu J-E., Koh Y-S, **Experimental Study of the Effect of Wavelength in the Laser Cleaning of Silver Threads**, LACONA IV Proc. in J. Cultural Heritage, Vol. 4 S 1 (2003) 157-161

19. Sokhan M, Hartog F, McPhail D, **Surface Analysis of Laser Cleaned Metal Threads**, Proc. Lasers in the Conservation of Artworks LACONA V Osnabrueck, Set. 2003, (2005) 237-244

20. Siatou A, Charalambous D, Argyropoulos V, Pouli P, **A Comprehensive Study for the Laser Cleaning of Corrosion Layers due to Environmental Pollution for Metal Objects of Cultural Value: Preliminary Studies on Artificially Corroded Coupons**, Hindawi Publishing Co. Laser Chemistry Article ID 85324 (2006) 7 pages

21. Gusmano G, Montanari R, Kaciulis G, Montesperelli G, Denk R, **"Gold Corrosion": Red Stains on a Gold Austrian Ducat**, Applied Physics A, Vol 79 No 2 (2004) 205-211

22. Georges C, Sanchez H, Semmar N, Boulmer-Leborgne C, Perrin C, Simon D, **Laser Treatment for Corrosion prevention of Electrical Contact Gold Coating**, Applied Surface Science, Vol 186 (2002) 117-123

23. Ohba M, Kuzukawa K, Sakairi K, **Experimental Study on the Process of Cleaning the Contacts of Signal Control Relays**, Proc. "34th Meeting of the IEEE Holm Conference - Electrical Contacts" (1998) 311-320

24. Menzel R, Photonics, **Linear and Non-Linear Interactions of Laser Light and Matter**, Springer Advanced Texts in Physics, Springer-Verlag Berlin, Heidelberg, New York 2001 101

25. Hecht, E. **Optics**, 3rd ed., Addison Wesley Longmann ed, 1998 147

26. Huang C, Zhang G, Chen Z, Huang X, Shen H, **Calculation of the Absorption Coefficients of Optical Materials by Measuring the Transmissivities and Refractive Indices**, Optics & Laser Technology, Vol. 34 No 3 (2002) 209-211

27. Pasquet P, Coso R, Boneberg J, Leiderer P, Oltra R, Bouquillon J P, **Laser Cleaning of Oxide Iron Layer: Efficiency Enhancement Due to Electrochemical Induced Absortivity Change**, Applied Physics A, Vol. 69 Sup 1, (1999) S727-S730

28. Pasquet P, Psyllaki P, Oltra R, Meja P, Autric M, **Laser Cleaning of Oxidized Fe-Alloys**, Surface Modification Technologies, XIV (2000) 7 pages

29. Pasquet P, Psykally P, Oltra R, Boquillon J, Leiderer P, Boneberg J, Joiret S, Hugot-Le Goff A, **Laser Cleaning of Oxidized Metallic Materials: Role of the Optical Properties of the Oxide Film**, SPIE Proc. "Laser Techniques and Systems in Art Conservation", Munich Germany June 2001 (2001) 38-41

30. Autric M, Oltra R, **Basic Processes of Pulsed Laser Materials Interaction. Applications to Laser Cleaning of Oxidized Surfaces**, Proc. "XV Int Symp on GCL&HPL", Prague Aug. 2004, SPIE Vol. 5777 (2005) 982-985

31. Steen W M, **Modelling** in "Handbook of the Eurolaser Academy", Vol. 2, Dieter Shuocker ed. Chapman & Hall 1998 622-624

32. Zhou X, Imasaki K, Furukawa H, Umino H, Skagishi, K, Nakai S, Yamanaka, C, **Simulation Study and Experiment on Laser Ablation Surface Cleaning**, Optics and Laser Technology, Vol. 33 No 3 (2001) 189-194

33. Carslaw H S, Jaeger J C, **Conduction of Heat in Solids** 2nd edition Oxford Science Publications, Oxford University Press 1959

34. Ready J F, **Effects of High Power Laser Radiation** Academic press Inc 1971

35. Duley W W, **CO2 Lasers, Effects and Applications**, Academic Press Inc. 1976

36. Duley W W, **Laser Processing and Analysis of Materials**, Plenum Press 1983

37. Steen W M, **Laser Material Processing** Springer-Verlag 1991

38. Watkins K G, **Laser Cleaning** in Laser Material Processing, 3rd ed. W. Steen Springer-Verlag London, Berlin, Heidelberg 2003

39. Siano S, Fabiani F, Pini R, Salimbeni R, Giamello M, Sabatini G, **Determination of Damage Thresholds to Prevent Side Effects in Laser Cleaning of Pliocene Sandstone of Siena**, J. Cultural Heritage, Vol. 1 (2000) S47-S53

40. Siano S, Margheri F, Pini R, Mazzinghi P, Salimbeni R, **Cleaning Processes of Encrusted Marbles by Nd:YAG Lasers Operating in Free–Running and Q-Switching Regimes**, Applied Optics, Vol. 36 (1997) 7073-7079

41. Mazzinghi P, Margheri F, **A Short Pulse Free Running, Nd:YAG Laser for the Cleaning of Stone Cultural Heritage**, Optics and Lasers in Eng., Vol. 39 No 2 (2003) 191-202

42. Burmester T, Meier M, Haferkamp H, Barcikowski F, Bunte J, Ostendorf A, **Femtosecond Laser Cleaning of Metallic Cultural Heritage and Antique Artworks**, Proc. Lasers in the Conservation of Artworks LACONA V Osnabrueck, Set. 2003 (2005) 61-69

43. Bäuerle D, **Laser Processing and Chemistry**, Springer, 3rd ed., 2000

44. Fotakis C, Athanassiou A, Andreou E, Tornari, V, Bonarou A, Antonucci L, Anglos D, Georgiou S, Zafiropoulos V, **Modelling of Chemical and Mechanical Aspects in Laser Restoration of Artworks**, Proc. "Second International Symposium on Laser Precision Micro fabrication", SPIE Vol. 4426 (2002) 296-301

45. Watkins K; Curran C; Lee J, **Two New Mechanisms for Laser Cleaning Using Nd:YAG Sources**, J. Cultural Heritage, Vol. 4, S 1 (2003) 59s -64s

46. Tam A C, Leung W P, Zapka W, Ziemlich W, **Laser Cleaning Techniques for Removal of Surface Particulates**, J. Applied Physics, Vol. 71 No 7 (1992) 3515-3523

47. Lu Y F, Song W D, Ye K D, Lee Y P, Chan D H, Low T S, **A Cleaning Model for Removal of Particles Due to Laser Induced Thermal Expansion of Substrate Surface**, Jpn. J. Applied Physics, Vol. 36 Part 2 No. 10A (1997) L 1304-L 1306

48. Halfpenny D R, Kane D M, **A Quantitative Analysis of Single Pulse Ultraviolet Dry Laser Cleaning**, J. of Applied Physics, Vol. 86, No 12 (1999) 6641-6646

49. Arnold N, **Theoretical Description of Dry Laser Cleaning**, Applied Surface Science, Vol. 208-209 (2003) 15-22

50. Luk'Yanchuk B, Arnold N, Huang S, Wang Z, Hong M, **Three Dimensional Effects in Dry Laser Cleaning**, Applied Physics A, Vol. 77 No 2 (2003) 209-215

51. Pleasants S, Arnold N, Kane D M, **Acoustic Substrate Expansion in Modelling Dry Laser Cleaning of Low Absorbing Substrates**, Applied Physics A, Vol. 79 No 3 (2004) 507-514

52. Hsu H-T, Lin J, **Thermal -Mechanical Analysis of the Surface Waves in Laser Cleaning**, Int. J. Machine Tools and Manufacture, Vol. 45, No 5-6 (2005) 979-985

53. Bloisi F, Barone A, Vicari L, **Dry Laser Cleaning of Mechanically Thin Films**, Applied Surface Science, Vol. 238 No 1-4 (2004) 121-124

54. Bloisi F, Blasio G, Vicari L, Zoncheddu M, **One-Dimensional Modelling of 'Verso' Laser Cleaning**, J. of Modern Optics, Vol. 53 No 8 (2006) 1121-1129

55. Watkins K, **Mechanisms of Laser Cleaning**, Proc. Conference on High Power Lasers in Manufacturing Nov. 1999 SPIE Vol. 3888 (2000) 165-174

56. Aden M, Kreutz E, Schlüter H, Wissenbach K, **The Application of the Sedov-Taylor Scaling during Material Removal of Metals and Oxide Layers with Pulsed CO2 and Excimer Laser Radiation**, J. Physics D: Applied Physics, Vol. 30 No 5 (1997) 980-989

57. Siano S, Pini R, **Analysis of Blast Waves Induced by Q-Switched Nd:YAG Laser Photodisruption of Absorbing Targets**, Optics Communications, Vol. 135 (1997) 279-284.

58. Dimogerontakis T, Oltra R, Heintz O, **Thermal Oxidation Induced During Laser Cleaning of an Aluminium Magnesium Alloy**, Applied Physics A, Vol. 81 No 6 (2005) 943-95

59. von Allmen, M; **"Laser Beam Interactions with Materials, Physical Principles and Applications"** Springer Series in materials Science, Aram Mooradian and Morton B Panish, ed. (1987) 6-18.

60. Rethfeld B, Sokolowski- Tinten K, Von der Linde D, Anisimov S, **Timescales in the Response of Materials to Femtosecond**

Laser Excitation, Applied Physics A, Vol 79 No 767-769 (2004) DOI: 10.1007/ s00339-004-2805-9

61. Gamaly E, Rode A, Tikhonchuk V, L-Davies B, **Ablation of Solids by Femtosecond Lasers: Ablation Mechanisms and Ablation Thresholds for Metals and Dielectrics**, Physics of Plasmas, Vol. 9 No 3 (2002) 949

62. Gamaly E, Rode A, Tikhonchuk V, L-Davies B, **Electrostatic Mechanism of Ablation by Femtosecond Laser,** Applied Surface Science, Vol. 197-198 (2002) 699-704

63. Maznev A, Holfeld J, Gudde J, **Surface Thermal Expansion Under Femtosecond Laser Irradiation**, J. Applied Physics, Vol 82 No 10 (1997) 5082-5085

64. Perez D, Lewis L, **Molecular Dynamics Study of Ablation of Solids under Femtosecond Laser Pulses**, Physical Review Letters, Vol. 89 (2002) 255504

65. Perez D, Lewis L, **Molecular-Dynamics Study of Ablation of Solids under Femtosecond Laser Pulses**, Physical Review B, Vol. 67, No. 18 (2003) 18410201-15

66. Perez D, Lewis L, **Thermodynamic Evolution of Materials during Laser Ablation under Pico and Femtosecond Pulses**, Applied Physics A, Vol. 79 (2004) DOI 10.1007/s00339-004-2611-4

67. Yang J, Zhao Y, Zhu X, **Theoretical Studies of Ultrafast Ablation of Metal Targets Dominated by Phase Explosion**, Applied Physics A, Vol. 89 (2007) DOI 10.1007/s00339-007-4141-3

68. Zighilei L, Kodali P, Garrison B, **On The Threshold Behaviour in Laser Ablation of Organic Solids**, Chemical Physics Letters, Vol 276 (1997) 269-273

69. Zeng X, Mao X, Greif R, Russo E, **Ultraviolet Femtosecond and Nanosecond Ablation of Silicon: Ablation Efficiency and Laser Induced Plasma Expansion**, Proc. "High Power Laser Ablation V" Taos USA, SPIE Vol 5448 (2004) 1150-1158

70. B- Leborgne C, Benzerga R, Scuderi D, Perrière J, Albert O, Etchepare J, Millon E, **Femtosecond Laser Beam in Interaction with Materials for Thin Film Deposition**, Proc. "High Power Laser Ablation VI", SPIE Vol 6261 (2006) 626120

71. Watkins K G, **Mechanisms of Laser Cleaning**, SPIE Vol. 3888 Proc. High Power Lasers in Manufacturing (1999) 165-174.

72. Asmus J F, Murphy C G, Munk W H, **Studies on the Interaction of Laser Radiation with Art Artefacts**, Proc. Society Photo-Optical Instrument Eng., Vol. 41 (1973) 19-27.

73. Lazzarini L, Asmus J F, Marchesini M L, **Lasers for the Cleaning of Statuary- Initial Results and Potentialities**, Proc.1st Int. Symposium on the Deterioration of Building Stone, La Rochelle (1972) 89-94.

74. Asmus J F, Munk W H, Wuerker R, **Lasers and Holography in Art Preservation and Restoration**, Proc. NEREM IEEE (1972) 5-8.

75. Kautek W, Pentzien S, Rudolph P, Kruger J, Konig E, **Laser Interaction with Coated Collagen and Cellulose Fibre Composites: Fundamentals of Laser Cleaning of Ancient Parchment and Paper**, Applied Surface Science No 127-129 (1998) 746-754.

76. Salimbeni R, Pini R, Siano S, **Achievement of Optimum Laser Cleaning in the Restoration of Artworks: Expected Improvements by On-Line Optical Diagnostic**, Spectrochimica Acta – B, Vol. 54 No 6 (2001) 877-885

77. Imen K, Lee S J, Allen S D, **Laser Assisted Micro Scale Particle Removal**, Applied Physics Letters, Vol. 58, No 2 (1991) 203-205

78. Yavas O, Schiling A, Bischof J, Boneberg J, Leiderer P, **Bubble Nucleation and Pressure Generation during Laser Cleaning of Surfaces**, Applied Physics A, Vol. 64 No 4 (1997) 331-339

79. Siano, S. Salimbeni, R, **The Gate of Paradise: Physical Optimisation of the Laser Cleaning Approach**, Studies in Conservation, Vol. 46 (2001) 269-281

80. Lee J M, Watkins K G, Steen W M, **Laser Shock Cleaning**, LIA Proc. "ICALEO' 2000", Dearborn, USA, Oct. 2000, Section D, (2000) 171-177

81. Cetinkaya C, Peri M M, **Non-Contact Nanoparticle Removal with Laser Induced Plasma Pulses**, Nanotechnology, Vol. 15 No 5 (2004) 435-440

82. Lim H, Kim D, **Optical Diagnostics for Particle-Cleaning Process Utilizing Laser Induced Shockwave**, Applied Physics A, Vol. 79 No 4-6 (2004) 965-968

83. Song W, Lu Y, Hong M, Chong T, Low T, **Theoretical and Experimental Investigations on Laser Dry Cleaning of Particles from Substrate Surfaces**, Proc. "Advanced Applications of Lasers in Materials Processing" IEEE/LEOS Summer Topical Meetings, (1996) 69-70

84. Grojo D, Onana M, Cros A, Delaporte P, **Influence of Laser Pulse Shape on Dry Laser Cleaning**, Applied Surface Science, Vol 252 No 13 (2006) 4786-4791

85. Grojo D, Cros A, Delaporte Ph, Sentis M, **Experimental Investigation of Ablation Mechanisms Involved in Dry Laser Cleaning**, Applied Surface Science, Vol 253, No 19 (2007) 8309-8315

86. Watkins K, Lee J-M, Curran C, **Underlying Mechanisms in Laser Techniques for Art Conservation: Two Improved Cleaning Mechanisms**, Proc. "Laser Techniques and Systems in Art Conservation", Munich June 2001, SPIE Vol. 4402 (2001) 73-81

87. Lee J M, Watkins K G, Steen W M, **Angular Laser Cleaning for Effective Removal of Particles from a Solid Surface**, Applied Physics A, Vol. 71 No 6 (2000) 671-674

88. Lu Y F, Song W D, Ang B W, Hong M H, Chan D S H, Low T S, **A Theoretical Model for Laser Removal of Particles from Solid Surfaces**, Applied Physics A, Vol. 65 No 1 (1997) 9-13

89. Barone A, Bloisi F, Vicari L, **"Verso" Laser Cleaning of Mechanically Thin Films**, Applied Surface Science, Vol. 208-209 (2003) 468-473

90. Leveugle E; Zhigilei L V, **Microscopic Mechanisms of Short Pulse Laser Spallation of Molecular Solids**, Applied Physics A, Vol. 79 No 4-6 (2004) 753-756

91. Oltra R, Yavas O, Cruz F, Bouquillon J P, Sartori C, **Modelling and Diagnostic of Pulsed Laser Cleaning of Oxidized Metallic Surfaces**, Applied Surface Science No 96-98 (1996) 484-490

92. Strzlec M, Marczak J, **Interferometric Measurements of Acoustic Waves Generated during Laser Cleaning of Works of Art**, Proc. "Laser Techniques and Systems in Art Conservation", Munich June 2001, SPIE Vol. 4402 (2001) 235-241

93. Jezersek M, Milanic M, Babnik A, Mozina J, **Real-time Optodynamic Monitoring of Pulsed Laser Decoating Rate**, Ultrasonics, Vol. 42 No 1-9 (2004) 37-41

94. Bregar V B, Mozina J, **An Optodynamic Characterisation of a Laser Cleaning Process**, Proc. "Laser Techniques and Systems in Art Conservation", Munich June 2001, SPIE Vol. 4402 (2001) 82-92

95. Vereecke G, Rohr E, Heyns, M M, **Influence of Beam Incidence Angle on Dry Laser Cleaning of Surface Particles**, Applied Surface Science, Vol. 157 No 1-2 (2000) 67-73

96. Perrie W, Rushton A, Gill M, Fox P, O'Neill W, **Femtosecond Laser Microstructuring of Alumina Ceramic**, Applied Surface Science, Vol. 248 (2005) 213-217

97. Steen, W, **Foreword in Special Issue dedicated to Laser Material Processing**, J. Optics and Lasers in Eng., Vol. 34 No 4-6 (2000) 203-204

98. Hallet K, Thickett D, McPhail D, Chater R, **Application of SIMS to Silver Tarnish**, Applied Surface Science, Vol. 203-204 (2003) 789-792

99. **SOLID State Lasers for Materials Processing**, R. Ifflander, Springer Ed (2001) pp 323

100. Lima M, Wagniere J, Morato S, Vieira N, **Elimination of Lubricants from Aluminium Cold Rolled Products, Using Short Laser Pulses** Materials Research, Vol 5 No 2 (2002) 205-208

101. Perrie W, Baum A, Scully P, Sharp M, Edwardson S, Watkins K, **NIR and UV Femtosecond Laser Micro-Structuring of Materials**, Photon06 Conference Manchester, September 2006